EFFECTS OF HYDRAULIC ROUGHNESS AND SEDIMENT SUPPLY ON SURFACE TEXTURES OF GRAVEL-BEDDED RIVERS

By

John M. Buffington

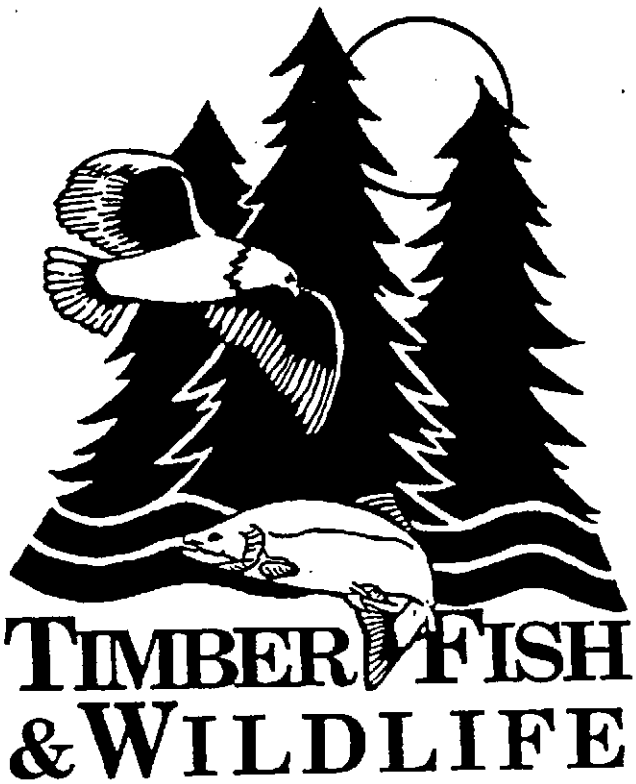

March 8, 1995

Effects of Hydraulic Roughness and Sediment Supply on Surface Textures of Gravel-bedded Rivers

by

John M. Buffington

A thesis submitted in partial fulfillment
of the requirements for the degree of

Master of Science

University of Washington

1995

Approved by _____
(Chairperson of Supervisory Committee)

_____

Program Authorized
to Offer Degree Department of Geological Sciences

Date March 8 1995

In presenting this thesis in partial fulfillment of the requirements for a Master's degree at the University of Washington, I agree that the Library shall make its copies freely available for inspection. I further agree that extensive copying of this thesis is allowable only for scholarly purposes, consistent with "fair use" as prescribed in the U.S. Copyright Law. Any other reproduction for any purposes or by any means shall not be allowed without my written permission.

Signature 

Date 3/6/95

University of Washington

Abstract

Effects of Hydraulic Roughness and Sediment Supply on Surface Textures of Gravel-bedded Rivers

by John M. Buffington

Chairperson of Supervisory Committee: Research Assistant Professor D. R. Montgomery
Department of Geological Sciences

Textural response to sediment supply and other hydraulic roughness elements in gravel-bedded rivers is examined by comparing reach-average median surface grain sizes (D_{50s}) with those predicted from a simple threshold channel model. An extensive literature review of bedload transport studies indicates that sediment transport in gravel-bedded channels is to a first approximation bankfull threshold. Using Shields' equation D_{50s} is predicted from bankfull depth and slope, providing a theoretical reference point for examining textural response. The model, however, requires specification of a dimensionless critical shear stress parameter (τ^*_{c50s}), which is made uncertain by the current state of the incipient motion literature. A detailed review of this literature demonstrates distinct methodological biases in previously reported results (commonly assumed, but poorly documented) and it is concluded that of the τ^*_{c50s} values currently available 0.032 is the most appropriate for natural channels.

Previously documented textural response to sediment supply is examined within the bankfull-threshold framework, showing that increased sediment loading causes a systematic textural fining and deviation from model predictions. Textural response to bedform and large woody debris (LWD) roughness is investigated through a field study of gravel-bedded channels in forest environments of western Washington and southeast Alaska. Surface textures are examined in three distinctly different channel morphologies representing an increasing complexity of channel roughness: plane-bed, LWD-poor pool-riffle, and LWD-rich pool-riffle. Results show that textural fining in response to hydraulic roughness features occurs at both reach and local scales and that the number and spatial complexity of textural patches increases with greater complexity of channel roughness. Within the bankfull-threshold framework, reach-average median surface grain sizes segregate by channel type into distinct zones of textural response, with plane-bed channels

showing the least deviation from model predictions and LWD-rich pool-riffle channels the most. Median values of textural response distributions reveal that roughness caused by bedforms and minimal LWD result in a two-and-half-fold decrease in D_{50s} relative to model predictions, while pool-riffle channels with abundant LWD exhibit a four-and-a-half-fold decrease.

In the channels studied, non-catastrophic levels of sediment loading are apparently subordinate to the controls on surface texture caused by bedform and LWD roughness. Although there is the potential for severe sediment impacts (and hence sediment-induced textural fining) in the study areas, such occurrences tend to be infrequent pulsed events compared to the pervasive influence of stable bedforms and LWD. Consequently, bedforms and LWD provide long term influences that dominate surface textures of the study sites, while sediment supply effects are either relatively less significant or transient.

Coupled with subsurface grain size sampling, the bankfull-threshold model allows evaluation of the degree of textural fining within theoretical grain size limits and is proposed as a management tool for assessing channel textural-response condition. Naturally large degrees of textural fining in LWD-rich pool-riffle channels generally correspond with small capacities for further surface fining. The bankfull-threshold model and empirically determined response ranges also offer an opportunity to examine geomorphic controls on the availability of salmonid spawning gravels. Textural fining due to sediment supply and hydraulic roughness elements significantly increases spawning habitat availability.

TABLE OF CONTENTS

LIST OF FIGURES

LIST OF MAPS

LIST OF TABLES

ACKNOWLEDGMENTS

The initial impetus for this work and the development of an assessment technique combining q* with a threshold channel model was provided by Bill Dietrich and originally presented as part of the proposal for the Geomorphological Watershed Analysis Project (Dunne et al., 1991).

A tremendous amount of work went into collecting field data and processing gravel samples in the lab, and I am indebted to all those who provided muscle, thoughtful comments, patience, and encouragement: my wife Mélanie, Jennette deLeeuw, Heidi Fassnacht, Lisa Hackney, Kirt Hansen, Tammy Lealand, Tamara Massong, Kevin Schmidt, Rick Smith, Todd Stubbs, and Carolyn Trayler. Many valuable comments and criticisms at various stages of this work were provided by Derek Booth, Bill Dietrich, Tom Dunne, Jim Kirchner, Tom Lisle, Gerry Middleton, Dave Montgomery, Ron Shreve, Rick Smith, and Kelin Whipple. Financial support was provided by the Sediment, Hydrology, and Mass Wasting Committee of the Washington State Timber, Fish & Wildlife agreement and by the Pacific Northwest Research Station of the USDA Forest Service, Juneau. ITT Rayonier Corporation graciously provided access to their land on the Olympic Peninsula. My wife Mélanie provided much love and encouragement.

INTRODUCTION

A rising environmental consciousness coupled with an acceleration in the rate of land development and timber harvesting in North America have created a need for a better understanding of physical and biologic processes in watersheds. River channels integrate the effect of watershed processes, and as such provide an expression of basin condition. Thus a better understanding of river processes is of particular importance for both interpreting watershed condition and assessing potential land use impacts to human and animal uses of a watershed.

Successful development and application of any form of channel assessment requires a process-based understanding of fluvial systems. State and federal agencies are developing process-based watershed analysis programs (FEMAT, 1993; WFPB, 1993; USDA, 1994) and are currently investigating some of the available channel assessment techniques [see review in Montgomery and Buffington (1993)]. Bed surface textures are an important characteristic of rivers, and several assessment methods rely on textural analysis as an indicator of channel processes and condition (e.g., Dietrich et al., 1989; Lisle and Hilton, 1992; Kappesser, 1993).

Based on the premise that surface textures are responsive to and indicative of shear stress, sediment supply, and the presence of other roughness elements, I propose and investigate the use of a simple threshold-channel model that allows prediction of surface grain size from bankfull shear stress and provides a theoretical reference point from which to analyze textural response to sediment supply and hydraulic roughness. Textural response to sediment supply has been documented by several researchers (i.e., Dietrich et al., 1989), however response to hydraulic roughness, particularly in forest environments, has not been well studied. Textural response to both sediment supply and other hydraulic roughness is examined within the model framework through analysis of published data, as

well as through a field investigation that documents surface texture characteristics in gravel-bedded channels exemplifying different scales and complexity of roughness.

Implications of this work have several direct applications to land management concerns. A better understanding of 1) the factors that control streambed textures and 2) the characteristic ranges of textural response to these factors will aid assessment of channel condition and prediction of channel response to natural and anthropogenic disturbances. Combined with subsurface grain size measurements, the bankfull-threshold model is proposed as a management tool for evaluating both the general textural-response condition of a channel and its capacity for further response; use of the bankfull-threshold model in this fashion is essentially an extension of the q* technique (Dietrich et al., 1989) for assessing the sediment supply of a channel relative to its transport capacity. Finally, empirical findings of the current study are used to examine the geomorphic controls on availability of salmonid spawning habitat.

Chapter 1: The Bankfull Threshold Model

THRESHOLD CHANNEL CONCEPT

It is commonly observed that there are differences between sediment transport characteristics and bedform stability in fine-grained and coarse-grained channels. Fine-grained channels transport sediment at almost all stages and adjust their bed morphology to changing hydraulic regimes, whereas coarse-grained channels exhibit relatively stable bedforms and generally transport significant amounts of sediment only beyond some critical discharge. Thus there is a basic dichotomy between what are termed "live-bed" and "threshold" channels (Henderson, 1966; Parker 1978a; b; Howard, 1980). Live-bed streams have also been termed "regime" channels (Henderson, 1961; Howard, 1980), although, Inglis (1961) warns against such usage, as it befuddles Lindley's (1919) concept of "in regime". A channel is said to be "in regime" when it exhibits a stable morphologic state for the imposed sediment supply and hydraulic discharge (Lacey, 1961); as such, the regime concept can be applied to any alluvial channel type.

The term "threshold channel" was coined by Henderson (1963) and refers to Lane's (1953; 1955) examination of engineering designs aimed at producing "stable channels" in coarse alluvium. A stable channel was defined by Lane (1953) as an ". . . earth channel for carrying water, the banks and bed of which are not scoured by the moving water, and in which objectionable deposits of sediment do not occur." The point of this design is to engineer a channel which will neither degrade through scour nor be incompetent to carry the imposed sediment load, which would otherwise lead to deposition and aggradation within the channel. Lane proposed that an analysis of tractive forces could be used to determine the minimum bed material size that would be stable for a given channel geometry, slope, and discharge. As Henderson (1963) later points out, Lane's analysis

examines bed material at the "threshold" of mobility for given hydraulic geometry conditions.

Henderson (1963) examined differences in hydraulic geometry relations between threshold and live-bed channels and used Lane's tractive force model to approximate sediment mobility conditions in natural coarse-grained channels. Henderson reasoned that the threshold for mobility in coarse-grained channels was that of the dominant or channel-forming discharge, which based on considerations of channel morphology was interpreted to be the bankfull flow (Wolman and Leopold, 1957). However, it is not readily obvious that bankfull stage, as opposed to some other moderate discharge, is the threshold stage for grain mobilization. For example, live-bed channels also have a characteristic bankfull morphology, yet these channels do not exhibit a bankfull threshold for grain mobility. Nevertheless, it does seem reasonable that the critical grain-mobilizing stage for coarse-grained channels should lie somewhere within the limits of moderate to bankfull flow; this follows both from observation of little to no transport at low flows and from recognition that channels with well-developed floodplain morphology limit the effectiveness of flows beyond the bankfull stage (Henderson, 1963; Leopold et al., 1964; Andrews and Erman, 1986). While arguments for using bankfull stage to characterize channel- and bed-forming conditions are intuitively attractive (e.g., Wolman and Leopold, 1957; Henderson, 1963; Li et al., 1976), it remains to justify them. As such, I will briefly summarize some of the pertinent literature in order to examine the validity and limits of bankfull threshold representation of sediment transport in coarse-grained channels.

A further complicating issue not discussed above is the assertion by some investigators that sediment transport in heterogeneous coarse-grained channels is characterized by stage-dependent selective transport (Gilbert, 1914; Day, 1976; Little and Mayer, 1976; Proffit, 1980; Komar, 1987a; b; Rakoczi, 1987; Komar and Li, 1988; Wilcock and McArdell, 1993) rather than by threshold mobility at a single stage. Selective

transport is an important process and does occur in gravel-bedded channels due to effects of grain hiding (relative protrusion), imbrication, and friction angle distributions (a function of grain size, packing, and sorting) (Li and Komar, 1986; Kirchner et al., 1990; and Buffington et al., 1992). Selective transport must indeed occur to produce armored bed surfaces that are typical of most gravel-bedded streams. However, bed armoring is due to selective removal of the most easily mobilized grains (i.e., those of small size with high protrusion and low friction angle) leaving behind a more stabile, armored bed surface that inhibits further significant grain transport, protecting the underlying, finer subsurface material (Milhous, 1973). Significant bedload transport occurs with the breaching of the armor surface, which as will be demonstrated below is typically a bankfull-threshold phenomenon. Consequently, *to a first approximation* sediment transport in coarse-bedded rivers can be considered bankfull threshold. This viewpoint is reinforced in the following literature review.

EVIDENCE OF BANKFULL THRESHOLD MOBILITY

Wolman and Miller (1960) examined the frequency and magnitude of geomorphic forces and proposed that both the effective discharge, that which accomplishes the most work of sediment transport, and the channel-forming discharge are equivalent frequent occurrences characterized by the bankfull flow [see also Wolman and Leopold (1957)]. In a subsequent study Andrews (1980) substantiated Wolman and Miller's concept of effective discharge and correlated it with near-bankfull stages. Although these studies demonstrate that bankfull stage is identified with both the channel-forming and sediment-transporting flows, it is not clear that bankfull is the threshold discharge for incipient motion.

Carling (1988) examined effective discharges and entrainment thresholds in two gravel-bedded channels. Over a six year period the effective discharges for the two channels were on average 94% and 100% bankfull respectively, further substantiating Wolman and Miller's (1960) findings. Furthermore, Carling observed three phases of grain mobility: phase 1 transport (discharge ≤ 60% bankfull) characterized movement of fine material (< 4 mm) winnowed from the coarser framework (armor); phase 2 transport (>60% bankfull) represented threshold mobility of the coarse surface layer and entrainment of small framework gravels, but without significant exposure of subsurface material; and phase 3 transport (>130% bankfull) characterized extreme mobility of the coarse surface layer, significant scour, and the potential for major morphologic change. Discharges that significantly modified the coarse surface layer averaged 75% and 94% bankfull in the two study sites (Carling, 1987). These observations demonstrate the threshold nature (> 60% bankfull) of mobility of the coarse surface layer. Furthermore, while the mobilization of the coarse surface layer occurs over a range of discharges (60-130% bankfull), the bankfull stage can be considered a first-order approximation of the threshold discharge for significant bed mobility in these channels. Carling (1988) argues that the near-bankfull flow is dominant in terms of transporting bedload and maintaining channel form, while the catastrophic phase 3 transport is responsible for major but infrequent channel changes; similar ideas were expressed by Wolman and Miller (1960). Carling also presents evidence suggesting that the equivalence of sediment-transporting and channel-forming flows occurs only for channels that have achieved steady-state conditions [see also Richards (1982)].

Other investigators have also noted phases of bedload transport (Bathurst, 1987b) and a near-bankfull flow threshold for significant grain mobility in coarse-bedded channels. In a study of bedload transport in an armored gravel-bedded stream in coastal Oregon Milhous (1973) reported that "bed material is essentially stable during all but the highest flows." He observed that at low flows only exposed sand-sized material was transported,

while above a critical discharge of about 40 cfs the armor layer mobilized, exposing finer substrate and rapidly increasing both the rate of bedload transport and the size of bedload material [see also Parker et al. (1982a)]. Furthermore, he suggested that the armor layer effectively limits the availability of fines below this critical stage. Milhous estimated that 98% of the sediment transport occurs during flows in excess of 40 cfs. On a duration curve these flows occur about 3% of the time each year, which is within the range of other reported bankfull durations (Andrews, 1980; 1984). Milhous' observations exemplify bankfull threshold conditions.

In a separate study of another coastal Oregon stream Jackson and Beschta (1982) noted two similar grain mobility thresholds. Phase I transport is characterized by low-flow movement of sand-sized material over a stable armor, and Phase II transport, occurring at 108% bankfull, represents high-flow mobilization of the armor surface and a rapid rise in bedload transport. Again, demonstrating a near-bankfull threshold for significant mobility. In this case, transport rates continued to increase beyond the bankfull threshold, presumably because of channel confinement. Many other researchers also report rapid increases in bedload size and transport rate associated with high-flow mobilization of bed armor (Emmett, 1984; Ashida, 1981; Gomez, 1983; Sawada et al., 1983; Sidle, 1988; Ashworth and Ferguson, 1989; Warburton, 1992), emphasizing the characteristic quality of threshold mobility in coarse-bedded channels.

In contrast to the above investigations, Reid et al. (1985) found no clear relation between stage and bedload movement in a study of Turkey Brook, a gravel-bedded channel in England. They argue that bedload transport in Turkey Brook is a function of both kinematic wave phenomena (Langbein and Leopold, 1968) and the degree of bed "conditioning" by antecedent flow events. Conditioning refers to the packing, imbrication, and degree of armoring as controlled by the preceding discharge history (magnitude, frequency, duration, and chronologic order of events) and seasonal sediment inputs

(Nanson, 1974; Milhous, 1973; Griffiths, 1980; Jackson and Beschta, 1982; Campbell and Sidle, 1985; Bathurst, 1987b; Sidle, 1988). However, Reid et al. (1985) report significant transport during most flows observed, even though the largest flow attains a depth of only 70% bankfull, and the average recorded flood depth for all storms presented is less than 40% bankfull; significant bedload transport under these flow conditions is suggestive of live-bed transport. It is my opinion that the high transport rates that accompany these low flows are the result of high sediment loading. Dietrich et al. (1989) suggested that the closer the surface and subsurface median grain sizes (D_{50s} and D_{50ss}) are to one another, the higher the sediment loading. D_{50s} and D_{50ss} in Turkey Brook are 22 and 16 mm respectively, indicating only weak armoring and suggesting a fairly high sediment supply relative to transport capacity. In general, streams with high sediment loading typically behave more like live-bed channels than threshold channels, and Turkey Brook appears to demonstrate this.

Studies of Bambi Creek in southeast Alaska show an exponential transport-discharge relation, but do not clearly document a bankfull threshold of bed mobility (Campbell and Sidle, 1985; Sidle, 1988; Smith et al., 1993). The channel is armored and it is observed that fine (< 1 mm) material moves more frequently than coarse (> 8 mm) material (Sidle, 1988), suggesting that the coarse surface layer functions similarly to other armored channels and limits the availability of fine material below armor-mobilizing thresholds. However, Bambi Creek exhibits extreme variability in transport rates between and within storms and it is unclear if there is a single threshold for mobilization of the coarse surface layer. Transport variability is attributed to bed conditioning by antecedent flow events and to capacitance of morphologic sediment storage sites (pools and woody debris-buttressed reservoirs) (Sidle, 1988).

A variety of other studies also provide information regarding the threshold nature of sediment transport in coarse-grained channels. Leopold et al. (1964) observed that over a

seven year period in Seneca Creek transport of bar-forming material occurs at discharges near bankfull stage; sand-sized material is virtually immobile at or below mean flow heights. Andrews (1983; 1984) calculated that in twenty-four Colorado rivers the threshold for grain mobility occurs at stages "slightly less than bankfull." Based on the predicted and calculated critical dimensionless shear stress values presented by Andrews (1984) I calculate that on average grain mobility occurs at stages that are approximately 70% bankfull. Similar calculations for Sagehen Creek in northern California indicate a mobility threshold of 93% bankfull (Andrews and Erman, 1986). Using data from Lane and Carlson (1953), Kellerhals (1967) found a clear relation between observed D_{50s} and the boundary shear stress associated with the "maximum sustained discharge" [i.e., bankfull discharge (Andrews, 1984)]. In a tracer study of a coarse-grained river in northern California, Helley (1969) determined that the critical mobilizing stage occurs 5% of the time (based on mean monthly discharge records). Although 5% is a frequent event, it is well within the range of typical bankfull durations (0.12-6.0%) reported by Andrews (1984).

The weight of evidence in the literature summary presented above indicates that to a first approximation coarse-grained channels are bankfull threshold. This conclusion will be used in the model formulation presented in the next section. However, it is recognized that a bankfull threshold theory is only a useful approximation of the complex nature of bed mobility in coarse-grained channels.

BANKFULL THRESHOLD MODEL

A major premise of this study is that bed surface textures are responsive to, and thus indicative of, shear stress, sediment supply, and the presence of other hydraulic roughness elements within a channel. Consequently surface textures can be used as

indicators of channel condition with respect to these factors, provided that the potential range of textural response to each factor is known and that the process-driven mechanics of textural response are understood.

Calculation of flow competence from surface grain sizes is a classic use of textures as indicators of current or past fluvial conditions. Equations of flow competence are commonly used to predict the critical mobilizing shear stress for a given grain size of interest (Helley, 1969; Baker and Ritter, 1975; Church, 1978; Bradley and Mears, 1980). In contrast, the bankfull threshold model utilized here predicts grain size based on the hypothesis that the bankfull boundary shear stress provides the critical tractive force for general incipient motion of the bed. By adopting a simplistic prediction of grain size the model provides a theoretical reference point from which to analyze textural response to sediment supply and hydraulic roughness elements other than bed surface grains. Textural response within the bankfull threshold model framework can be quantified by the magnitude of deviation from the theoretical grain size prediction. Recognition and quantification of textural response caused by a specific process provides valuable channel assessment information. Derivation of the model and textural response hypotheses are examined in the remainder of this chapter.

In the absence of other influences the critical grain-mobilizing shear stress, τ_c, in a bankfull threshold channel can be characterized by the mean total bankfull boundary shear stress, τ_0

$$\tau_0 = \tau_c = \rho g h S \qquad (1)$$

where ρ is the fluid density, g is the gravitational acceleration, h is the average bankfull flow depth, and S is the energy slope. The above expression for total boundary shear stress assumes steady incompressible flow, but can be used to describe either uniform or

non-uniform flow (Henderson, 1966). Equation (1) is a time-averaged representation of the channel shear stress, best applied on a reach scale.

At the bankfull threshold there is general mobilization of most size fractions on the bed. The phenomenon of general motion is attributed to the effects of both armoring and physical interactions of heterogeneous grains. Mobilization of armor particles releases finer material trapped under and around the coarser armor grains, resulting in a sudden entrainment of numerous sizes and giving rise to the observation of general motion (Fig. 1.1). In addition, because of grain interactions caused by the natural heterogeneity of bed surface material, the coarse surface layer tends to exhibit equal grain mobility (Parker and Klingeman, 1982), at least initially (Buffington et al., 1992), resulting in general motion of the bed at a common threshold shear stress. Grain interactions caused by the size, sorting, shape, and packing of bed material control physical features of the bed, such as friction angles and grain protrusion (Fig. 1.2), which dictate relative entrainment thresholds for bed surface grains (Fenton and Abbott, 1977; Kirchner et al., 1990). Friction angles cause bed surfaces to be relatively rougher for small grains and smoother for large grains (Fig. 1.2), resulting in an initial near-equal mobility of bed surface material at a common critical shear stress. However, the bed is rarely mobilized *en masse*, and due to friction angle controls strict equal mobility may only occur for the first 1-10% of mobilized grains, after which selective transport may become increasingly important (Kirchner et al., 1990; Buffington et al., 1992). Nevertheless, bed mobility as indicated by friction angle distributions corroborates observations that beyond threshold conditions there is a general and significant mobility of grains, as evidenced by the well-known rapid rise in bedload transport.

Due to the grain interactions discussed above, mobility of the median surface grain size, D_{50s}, will be used in this analysis to approximate incipient motion of the bed as a

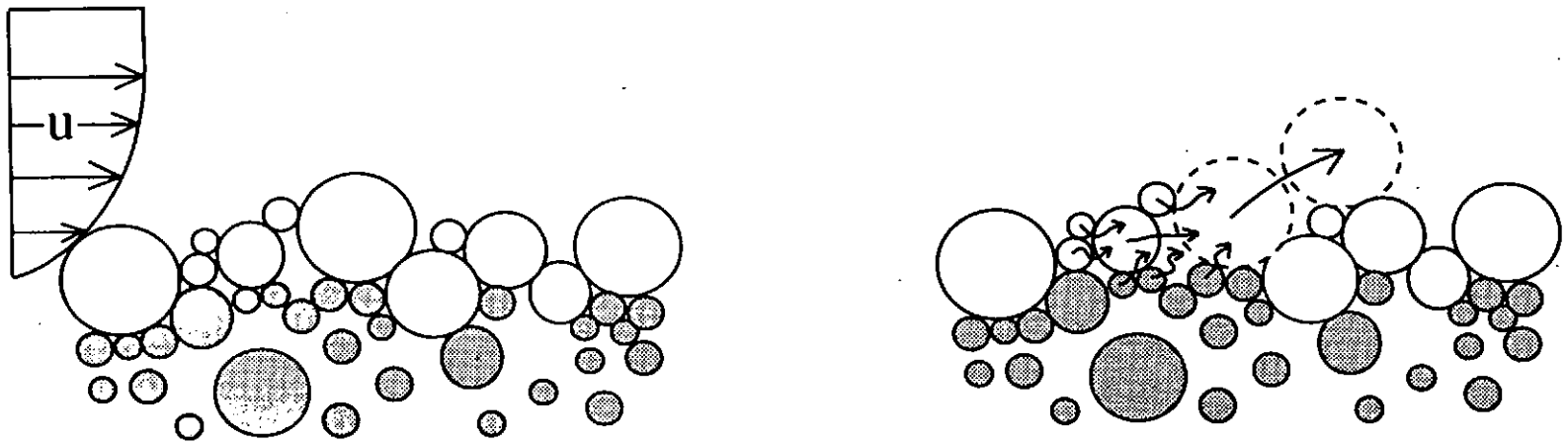

Figure 1.1 Movement of an armor particle releases finer material trapped under and behind the grain, resulting in the sudden entrainment of numerous grain sizes at a common shear stress.

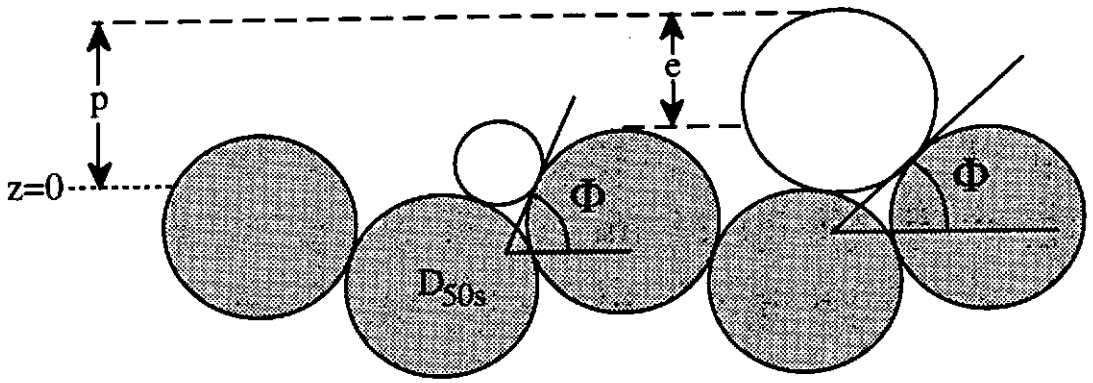

Figure 1.2 Friction angle, Φ, and relative grain protrusion, p-e, for two different grain sizes on a uniform streambed surface. Larger grains typically have lower friction angles and protrude higher into the flow than smaller grains, resulting in an initial near-equal mobility of different grain sizes at a common critical shear stress (Kirchner, 1990; Buffington et al., 1992).

whole. The median surface grain size can be related to its critical boundary shear stress, τ_{c50s}, through Shields' (1936) expression for dimensionless critical shear stress

$$\tau^*_{c50s} = \left(\frac{\tau_{c50s}}{(\rho_s - \rho)\, g D_{50s}} \right) \tag{2}$$

where τ^*_{c50s} is the dimensionless critical shear stress for D_{50s} and ρ_s is the sediment density. For a bankfull threshold of mobility, τ_{c50s} must equal the bankfull boundary shear stress. Thus combining (1) and (2) produces the simple bankfull threshold model enabling D_{50s} to be theoretically predicted from bankfull depth and slope

$$D_{50s} \approx 0.61 hS/\tau^*_{c50s} \tag{3}$$

Here ρ and ρ_s are 1000 and 2650 kg/m^3 respectively and τ^*_{c50s} is a constant that will be evaluated later in the chapter.

Past investigations of the threshold channel concept have considered the entire channel, including the sidewalls, to be composed of loose alluvium at the threshold of motion and as such have discussed sidewall equations of motion (Lane, 1953; 1954; Lane and Carlson, 1953; Parker, 1978b). In this regard Parker (1978b) has commented on the apparent paradox of cross-section stability in threshold channels, in that beyond the threshold of motion active bedload transport occurs, yet the inherently more mobile sidewall grains remain stable. Parker (1978b) argues that outward turbulent momentum flux between the channel center and walls (i.e., sidewall effects) stabilizes sidewall grains that would otherwise tend to move down the bank toward the channel center. While sidewall effects will be accounted for in the current analysis, mobility of bank material as

conceptualized in past threshold channel studies is of little significance here, as most of the channels examined in the current study are forest streams with cohesive soil banks reinforced by shrub and tree roots.

The bankfull threshold model assumes that all channel roughness can be attributed to particle roughness, as indicated by the scaling of τ_{c50s} by D_{50s} in (2). While this is a common assumption for gravel-bedded rivers, it is usually an oversimplification. Other sorts of in-channel roughness are typically present, such as bedforms and large woody debris (LWD). Nevertheless, because (3) neglects these other roughness features, their effects can be investigated by examination of textural deviation from the simple model prediction. It is hypothesized that the presence of in-channel roughness elements other than grain roughness will cause increased momentum extraction resulting in reduced basal shear stress. Consequently, momentum extraction will be reflected by surface textures that are finer than the model prediction. In this analysis investigation of textural response to hydraulic roughness features will be limited primarily to effects caused by bedform and LWD roughness typical of forest channels. Wall effects will also be quantified, but roughness elements other than LWD and bedforms will only be given qualitative consideration.

Multiple scales of roughness are commonly accounted for through roughness or shear stress partitioning, which is predicated on the hypothesis that the total channel roughness and shear stress can be decomposed into linearly additive components each characterizing a particular roughness element (Einstein and Barbarossa, 1952; Engelund, 1966; Johnson, 1973; Smith and McLean, 1977; Hey, 1979; Parker and Peterson, 1980; Prestegaard, 1983; Dietrich et al., 1984 ; Hey, 1988; Griffiths, 1989; Nelson and Smith, 1989b; Wiberg and Smith, 1989; Petit, 1989; 1990; Robert, 1990; Clifford et al., 1992; Yalin, 1992; Li, 1994; Milar and Quick, 1994). The relevant shear stress partitioning equation for the current investigation is

$$\tau_0 = \tau_g + \tau_w + \tau_f + \tau_l \quad (4)$$

where the total bankfull boundary shear stress is partitioned into components expended on grains, τ_g, sidewalls, τ_w, bedforms, τ_f, and LWD, τ_l. Other components could also be included, representing shear stress dissipation caused by, for example, channel curvature, saltating grains, and live in-channel vegetation. The effective shear stress, τ', is the shear stress that is available for sediment transport after correction for roughness features other than grain roughness, and is defined here as

$$\tau' = \tau_0 - \tau_w - \tau_f - \tau_l \quad (5)$$

In the case of a bankfull threshold channel, $\tau'=\tau_g$. Bankfull threshold channels that are only characterized by τ_g have a plane-bed morphology similar to the coarse-grained canals studied by Lane (1953; 1955) and Lane and Carlson (1953). As such, (3) predicts the median surface grain size of a wide, straight, bankfull threshold, plane-bed channel.

Sidewalls, bedforms, and LWD each dissipate channel shear stress in different ways. Sidewall effects are particularly influential in narrow channels ($W/h \leq 10$), causing turbulence due to momentum differences between the channel center and margins, effectively transferring a portion of the total boundary shear stress to the channel walls and reducing that over the channel bed (Parker, 1978b). The shear stress dissipated by channel walls additionally depends on the relative magnitude of bed and wall roughness length scales (Shimizu, 1989). Bedforms dissipate shear stress through simple form drag that is a function of bedform amplitude and wavelength (Smith and McLean, 1977; Nelson and Smith, 1989b). Woody debris roughness is a function of its amount, size, pitch, and orientation with respect to the flow. Mechanics of flow perturbance caused by LWD that

result in momentum extraction and consequent textural fining include: flow deceleration caused by woody debris skin roughness; form drag and turbulent energy dissipation around LWD obstructions; hydraulic jumps over woody debris steps; and general decline in water surface slope, and thus energy gradient, due to physical blockage of flow and back-water effects caused by LWD obstructions. It is hypothesized, through analogy with flow mechanics in meandering rivers (i.e., Furbish, 1991), that LWD roughness and its effects are locally intensive and progressively damped downstream away from a given obstruction.

In addition to hydraulic roughness features, the model prediction of grain size does not take into account effects of sediment supply. Dietrich et al. (1989) demonstrated that surface textures of laboratory plane-bed channels are responsive to sediment load (i.e., volume), fining when inundated with sediment, and coarsening when deprived. When deprived of sediment, small grains are selectively winnowed from exposed or low friction angle locations, ultimately resulting in an armored surface that is coarser and hydraulically rougher, compensating for any previous excess shear stress. In contrast, rough bed-surfaces that are inundated with sediment tend to trap smaller grains in sheltered or high friction angle locations, causing an overall surface fining and reduction in bed roughness that results in increased mobility of both material on and passing over the bed surface (see also Whiting et al., 1988); thus by decreasing surface roughness, textural fining allows increased sediment loads to be accommodated without significant bed aggradation (Dietrich et al., 1989).

Based on the findings of Dietrich et al. (1989), it is expected that within the threshold model framework textural fining in response to increased sediment loads will be expressed as a deviation from the predicted surface grain size. Furthermore, combining the bankfull threshold model with the dimensionless bedload transport rate, q*, proposed by Dietrich et al. (1989) allows quantification of the degree of sediment loading. Dietrich et al.

(1989) defined q* as the bedload transport rate of the surface material normalized by that of the load, where grain sizes of the load are approximated by the subsurface distribution (Milhous, 1973; Kuhnle, 1993)

$$q^* = \left(\frac{\tau_0 - \tau_{c50s}}{\tau_0 - \tau_{c50ss}}\right)^{1.5} = \left(\frac{\frac{\tau_0}{\tau_{c50ss}} - \frac{D_{50s}}{D_{50ss}}}{\frac{\tau_0}{\tau_{c50ss}} - 1}\right)^{1.5} \quad (6)$$

Commensurate with the discussion preceding (2), the q* formulation assumes that general mobility of heterogeneous material can be approximated by mobility of the median grain size and so employs τ_{c50s} and τ_{c50ss} (Dietrich et al., 1989; Kinerson, 1990). The dimensionless bedload transport rate is essentially a sediment transport efficiency equation, ranging from 0 for armored, low sediment supply channels to 1 for unarmored channels with high sediment loading (Dietrich et al., 1989). A q* of 0 indicates low sediment transport efficiency, while a q* of 1 indicates maximum transporting efficiency.

The theoretical limits of textural response to changes in sediment supply can be determined by comparing the bankfull threshold model with (6). The threshold model assumes that τ_0 is equal to τ_{c50s}, which in terms of (6) corresponds to a q* of 0. Thus, the bankfull threshold model represents armored conditions and the coarse limit of textural response described by q*. The opposite extreme is a q* of 1, which occurs when surface fining approaches the subsurface median grain size. Maximum transporting capacity and equilibrium conditions between bed surface and bedload occur at q* values of 1. Under these later conditions, increases in bedload supply can only be accommodated by deposition. Consequently, D_{50ss} is the theoretical limit of sediment-induced textural fining. Examination of textural response within the grain size limits of D_{50s} and D_{50ss} provides a means to quantify the degree of sediment loading within a channel. Although developed

from studies of plane-bed channels, the q* theory is applicable to other channel types provided that roughness effects are accounted for.

Threshold model predictions of median surface grain size and hypothesized textural responses to both sediment supply and in-channel roughness features are shown schematically in Figure 1.3. The bankfull threshold prediction of surface grain size corresponds to a plane-bed morphology with $q^*=0$ (i.e., low sediment supply and fully armored streambed). The subsurface median grain size is the limit of sediment-induced textural fining ($q^*=1$), but unfortunately cannot be predicted theoretically and must be determined by field investigation, as discussed further in the next chapter. Expression of these textural limits within the bankfull threshold model is simply another way to visualize the q* theory. However, the threshold model has the further advantage of providing a means to assess textural response caused by hydraulic roughness elements.

DIMENSIONLESS CRITICAL SHEAR STRESS

Application of the threshold channel model and investigation of the preceding hypotheses requires choice of an appropriate dimensionless critical shear stress value for the median surface grain size, τ^*_{c50s}, for use in (3). Shields (1936) demonstrated that τ^*_{c50} of near-uniform grains varies with critical boundary Reynolds Number, Re^*_c, from $1.8 \leq Re^*_c \leq 490$ and hypothesized based on analogy with Nikuradse's (1933) findings that τ^*_{c50} attains a constant value of about 0.06 beyond $Re^*_c \approx 490$ (Fig. 1.4). The critical boundary Reynolds Number is defined as $Re^*_c = u^*_c k_s / \nu$, where u^*_c is the critical shear velocity for incipient motion [$u^*_c = (\tau_c/\rho)^{0.5}$], k_s is the boundary roughness length scale, and ν is the kinematic viscosity. While Shields' (1936) boundary Reynolds Numbers are not the same as Nikuradse's (1933), the general form of Shields' (1936) curve (Fig. 1.4) is quite similar to Nikuradse's (1933), indicating regions of hydraulically smooth,

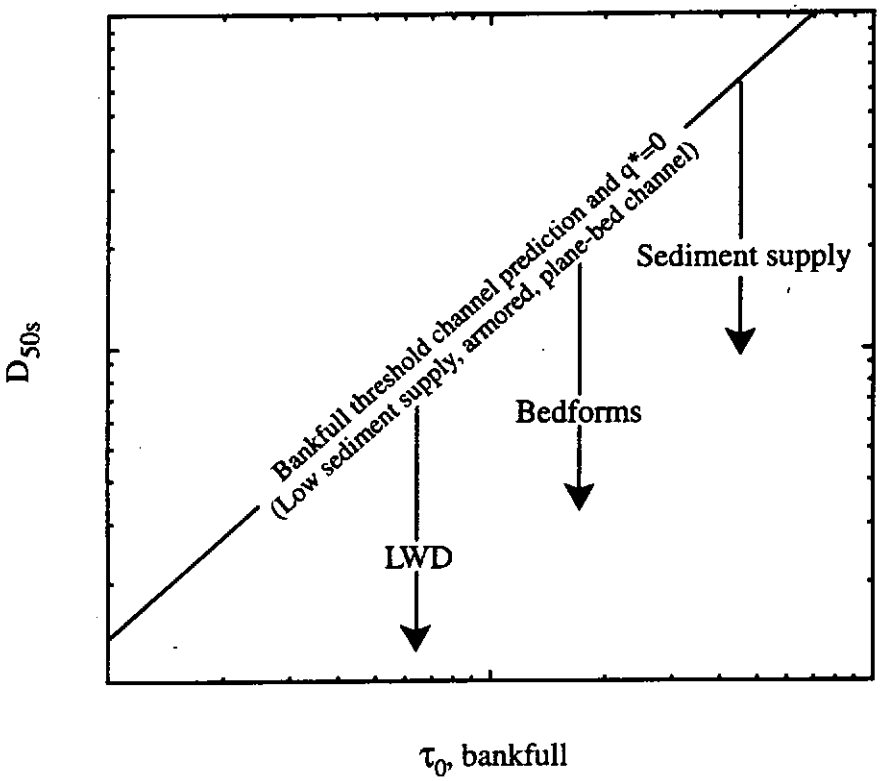

Figure 1.3 Schematic representation of the bankfull threshold model prediction of median surface grain size and hypothesized textural response to sediment supply and other hydraulic roughness elements.

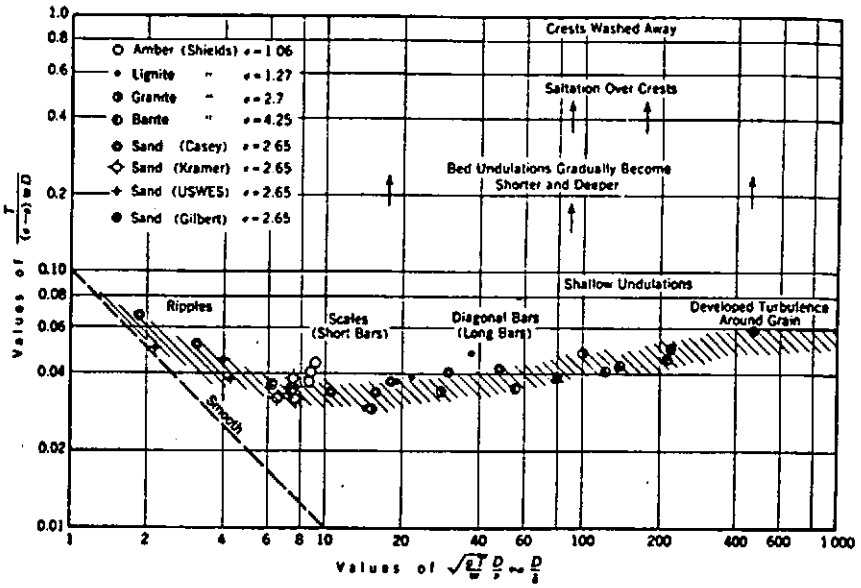

Figure 1.4 Shields' (1936) curve as presented by Rouse in Chang (1939).

transitional, and rough turbulent flow. Because bedload transport in most gravel-bedded streams is characterized by rough turbulent flow, the appropriate τ^*_{c50} value based on the Shields curve would be 0.06 for the current study. However, there have been numerous additions, revisions, and modifications of the Shields curve over the years, complicating the choice of τ^*_{c50}.

Gessler (1971) recognized that the incipient motion of a particular grain size is inherently a statistical problem, depending on probability functions of both turbulent shear stress at the bed and intergranular geometry (i.e., friction angles) of the bed material, the later being controlled by grain shape, sorting, and packing (Miller and Byrne, 1966; Li and Komar, 1986; Kirchner et al., 1990; Buffington et al., 1992). Re-analyzing Shields' (1936) data and correcting for sidewall effects and form drag, Gessler (1971) reports $\tau^*_{c50} \approx 0.046$ for a 50% probability of movement in rough turbulent flow. Without consideration of the probability of movement Miller et al. (1977) arrived at a similar rough turbulent-flow value, $\tau^*_{c50} \approx 0.045$, using compiled flume data from various sources. Miller et al. (1977) claim to have used "carefully selected data" to maximize the compatibility of their compiled data sources and avoid an otherwise "unmanageable amount of scatter." They only employed data that were derived from experiments using "flumes with parallel sidewalls where flows were uniform and steady over flattened beds of unigranular, rounded sediments"; sidewall corrections were applied and each source used a consistent definition of incipient motion. However, closer scrutiny of their compiled data shows that it is based on both uniform and non-uniform sediment mixtures, differing incipient motion definitions between studies, and in some cases bedload transport rates influenced by the presence of dune-ripple bedforms. Consequently, their data is much less controlled then a casual reading of their article would indicate.

Using a larger data set without any concern for differences in sediment characteristics, channel roughness, or definition of incipient motion, Yalin and Karahan

(1979, Fig. 5) also report τ^*_{c50}≈0.045 for rough turbulent flow. They further demonstrate the existence of a second "Shields curve" for fully laminar flow, which for the same Re^*_c values behaves differently than the traditional Shields curve (derived from turbulent flow with variable hydrodynamic boundary roughness). The τ^*_{c50} values reported by Miller et al. (1977) and Yalin and Karahan (1979) are based on curves fit by eye through data sets with considerable scatter; in both studies τ^*_{c50} for rough turbulent flow has a range of about 0.02-0.065.

While the compilation studies of Miller et al. (1977) and Yalin and Karahan (1979) are fairly consistent with one another in their findings, they unfortunately combine data sets derived from quite different experimental conditions and methodologies without any assessment of compatibility. This casts some doubt on the veracity of such compilations. Continued proliferation of incipient motion studies using new definitions of initial motion further complicates comparison and understanding of published studies. Miller and others' (1977) quote of Mark Twain is even more appropriate today: "Researchers have already cast much darkness on the subject, and if they continue their investigations we shall soon know nothing at all about it."

In an attempt to make some sense of previous findings I have compiled all available τ^*_{c50} values, categorizing them on the basis of τ^*_{c50} type and incipient motion definition (Table 1.1). By τ^*_{c50} type I mean that τ^*_{c50} values have been variously reported for the median grain size of the surface, D_{50s}, subsurface, D_{50ss}, and laboratory sediment mixture, D_{50m}, the three of which are equal only for uniform grain sizes; corresponding dimensionless critical shear stress types are denoted here as τ^*_{c50s}, τ^*_{c50ss}, and τ^*_{c50m}. Expression of dimensionless critical shear stress in terms of the subsurface grain size distribution was popularized by Andrews (1982) who expressed the Shields stress of a given grain size of interest, $\tau^*_{c_i}$, as a power-law function of the ratio D_i/D_{50ss}; Andrews (1982) found that for his data, D_i/D_{50ss} was better correlated with $\tau^*_{c_i}$ than was D_i/D_{50s}

(r^2=0.98 vs. 0.89). Unfortunately the Andrews (1982) expression introduced great confusion to the incipient motion literature in that some investigators subsequently used mobility thresholds of subsurface material in discussions of incipient motion of the bed *surface* (Parker et al., 1982; Parker and Klingeman, 1982; Komar, 1987a; Wilcock and Southard, 1988; Komar and Carling, 1991). It is well known that most gravel-bedded rivers are armored and that the surface and subsurface grain size distributions can be significantly different from one another (Milhous, 1973). It seems fundamentally intuitive then that any analysis of incipient motion of the bed *surface* should employ surface parameters (D_{50s}, τ^*_{c50s}, τ^*_{c50s}, etc.) rather than subsurface ones (D_{50ss}, τ^*_{c50ss}, τ^*_{c50ss}, etc.). Furthermore, poor recognition of the difference between τ^*_{c50ss} and τ^*_{c50s} by authors and subsequent users of data has in some instances led to erroneous applications. For example, using a power-law function for dimensionless critical shear stress, $\tau^*_{ci}=\alpha(D_i/D_{50})^{\beta}$, Komar (1987a) reported that $\alpha\approx0.045$ for natural coarse-grained channels, but did not clearly specify that $D_{50}\equiv D_{50ss}$ and thus $\alpha=\tau^*_{c50ss}$ (Appendix I, note 6); the corresponding unreported τ^*_{c50s} value is about 0.021-0.027 (Table 1.1). Mistakenly assuming that Komar (1987a) reported τ^*_{c50s}, Dietrich et al. (1989) erroneously used $\alpha=\tau^*_{c50ss}$ to calculate surface critical shear stresses from the Shields equation.

Each τ^*_{c50} type given in Table 1.1 is subdivided by the method used to measure incipient motion. The three most widely used methods are: 1) visual observation; 2) bedload sampling and extrapolation of transport rates to either a zero or low reference value; and 3) bedload sampling and development of competence functions. Visual observation is direct, but can be subjective depending on one's definition of how much movement constitutes "initial motion" (e.g., Kramer, 1935; USWES, 1935). Dimensionless critical shear stress values of the median surface grain size determined by extrapolation of transport rates depend on the particular reference value that is chosen

TABLE 1.1: Previously Reported $\tau^*_{c_{50}}$ Values

Source[£]	$\tau^*_{c_{50s}}$	Proposed τ^*_c Function Other than the Shields Equation[†]	D_{50s} (mm)	Re^*_c[‡]	σ_{gs}	Experimental Conditions
		SURFACE				
		Reference Transport Rate				
Parker and Klingeman (1982)[1]	0.035 m	$\tau^*_{c_{ri}}=0.035(D_i/D_{50_s})^{-0.78}$	54	10,001	0.75	Natural pool-riffle channel, with relatively subdued topography in the study reach. No form drag or sidewall correction. D_{50s}/h_c≈0.15[¥].
In Wilcock and Southard (1988)[2] Milhous (1973)	0.027 m	$\tau^*_{c_{ri}}=0.073(D_i/D_{50_{ss}})^{-0.98}$	54	8,784	0.75	Same as Parker and Klingeman (1982), but with D_{50s}/h_c≈0.20.
Ashworth and Ferguson (1989)[3]	0.072 m	$\tau^*_{c_{ri}}=0.072(D_i/D_{50_s})^{-0.65}$	~50	~11,660		Natural pool-riffle channel, variable sinuosity. Sidewall effects accounted for. D_{50s}/h_c≈0.11.
	0.054 m	$\tau^*_{c_{ri}}=0.054(D_i/D_{50_s})^{-0.67}$	~57.5	~12,694		Natural pool-riffle channel, mildly braided. Sidewall effects accounted for. D_{50s}/h_c≈0.10.
	0.087 m	$\tau^*_{c_{ri}}=0.087(D_i/D_{50_s})^{-0.92}$	~69	~24,207		Natural braided channel. D_{50}/h_c≈0.13. Sidewall effects accounted for.
Parker (1990)[4]	0.033 m	$\tau^*_{c_{ri}}=0.039(D_i/D_{gs})^{-0.90}$	55	9,982	1.02	Same as Parker and Klingeman (1982), but with D_{50s}/h_c≈0.16.
		Largest Mobile Grain				
Andrews and Erman (1986)[5]	0.047 m	$\overline{\tau}^*_{c_{qi}}=0.083(D_i/D_{50_{ss}})^{-0.87}$	58	12,200	0.97	Natural, meandering, pool-riffle channel. No form drag or sidewall correction. D_{50s}/h_c≈0.15.

£ Italicised numbers are keyed to Appendix I notes.

† See p. 144 for notation not previously defined in text.

u=uniform grain sizes ($\sigma_g \leq 0.5\phi$), m=mixed grain sizes ($\sigma_g > 0.5\phi$), where σ_g is the graphic standard deviation defined as $(\phi_{84}-\phi_{16})/2$ (Folk, 1974).

‡ $Re^*_c=u^*_c D_{50}/\nu$. Most values calculated by JMB based on reported data. For example using $\tau^*_{c_{r50}}$ and D_{50s} reported by Parker and Klingeman (1982) I calculated $\tau_{c_{r50}}=\tau^*_{c_{r50}} D_{50s}(\rho_s-\rho)g$ and $u^*_c=(\tau_{c_{r50}}/\rho)^{0.5}$, allowing determination of $Re^*_c=u^*_c D_{50s}/\nu$. Where not reported, it was assumed that ρ_s and ρ were 2650 and 1000 kg/m^3, respectively, and that $\nu=10^{-6}$ m^2/s.

¥ Most h_c values back-calculated from depth-slope products using data reported by authors or calculated by JMB.

TABLE 1.1 cont.

Source[£]	$\tau^*_{c_{50s}}$	Proposed τ^*_c Function Other than the Shields Equation[†]	D_{50s} (mm)	Re^*_c[‡]	σ_{gs}	Experimental Conditions
In Komar (1987a)[6]						
Milhous (1973)[7]	0.027 m	$\tau^*_{c_{qi}}=0.044(D_i/D_{50ss})^{-0.43}$	60	10,288	0.71	Same as Parker and Klingeman (1982), but with $D_{50s}/h_c\approx0.20$.
Carling (1983)[8]	0.022 m	$\tau^*_{c_{qi}}=0.045(D_i/D_{50ss})^{-0.68}$	62	9,378		Natural, steep, gravel-bedded channel. No form drag or sidewall correction. $D_{50s}/h_c=0.27$.
Hammond et al. (1984)[9]	0.022 m	$\tau^*_{c_{qi}}=0.045(D_i/D_{50ss})^{-0.71}$	21	1,816	0.56	Natural tidal channel. Plane-bed.
In Komar (1987b)						
Fahnestock (1963)[10]	0.029 m		128	31,375	1.50	Natural, proglacial, braided channel. No form drag or sidewall correction.
In Komar and Carling (1991)[11]						
Milhous (1973)	0.029 m	$\tau^*_{c_{qi}}=0.059(D_i/D_{50ss})^{-0.64}$	60	10,662	0.71	Same as Parker and Klingeman (1982), but with $D_{50s}/h_c\approx0.19$.
Komar and Carling (1991)	0.039 m	$\tau^*_{c_{qi}}=0.039(D_i/D_{50s})^{-0.82}$	62	12,487		Same as Carling (1983) in Komar (1987a), but with $D_{50s}/h_c\approx0.15$.
Milhous (1973)[12]	0.025 m		60	9,900	0.71	Same as Parker and Klingeman (1982), but wtih $D_{50s}/h_c\approx0.22$.
Carling (1983)[13]	0.030 m	$\tau^*_{c_{qi}}=1.17Re^*_i{}^{-0.46}$	62	10,952		Natural, steep, gravel-bedded channel (Great Eggleshope Beck). No form drag or sidewall correction. $D_{50s}/h_c\approx0.19$.
	0.111 m	$\tau^*_{c_{qi}}=4.99Re^*_i{}^{-0.42}$	87	32,356		Natural, steep, gravel-bedded channel (Carl Beck). No form drag or sidewall correction. $D_{50s}/h_c\approx0.24$.
Ferguson (1994)[14]	0.074 m		106	37,770	1.06	Natural boulder-bed stream. Bedform type not reported. Form drag and sidewall correction not explicitly considered. $D_{50s}/h_c=0.31$.
	0.078 m		104	37,685	1.01	Same as above, but with $D_{50s}/h_c\approx0.28$.
	0.061 m		109	35,759	1.11	Same as above, but with $D_{50s}/h_c\approx0.33$.
	0.070 m		96	31,662	1.22	Same as above, but with $D_{50s}/h_c\approx0.42$.
	0.047 m		75	17,915		Natural channel. Bedform type not reported. Form drag and sidewall corrections not explicitly considered.
		Other				
Kalinske (1947)[15]	0.039 u					

TABLE 1.1 cont.

Source[£]	τ^*_{c50s}	Proposed τ^*_c Function Other than the Shields Equation[†]	D_{50s} (mm)	Re^*_c[‡]	σ_{gs}	Experimental Conditions
Çeçen and Bayazit (1973)[16]	0.044 m[48]		14.6	1,481	0.72	Straight, rectangular flume. Plane-bed. No sidewall correction. D_{50s}/h_c=0.26.
Kirchner et al. (1990)[17]	~0.100 m		3.74-4.85	291-430	~0.94-1.18	Straight, rectangular flume. Plane-bed (?).
		$\tau^*_{ci} = \left(\frac{1}{\tan\Phi_i} \frac{3C_D}{\pi\kappa^2} \int_{p_i^* - e_i^*}^{p_i^*} \sqrt{1-(2z^*-(2p_i^*-1))^2}\left[\ln(z^*D_i^*+1)\right]^2 dz^* + \frac{3C_L}{4\kappa^2}\left\{\left[\ln(p_i^*D_i^*+1)\right]^2 - \left[\ln(p_i^*D_i^*-D_i^*+1)\right]^2\right\} \right)^{-1}$				
Buffington et al. (1992)[18]	~0.100 ~u, m	"	4.1-45	334-12,145	0.67-1.50	Natural, pool-riffle channel.
Jiang and Haff (1993)[19]	0.086-0.161 m		7.2 (?)	700-1000		Simulated heterogeneous bed surface undergoing a "slab" shear.

MIXTURE

Source	τ^*_{c50m}	Proposed τ^*_c Function Other than the Shields Equation[†]	D_{50m} (mm)	Re^*[‡]	σ_{gm}	Experimental Conditions
			Reference Transport Rate			
In Shields (1936)[20]						
Shields (1936)	0.036 ~u		0.36	~6.3	0.30	Straight, rectangular flume. Various bedform types. Sidewall correction, but no form drag correction. Grains composed of barite.
	0.034 ~u		1.52	52	0.35	"
	0.043 ~u		2.76	127	0.41	"
	0.045 ~u		3.44	205	0.16	"
	0.039 ~u		2.46	115	0.22	"
	0.031 ~u		0.69	15	0.33	"
	~0.037 m		1.56	~8.7	0.59	Same as above, but with amber grains.
	~0.041 m		1.56	~8.9	0.59	"
	~0.044 m		1.56	~9.3	0.59	"
	~0.029 ~u		0.85	~15	0.23	Same as above, but with granitic (natural) grains.
	~0.034 ~u		1.23	~29	0.23	"

TABLE 1.1 cont.

Source[£]	$\tau^*_{c_{50m}}$	Proposed τ^*_c Function Other than the Shields Equation[†]	D_{50m} (mm)	Re^*_c[‡]	σ_{gm}	Experimental Conditions
	-0.047 -u		2.44	100	0.23	"
	-0.029 m		1.77?	~14	0.78?	Same as above, but with lignite breeze grains.
	0.037 m		1.77	20	0.78	"
	-0.039 m		1.88	-23	0.72	"
	-0.047 m		2.53	-37	0.56	"
Casey (1935)[21]	-0.068 -u?			~1.8		Straight, rectangular flume. Bedform types not reported by Shields (1936) Sidewall correction (?)[20], but no form drag correction.
	-0.052 -u?			-3.2		"
	-0.034 -u?			-11		"
	-0.034 -u?			-16		"
	-0.037 -u?			-18		"
	-0.041 -u?			-31		"
	-0.041 -u?			-47		"
	-0.039 -u?			80		"
Kramer (1935)[22]	-0.032 m		0.51	-6.7	0.74	Straight, rectangular flume. Various bedforms. Sidewall correction (?), but no form drag correction.
	-0.032 m		0.52	-7.9	0.81	"
	-0.039 m		0.56	-7.6	0.62	"
USWES (1935)[23]	-0.051 -m?			-2.2		Straight, rectangular flume. Bedform types not reported by Shields (1936). Sidewall correction(?), but no form drag correction.
	-0.045 -m?			4.0		"
	-0.039 -m?			-4.4		"
	-0.034 -m?			-7.5		"
	-0.036 -m?			-7.4		"
	-0.036 -m?			-7.9		"
Gilbert (1914)[24]	-0.059 -u		7.01	-491	<0.22	Straight, rectangular flume. Bedform types not reported. Sidewall correction (?), but no form drag correction.
	-0.051 -u		4.94?	-225	<0.26	"
Paintal (1971)[25]	0.050 -u		2.5-7.95	112-638	0.14-0.18	Straight, rectangular flume. Plane-bed. (?) Sidewall correction.
	0.020 -u, m		2.5-22.2	71-13,308	0.14-1.39	"
Mizuyama (1977)[26] [also published as Ashida and Bayazit (1973)]	0.044 -u	$\tau^*_{c_{r50m}}=\tau_{c_{r50m}}/[(\rho_s-\rho)gD_{50m}(\tan\Phi\cos\theta-\sin\theta)]$	6.4	468	<0.12	Straight, rectangular flume. Bedform type not reported. Sidewall correction, but no form drag correction. D_{50m}/h_c=0.12
	0.049 -u	"	6.4	491	"	Same as above, but with D_{50m}/h_c=0.27.

TABLE 1.1 cont.

Source[£]	τ^*_{c50m}	Proposed τ^*_c Function Other than the Shields Equation[†]	D_{50m} (mm)	Re^*_c[‡]	σ_{gm}	Experimental Conditions
	0.054 ~u	"	"	511	"	Same as above, but with D_{50m}/h_c=0.49.
	0.050 ~u	"	12.0	1,174	<0.21	Same as above, but with D_{50m}/h_c=0.12.
	0.047 ~u	"	"	1,135	"	Same as above, but with D_{50m}/h_c=0.33.
	0.054 ~u	"	"	1,203	"	Same as above, but with D_{50m}/h_c=0.59.
	0.059 ~u	"	"	1,239	"	Same as above, but with D_{50m}/h_c=0.83.
	0.067 ~u	"	"	1,302	"	Same as above, but with D_{50m}/h_c=1.00.
	0.083 ~u	"	"	1,425	"	Same as above, but with D_{50m}/h_c=1.04.
	0.056 ~u	"	22.5	3,015	<0.08	Same as above, but with D_{50m}/h_c=0.25.
	0.056 ~u	"	"	2,969	"	Same as above, but with D_{50m}/h_c=0.63.
	0.061 ~u	"	"	3,052	"	Same as above, but with D_{50m}/h_c=0.90.
	0.072 ~u	"	"	3,268	"	Same as above, but with D_{50m}/h_c=1.05.
	0.081 ~u	"	"	3,376	"	Same as above, but with D_{50m}/h_c=1.47.
	0.099 ~u	"	"	3,593	"	Same as above, but with D_{50m}/h_c=1.73.
Misri et al. (1984)[27]	~0.023 m		6.02	~285	1.65	Straight, rectangular flume. Bedform type not reported. Sidewall effects and (?) form drag corrected.
In Bridge and Dominic (1984)[28]						
Upper stage plane-bed:						
Gilbert (1914)	0.040 ~u		0.30	4.2		Straight, rectangular flume. Upper stage plane-bed. Sidewall correction.[28]
	0.052 ~u		0.38	6.9		"
	0.042 ~u		0.51	9.6		"
	0.030 ~u		0.79	16		"
Guy et al. (1966)[29]	0.040 ~u		0.19	2.1	0.45	"
	0.040 m		0.28	3.3	0.81	"
	0.040 m		0.32	4.6	0.65	"
Williams (1970)[30]	0.040 ~u		1.35	40	0.20	"
Lower stage plane-bed:						
Gilbert (1914)	0.040 ~u		3.17	145		Straight, rectangular flume. Lower stage plane-bed. Sidewall correction.[28]
	0.041 ~u		4.94	286		"
Williams (1970)[30]	0.040 ~u		1.35	40	0.20	"
Fernandez Luque and van Beek (1976)[31]	0.040 ~u		0.9-3.3	22-152	<0.49	"
In Bathurst et al. (1987)[32]						
EPFL (Ecole Polytechnique Fédérale de Lausanne)	0.052 ~u?	$\tau^*_{cr50m}=\tau_{cr50m}/[(\rho_s-\rho)gD_{50m}(\tan\Phi\cos\theta-\sin\theta)]$	11.5	~900		Straight, rectangular flume. Various bedforms. Sidewall correction, but no form drag correction. D_{50m}/h_c=0.08.
	0.063 ~u?	"	"	~951		Same as above, but with D_{50m}/h_c=0.10.

TABLE 1.1 cont.

Source[£]	$\tau^*_{c_{50m}}$	Proposed τ^*_c Function Other than the Shields Equation[†]	D_{50m} (mm)	Re^*_c[‡]	σ_{gm}	Experimental Conditions
	0.070 ~u?	"	"	~1,069		Same as above, but with D_{50m}/h_c=0.12.
	0.062 ~u	"	22.2	~3,162	0.34	Same as above, but with D_{50m}/h_c=0.12.
	0.087 ~u	"	"	~3,381	"	Same as above, but with D_{50m}/h_c=0.27.
	0.102 ~u	"	"	~3,614	"	Same as above, but with D_{50m}/h_c=0.39.
	0.113 ~u	"	"	~3,799	"	Same as above, but with D_{50m}/h_c=0.50.
	0.115 ~u	"	"	~3,929	"	Same as above, but with D_{50m}/h_c=0.65.
	0.061 ~u?	"	44.3	~8,050		Same as above, but with D_{50m}/h_c=0.35.
	0.068 ~u?	"	"	~8,463		Same as above, but with D_{50m}/h_c=0.53.
	0.087 ~u?	"	"	~8,750		Same as above, but with D_{50m}/h_c=0.59.
	0.088 ~u?	"	"	~9,354		Same as above, but with D_{50m}/h_c=0.79.
Bathurst et al. (1979)[33]	~0.094 ~u?	"	8.8	~8,075		Flume. Bedform types not reported by Bathurst et al. (1987). Sidewall correction? D_{50m}/h_c≈0.14.
	~0.126 ~u?	"	"	~1,000		Same as above, but with D_{50m}/h_c≈0.27.
	~0.182 ~u?	"	"	~1,160		Same as above, but with D_{50m}/h_c≈0.31.
	~0.097 ~u?	"	34	~6,310		Same as above, but with D_{50m}/h_c≈0.57.
In Day (1980b)[34]						
USWES (1935)	~0.050 m		0.42	7.7	0.86	Flume. Bedform type not reported. No form drag or sidewall correction.
	~0.047 m		0.44	8.1	0.59	"
	~0.034 m		4.10	195	0.54	"
Day (1980a)	~0.024 m		1.75	46	2.10	"
	~0.029 m		1.55	42	1.70	"
In Wilcock and Southard (1988)[35]						
Day (1980a)	0.037 m	$\tau^*_{c_{ri}}=0.037(D_i/D_{50m})^{-0.81}$	1.82	60	2.10	Flume. Bedform type not reported. No form drag or sidewall correction (?).
	0.037 m	$\tau^*_{c_{ri}}=0.037(D_i/D_{50m})^{-0.95}$	1.57	48	1.70	"
Dhamotharan et al. (1980)	0.071 m	$\tau^*_{c_{ri}}=0.071(D_i/D_{50m})^{-1.1}$	2.16	108	1.43	Flume. Bedform type not reported. No form drag or sidewall correction (?).
Misri et al. (1984)	0.048 m	$\tau^*_{c_{ri}}=0.048(D_i/D_{50m})^{-1.0}$	2.36	101	1.05	Straight, rectangular flume. Bedform type not reported. Sidewall and (?) form drag correction.
	0.042 m	$\tau^*_{c_{ri}}=0.042(D_i/D_{50m})^{-0.95}$	3.81	194	1.65	"
	0.037 m	$\tau^*_{c_{ri}}=0.037(D_i/D_{50m})^{-0.92}$	4.00	196	1.29	"

TABLE 1.1 cont.

Source[£]	$\tau^*_{c_{50m}}$	Proposed τ^*_c Function Other than the Shields Equation[†]	D_{50m} (mm)	Re^*_c[‡]	σ_{gm}	Experimental Conditions
Wilcock (1987)[36]	0.030 m	$\tau^*_{c_{ri}}=0.030(D_i/D_{50m})^{-1.0}$	1.83	61	0.53	Straight, rectangular flume. Various bedforms. Sidewall and form drag correction applied.
	0.036 m	$\tau^*_{c_{ri}}=0.036(D_i/D_{50m})^{-0.97}$	1.83	67	1.06	"
	0.023 –u	$\tau^*_{c_{ri}}=0.023(D_i/D_{50m})^{-0.98}$	0.67	12	0.29	"
	0.037 –u	$\tau^*_{c_{ri}}=0.037(D_i/D_{50m})^{-1.1}$	5.28	332	0.20	Straight, rectangular flume. Plane-beds. Sidewall correction applied.
		Visual Observation				
Kramer (1935)[37]	0.048 m		0.52	8.5	0.81	Straight, rectangular flume. Plane-bed. No sidewall correction.
	0.055 m		"	9.1	"	"
	0.045 m		"	8.1	"	"
	0.047 m		"	8.5	"	"
	0.040 m		0.51	7.6	0.74	"
	0.042 m		"	7.6	"	"
	0.039 m		"	7.5	"	"
	0.034 m		"	6.9	"	"
	0.038 m		0.56	8.3	0.62	"
	0.043 m		"	8.8	"	"
	0.042 m		"	8.6	"	"
	0.041 m		"	8.7	"	"
Meyer-Peter and Müller (1948)[38]	0.033–u?	$\tau^*_{cv50m}=[\tau_{cv50m}(Q_s/Q)(n_g/n_0)^{3/2}]/[(\rho_s-\rho)gD_{50m}]$	3.2	127		Straight, rectangular flume. Plane-bed or very low amplitude bedforms. Form drag and sidewall correction applied. Rounded grains.
	0.032 –u?		2.7	98		"
	0.037 –u?		3.8	183		"
	0.030 –u?		3.6	157		"
	0.039 –u?		3.66	174		"
	0.040 –u?		3.66	190		"
	0.037 –u?		8.5	676		"
	0.050 –u?		7.4	603		"
	0.047 –u?		8.5	762		"
	0.040 –u?		3.14	152		"
	0.033–u?		1.86	57		Same as above, but with angular grains.
	0.025 –u?		3.14	107		"
	0.033 –u?		3.1	127		"

TABLE 1.1 cont.

Source[£]	τ^*_{c50m}	Proposed τ^*_c Function Other than the Shields Equation[†]	D_{50m} (mm)	Re^*_c[‡]	σ_{gm}	Experimental Conditions
	0.043 ~u?		3.14	165		"
	0.038 ~u?		3.66	179		"
	0.040 ~u?		3.06	144		"
	0.040 ~u?		2.58	112		"
	0.048 ~u?		2.61	124		"
	0.050 ~u?		4.04	233		"
	0.043 ~u?		4.34	275		"
	0.043 ~u?		2.190			"
White (1940)[39]	0.338 ~u		0.21	0.04		Straight, rectangular flume. Plane-bed. No sidewall correction. Fluid medium of lubricating oil. Entirely laminar flow.
	0.168 ~u		0.90	0.30		"
	0.180 ~u		0.122	2.4		Constant-drag nozzle. Plane-bed (?). No sidewall correction. Water fluid medium. Entirely laminar flow.
	0.119 ~u		0.90	33		Constant-drag nozzle. Plane-bed (?). No sidewall correction. Fully (?)turbulent flow.
	0.101 ~u		5.6	480		"
	0.064 ~u		0.71	35		Constant-drag nozzle. Plane-bed (?). No sidewall correction. Steel shot grains. Fully (?) turbulent flow.
	0.098 ~u		0.90	80		Constant-drag nozzle. Plane-bed (?). No sidewall correction. Fluid medium of air. Fully (?) turbulent flow.
	0.102 ~u		5.6	1,280		"
Neill (1967)	0.024 ~u?		6.2	297		Straight, rectangular flume. Plane-bed. No sidewall correction. D_{50m}/h_c=0.12.
	0.033 ~u?		"	347		Same as above, but with D_{50m}/h_c=0.11.
	0.038 ~u?		"	372		Same as above, but with D_{50m}/h_c=0.07.
	0.034 ~u?		"	351		Same as above, but with D_{50m}/h_c=0.07.
	0.042 ~u?		"	388		Same as above, but with D_{50m}/h_c=0.06.
	0.045 ~u?		"	404		Same as above, but with D_{50m}/h_c=0.05.
	0.034 ~u?		"	348		Same as above, but with D_{50m}/h_c=0.05.
	0.037 ~u?		"	364		Same as above, but with D_{50m}/h_c=0.04.
	0.035 ~u?		"	353		Same as above, but with D_{50m}/h_c=0.04.
	0.040 ~u?		8.5	606		Same as above, but with D_{50m}/h_c=0.28.
	0.040 ~u?		"	602		Same as above, but with D_{50m}/h_c=0.14.
	0.062 ~u?		"	755		Same as above, but with D_{50m}/h_c=0.07.
	0.058 ~u?		"	729		Same as above, but with D_{50m}/h_c=0.05.
	0.033 ~u?		20.0	1,969		Same as above, but with D_{50m}/h_c=0.55.
	0.034 ~u?		"	2,001		Same as above, but with D_{50m}/h_c=0.39.

TABLE 1.1 cont.

Source[£]	τ^*_{c50m}	Proposed τ^*_c Function Other than the Shields Equation[†]	D_{50m} (mm)	Re^*_c[‡]	σ_{gm}	Experimental Conditions
	0.029 ~u?		"	1,856		Same as above, but with D_{50m}/h_c=0.33.
	0.034 ~u?		"	2,007		Same as above, but with D_{50m}/h_c=0.23.
	0.040 ~u?		"	2,178		Same as above, but with D_{50m}/h_c=0.18.
	0.036 ~u?		"	2,073		Same as above, but with D_{50m}/h_c=0.14.
	0.043 ~u?		"	2,263		Same as above, but with D_{50m}/h_c=0.11.
	0.028 ~u?		5.0	228		Straight, rectangular flume. Plane-bed. No sidewall correction. Glass ball sediment. D_{50m}/h_c=0.08.
	0.042 ~u?		"	279		Same as above, but with D_{50m}/h_c=0.04.
	0.048 ~u?		"	295		Same as above, but with D_{50m}/h_c=0.04.
	0.044 ~u?		"	284		Same as above, but with D_{50m}/h_c=0.04.
	0.043 ~u?		"	280		Same as above, but with D_{50m}/h_c=0.03.
White (1970)	0.053 ~u		2.2	~38		Straight, rectangular flume. Plane-bed. Sidewall correction. Polystyrene grains.
	0.037 ~u		2	~53		Same as above, but with PVC grains.
	0.055 ~u		0.17	2.1		Same as above, but with natural grains.
	0.058 ~u		0.153	1.8		"
	0.071 ~u		0.133	1.6		"
	0.066 ~u		0.093	0.93		"
	0.073 ~u		0.077	0.73		"
	0.125 ~u		0.044	0.42		"
	0.112 ~u		0.033	0.26		"
	0.102 ~u		0.030	0.21		"
	0.103 ~u		0.029	0.20		"
	0.146 ~u		0.028	0.23		"
	0.110 ~u		0.024	0.16		"
	0.151 ~u		0.016	0.10		"
	0.037 ~u		2.2	~15		Straight, rectangular flume. Plane-bed. Sidewall correction. Polystyrene grains in Mentor 28 oil. Fully laminar flow (?).
	0.034 ~u		2	~40		Same as above, but with PVC grains.
	0.132 ~u		0.133	0.28		Same as above, but with natural grains
	0.122 ~u		0.093	0.16		"
	0.166 ~u		0.077	0.14		"
	0.218 ~u		0.046	0.07		"
	0.254 ~u		0.033	0.05		"
	0.288 ~u		0.030	0.04		"
	0.219 ~u		0.025	0.03		"
Grass (1970)[40]	0.141 (0.174) ~u		0.090	0.88 (0.97)		Straight, rectangular flume. Plane-bed. Sidewall effects accounted for.
	0.131 (0.154) ~u		0.090	0.84 (0.91)		"

TABLE 1.1 cont.

Source[£]	τ^*_{c50m}	Proposed τ^*_c Function Other than the Shields Equation[†]	D_{50m} (mm)	Re^*_c[‡]	σ_{gm}	Experimental Conditions
	0.110 (0.131)	~u	0.115	1.6 (1.7)		"
	0.086 (0.095)	~u	0.138	1.8 (1.9)		"
	0.069 (0.093)	~u	0.165	2.1 (2.5)		"
	0.072 (0.079)	~u	0.195	2.8 (2.9)		"
	0.058 (0.091)	m	0.143	1.6 (2.0)		"
Everts (1973)[41]	0.023	~u	3.57	145		Straight, rectangular flume. Plane-bed. Sidewall correction applied.
	0.027	~u	"	157		"
	0.029	~u	"	162		"
	0.023	~u	1.79	51		"
	0.025	~u	"	54		"
	0.019	~u	"	47		"
	0.017	~u	"	44		"
	0.017	~u	0.895	16		"
	0.021	~u	"	17		"
	0.018	~u	"	16		"
	0.020	~u	"	17		"
	0.020	~u	0.508	7.2		"
	0.024	~u	"	8.0		"
	0.022	~u	"	7.7		"
	0.025	~u	"	8.1		"
	0.029	~u	0.359	5.2		"
	0.026	~u	"	4.9		"
	0.027	~u	"	5.1		"
	0.023	~u	"	4.6		"
	0.032	~u	0.254	3.3		"
	0.035	~u	"	3.4		"
	0.041	~u	"	3.7		"
	0.039	~u	0.18	2.1		"
	0.046	~u	"	2.3		"
	0.052	~u	0.127	1.5		"
	0.052	~u	"	1.5		"
	0.040	~u	"	1.3		"
	0.056	~u	0.18	3.9		Same as above, but with ilmenite grains.
	0.056	~u	"	3.9		"
	0.062	~u	"	4.1		"
	0.058	~u	0.127	2.3		"
	0.060	~u	"	2.4		"
	0.059	~u	"	2.4		"
	0.063	~u	"	2.4		"
	0.057	~u	0.09	1.4		"

TABLE 1.1 cont.

Source[£]	$\tau^*_{c_{50m}}$	Proposed τ^*_c Function Other than the Shields Equation[†]	D_{50m} (mm)	Re^*_c[‡]	σ_{gm}	Experimental Conditions
	0.070 ~u		"	1.5		"
	0.058 ~u		"	1.4		"
	0.081 ~u		"	1.6		"
Fernandez Luque and van Beek (1976)[42]	~0.038 ~u		0.9	~18	<0.49	Straight, rectangular flume. Plane-bed. Sidewall effects accounted for.
	~0.037 ~u		1.8	~51	"	"
	~0.047 ~u		3.3	~127	"	"
	~0.043 ~u		1.8	~74	"	Same as above, but with magnitite grains.
	~0.038 ~u		1.5	~16	"	Same as above, but with walnut (shell?) grains.
Yalin and Karahan (1979)[43]	0.038 ~u, m?		1.00	25	~0.34-0.54	Straight, rectangular flume. Plane-bed. Sidewall effects corrected.
	0.030 ~u, m?		0.56	9.4	"	"
	0.113 ~u, m?		0.10	1.5	"	"
	0.036 ~u, m?		0.40	6.1	"	"
	0.053 ~u, m?		0.19	2.5	"	"
	0.079 u		0.14	1.8	"	Same as above, but with glass bead grains.
	0.178 ~u, m?		1.00	0.13	"	Straight, rectangular flume. Plane-bed. Sidewall effects corrected. Natural grains in water-glycerin mixture. Laminar flow.
	0.156 ~u, m?		1.88	0.30	"	"
	0.135 ~u, m?		2.86	0.55	"	"
	0.172 ~u, m?		0.56	0.05	"	"
	0.110 ~u, m?		1.00	0.78	"	"
	0.092 ~u, m?		1.88	1.9	"	"
	0.141 ~u, m?		0.56	0.38	"	"
	0.086 ~u, m?		2.86	3.4	"	"
	0.091 ~u, m?		2.86	3.5	"	"
	0.134 ~u, m?		1.00	0.86	"	"
	0.143 ~u, m?		0.56	0.38	"	"
	0.110 ~u, m?		1.88	2.0	"	"
	0.140 ~u, m?		0.56	0.80	"	"
	0.069 ~u, m?		2.86	6.4	"	"
	0.086 ~u, m?		1.88	3.8	"	"
	0.106 ~u, m?		1.00	1.6	"	"

TABLE 1.1 cont.

SUBSURFACE

Source	$\tau^*_{c_{50ss}}$	Proposed τ^*_c Function Other than the Shields Equation†	D_{50ss} (mm)	Re^*‡	σ_{gss}	Experimental Conditions
		Reference Transport Rate				
Parker and Klingeman (1982)[44]	0.088 m	$\tau^*_{c_{ri}}=0.088(D_i/D_{50_{ss}})^{-0.98}$	20	3,574	2.27	Same as Parker and Klingeman (1982).
In Wilcock and Southard (1988)						
Milhous (1973)	0.073 m	$\tau^*_{c_{ri}}=0.073(D_i/D_{50_{ss}})^{-0.98}$	19.5	3,134	2.27	Same as Parker and Klingeman (1982).
		Largest Mobile Grain				
Andrews (1982)	0.083 m	$\tau^*_{c_{qi}}=0.083(D_i/D_{50_{ss}})^{-0.87}$				
In Komar (1987a)[45]						
Milhous (1973)	0.044 m	$\tau^*_{c_{qi}}=0.044(D_i/D_{50})^{-0.43}$	20	2,528	2.67	Same as Parker and Klingeman (1982).
Carling (1983)	0.045 m	"	20	2,457		Same as in Komar (1987a).
Hammond et al. (1984)	0.045 m	$\tau^*_{c_{qi}}=0.045(D_i/D_{50_{ss}})^{-0.71}$	7.5	554		"
In Komar and Carling (1991)						
Milhous (1973)	0.059 m	$\tau^*_{c_{qi}}=0.059(D_i/D_{50_{ss}})^{-0.64}$	20	2,927	2.67	Same as Parker and Klingeman (1982).

£ Italicised numbers are keyed to Appendix I notes.

† See p. 144 for notation not previously defined in text.

u=uniform grain sizes ($\sigma_g \leq 0.5\phi$), m=mixed grain sizes ($\sigma_g > 0.5\phi$), where σ_g is the graphic standard deviation defined as $(\phi_{84}-\phi_{16})/2$ (Folk, 1974).

‡ $Re^*_c=u^*_cD_{50}/\nu$. Most values calculated by JMB based on reported data. For example using $\tau^*_{c_{r50}}$ and D_{50s} reported by Parker and Klingeman (1982) I calculated $\tau_{c_{r50}}=\tau^*_{c_{r50}}D_{50s}(\rho_s-\rho)g$ and $u^*_c=(\tau_{c_{r50}}/\rho)^{0.5}$, allowing determination of $Re^*_c=u^*_cD_{50s}/\nu$. Where not reported, it was assumed that ρ_s and ρ were 2650 and 1000 kg/m^3, respectively, and that $\nu=10^{-6}$ m^2/s.

¥ Most h_c values back-calculated from depth-slope products using data reported by authors or calculated by JMB.

(Paintal,.1971; Misri et al., 1984; Wilcock, 1988). Competence functions are based on relations between shear stress and the largest mobile grain size, from which one can establish the critical dimensional and dimensionless shear stresses for a given size of interest. Competence functions are, however, sensitive to the sampling device used, technique, and availability of coarse grain sizes (Wilcock, 1992). In this analysis τ^*_{c50} values corresponding to these three methods of measuring incipient motion are respectively symbolized as τ^*_{cv50}, τ^*_{cr50}, and τ^*_{cq50}.

Where data were available Table 1.1 also reports D_{50}, Re^*_c, and σ_g values, as well as experimental conditions and proposed τ^*_{ci} expressions other than Shields' (1936). In many cases Re^*_c values were not reported by a given source, but could be calculated from other presented data; to be consistent with Shields (1936) I took $k_s=D_{50}$, however, as will be discussed later it is recommended that this common practice be re-examined, particularly for data from natural, heterogeneous, gravel-bedded streams. The sorting coefficient, σ_g, is Folk's (1974) graphic standard deviation defined as $(\phi_{84}-\phi_{16})/2$, where ϕ_{84} and ϕ_{16} are the 84th and 16th percentiles of the grain size distribution expressed in units of the phi ($\log_2$) scale. In many cases τ^*_{c50} values (or particular types of τ^*_{c50}) were not explicitly reported by a source, but could be calculated from the equations and data presented by the author(s); detailed notes are given in Appendix I, keyed to italicized numerals in Table 1.1. Dimensionless critical shear stress values for subsurface median grain sizes (τ^*_{c50ss}) are presented in Table 1.1 for comparison with other τ^*_{c50} types, but will not be considered in this analysis as the concern here is choosing an appropriate τ^*_{c50} value for surface mobility.

By analogy with Folk's (1974) sorting definitions, near-uniform sediments (i.e., well-sorted) are defined here as those with $\sigma_g \leq 0.5$, while mixed-grain sediments are those with $\sigma_g > 0.5$. With this definition it can be seen that some of the laboratory sediment mixtures used by Shields (1936) are mixed-grain, contrary to popular belief (Table 1.1).

Sorting is of significance because of its influence on friction angles and hence critical dimensional and dimensionless shear stresses (Buffington et al., 1992). Poorer sorted sediments tend to have lower friction angles and correspondingly lower τ_{c_i} and $\tau^*_{c_i}$ values. Sorting is of further significance for establishing the reliability of mixture incipient motion as a measure of surface mobility (i.e., establishing that $\tau^*_{c50m} \approx \tau^*_{c50s}$). All experiments reporting dimensionless critical shear stress in terms of the sediment mixture (τ^*_{c50m}) were conducted in flumes. Of these the reference-based values (τ^*_{cr50m}) were determined from bedload transport data commonly collected after attainment of equilibrium conditions of slope, bedform character, and transport rate. As such, the actual surface grain size distribution of initially poorly sorted mixtures may not resemble, at the time of measurement, the initial mixture distribution due to potential textural responses to relative conditions of sediment supply and transport capacity. Dietrich et al. (1989) have shown that heterogeneous bed surfaces coarsen when deprived of sediment and fine when inundated, reflecting the magnitude of sediment supply relative to transport capacity. Because of this potential textural response, τ^*_{cr50m} values from mixed-grain experiments will not be considered here as they may not accurately represent the threshold of surface mobility; depending on the direction of textural response, τ^*_{cr50m} values could over- or underestimate actual dimensionless critical shear stress values of the surface (τ^*_{cr50s}). D_{50m} will only approximate D_{50s} when laboratory sediment mixtures are well-sorted, as there is little potential for textural response of a well-sorted bed material. Hence, only under these conditions will τ^*_{cr50m} approximate τ^*_{cr50s}. Potential textural responses are not an issue, however, for incipient motion of laboratory mixtures defined from visual observation (τ^*_{cv50m}).

Data from Table 1.1 are plotted in Figure 1.5 stratified by τ^*_{c50} type and incipient motion definition. Based on the above discussion, neither the subsurface dimensionless critical shear stress values (τ^*_{c50ss}) nor the reference-based mixture values (τ^*_{cr50m}) with

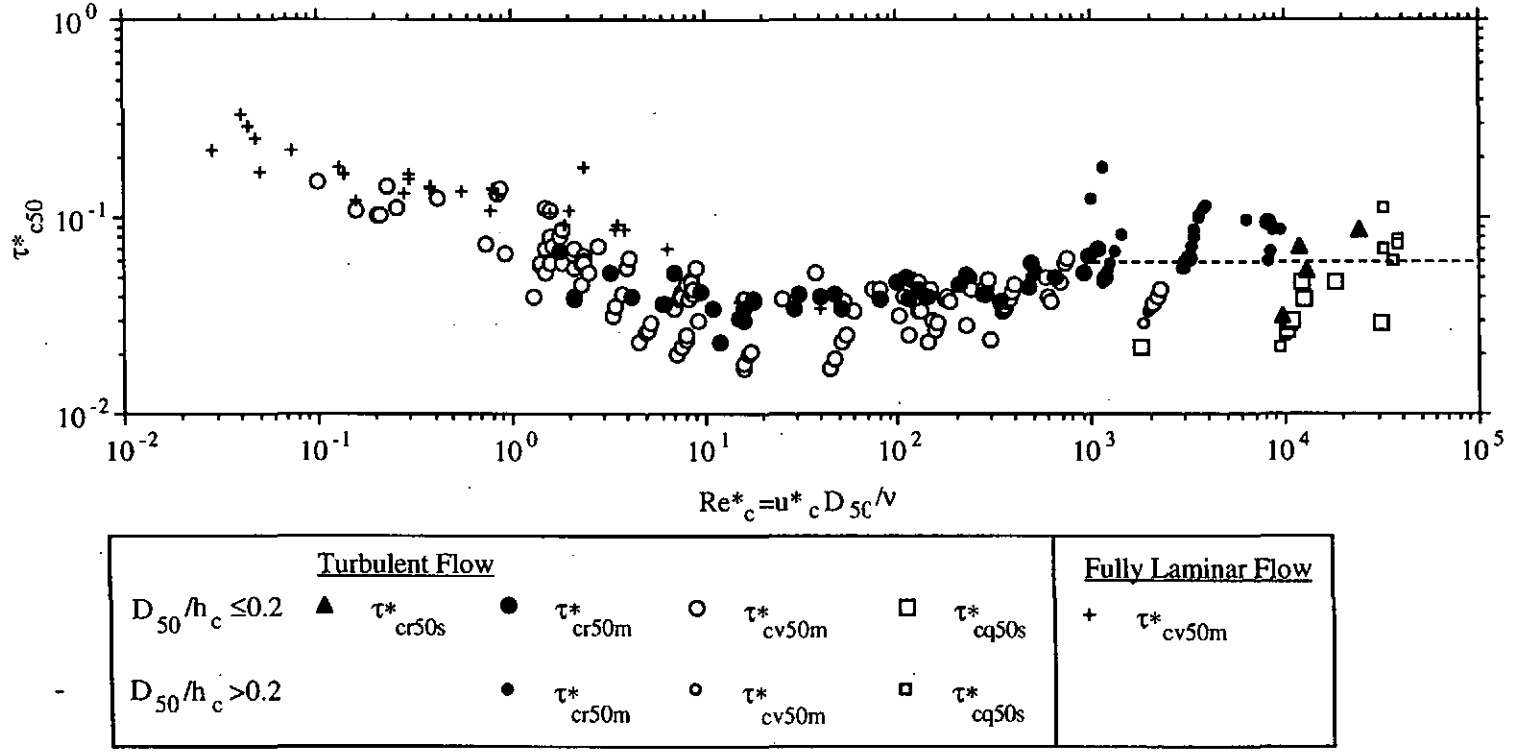

Figure 1.5 Composite Shields curve categorized by flow condition, relative roughness, τ^*_{c50} type, and incipient motion definition.

σ_g>0.5 are included. Furthermore, only data derived from time-averaged measures of shear stress are presented due to the potential incompatibility of τ^*_{c50} values determined from time-averaged versus instantaneous shear stress measures (e.g., Buffington et al., 1992); the majority of the data in Table 1.1 represent time-averaged shear stresses. The data plotted in Figure 1.5 are also segregated by flow condition [i.e., fully laminar versus (smooth, transitional, or rough) turbulent flow] and relative roughness, defined as the ratio of D_{50} to critical flow depth for incipient motion, h_c. As demonstrated by Yalin and Karahan (1979) two "Shields curves" are defined for laminar versus turbulent flow conditions over similar Re^*_c values (Fig. 1.5). The laminar data generally overlie the turbulent data and define a lower-sloped trend than predicted by Shields (1936) for low Re^*_c values.

Scatter within Shields curves has long been attributed to methodological differences between experiments (e.g., Tison, 1953), however a systematic examination of such influences has not been previously undertaken. When classified by incipient motion definition clear distinctions within the turbulent flow data are observed (Fig. 1.5). For laboratory sediment mixtures, two distinct sub-parallel Shields curves are evident for incipient motion defined by reference transport rate versus visual observation (i.e., τ^*_{cr50m} vs. τ^*_{cv50m} for turbulent flow), with the later generally underlying the former and suggesting a systematic methodological bias. Although there is considerable scatter, reference values of dimensionless critical shear stress for surface material (τ^*_{cr50s}) with low relative roughness (D_{50}/h_c<0.2) dove-tail with those of laboratory sediment mixtures (τ^*_{cr50m}), defining a constant average τ^*_{cr50} value of about 0.06 (fit by eye) for $Re^*_c>10^3$ (dashed line, Fig. 1.5). This value is identical to that originally proposed by Shields (1936) for fully turbulent flow. The surface dimensionless critical shear stress values determined from competence equations (τ^*_{cq50s}) define their own space separate from the

other data, indicating a third methodological bias. However, the τ^*_{cq50s} data are too scattered and too few to identify any structural similarities with that of the other data (Fig. 1.5).

Closer inspection of Figure 1.5 shows that many of the data cluster into steeply sloping lineaments. This observation has previously been explained by Bathurst et al. (1983) as a relative roughness effect. Bathurst et al. (1983) demonstrated that for a given median grain size, τ^*_{c50} systematically increases with greater relative roughness and that the rate of increase depends on channel slope. Greater form drag caused by increased relative roughness decreases the shear stress available at the bed for sediment transport, resulting in a higher *total* shear stress required for incipient motion, and thus an apparently greater τ^*_{c50} value. It is because of this effect that I have segregated the data in Figure 1.5 by relative roughness. $D_{50}/h_c<0.2$ was chosen as a value generally representative of gravel-bedded streams. Use of τ' rather than τ_0 in calculating τ^*_{c50} would likely collapse the observed relative roughness lineaments. The effect of bed slope on τ^*_{c50} values in Table 1.1 and Figure 1.5 is insignificant, as most of the data used are derived from experiments with bed slopes <0.01. The data of Bathurst et al. (1987) and Mizuyama (1977) are notable exceptions, however τ^*_{c50} values reported for these studies are based on a modified Shields stress that accounts for both bed slope and bulk material friction angle (Table 1.1).

Figure 1.5 is a useful addition to previous compilation studies (i.e., Miller et al., 1977; Yalin and Karahan, 1979), because it includes for the first time reference- and competence-based τ^*_{c50} values for surface material (τ^*_{cr50s} and τ^*_{cq50s}) and demonstrates methodological differences within compiled τ^*_{c50} data sets. The rough, turbulent flow value of $\tau^*_{c50}\approx0.045$ previously reported by Miller et al. (1977) and Yalin and Karahan (1979) is typical of visually determined mobility thresholds of laboratory mixtures (τ^*_{cv50m}), but underestimates dimensionless critical shear stresses determined from

reference transport rates ($\tau^*_{c_{r50m}}$ and $\tau^*_{c_{r50s}}$) (Fig. 1.5). Because the later are based on a less subjective incipient motion definition, they are preferred in this analysis. The competence-based data ($\tau^*_{c_{q50s}}$) are too few and too scattered to interpret at this time and are derived from a variety of sub-definitions of incipient motion (see Table 1.1 notes). In contrast, the majority of the $\tau^*_{c_{r50}}$ values for rough turbulent flow and low relative roughness are derived from surface-based studies employing Parker and others' (1982) incipient motion definition, adding a certain degree of consistency; it is the rough turbulent flow and low relative roughness portion of the Shields curve that is of significance for surface mobility in gravel-bedded streams. In this region the $\tau^*_{c_{r50s}}$ data with low relative roughness have a range of 0.032-0.087; the 0.032 value is an average of the data reported for Parker and Klingeman (1982), Wilcock and Southard (1988), and Parker (1990), as these values are variations of the same data set [that of Milhous (1973)] analyzed using Parker and others' (1982) definition of incipient motion.

Assuming similarity of incipient motion definition, the reported range of $\tau^*_{c_{r50s}}$ values can be attributed to neglect of roughness effects (i.e., sidewalls, form drag, etc.) and differences in bed material properties (i.e., grain sorting, packing, shape and rounding). Neglect of roughness effects (i.e., use of τ_0 rather than τ') causes overestimation of $\tau^*_{c_{50}}$. Differences in bed material properties can either increase or decrease particle mobility. Greater sorting and angularity cause grains to be more resistant to movement and increase $\tau^*_{c_{50}}$ values (Shields, 1936; Miller and Byrne, 1966; Li and Komar, 1986; Buffington et al., 1992). In contrast, increased sphericity, looser packing, and surfaces with protruding grains increase grain mobility, resulting in relatively lower $\tau^*_{c_{50}}$ values (Fenton and Abbott, 1977; Church, 1978; Reid et al., 1985; Li and Komar, 1986; Kirchner et al., 1990). Because none of the $\tau^*_{c_{r50s}}$ studies fully account for roughness effects (Table 1.1), the lowest $\tau^*_{c_{r50s}}$ value [e.g., the average Milhous value of 0.032] was selected for use in the threshold channel model; the lowest value likely

represents the least amount of overestimation caused by neglect of roughness elements. A low $\tau^*_{c_{r50s}}$ value is also an appropriate choice for natural gravel-bedded rivers as they are typically poorly sorted. It is cautioned, however, that this choice is based on a limited set of $\tau^*_{c_{r50s}}$ data, and as such is tentative.

Although the τ^*_{c50} data segregation presented in the above analysis provides some guidance for interpreting the myriad τ^*_{c50} values reported in the literature, it is likely that further insight can be achieved by explicitly accounting for bed material properties and roughness effects. It is commonly implied that because flume-based studies of incipient motion employ initially planar bed surfaces they are free of form drag influences caused by bedforms (e.g., Miller et al., 1977). This is true for the visually-based studies, but it is not so for most of the reference-based investigations, such as Shields' (1936). In the visual studies, flow is typically gradually increased until grains are observed to move from a plane-bed surface (Kramer, 1935; White, 1970; Yalin and Karahan, 1979). In contrast, most of the reference transport rate studies are based on bedload transport data collected after attainment of equilibrium conditions, which in many instances are characterized by the presence of bedforms (cf. Gilbert, 1914; Shields, 1936; Guy et al., 1966; Wilcock and Southard, 1988). Bedform drag in natural rivers has been estimated as comprising 10-75% of the total channel roughness (Parker and Peterson 1980; Prestegaard 1983; Dietrich et al., 1984; Hey 1988), indicating a potentially significant difference between τ' and τ_0, and hence the calculated τ^*_{c50} value if bedform roughness is not accounted for.

Our understanding of incipient motion studies would additionally be greatly improved from standardization of investigative methodology (Wilcock, 1988). Even within the methodological divisions presented here there are subtleties of definition that cause some of the observed scatter. For example, Wilcock (1988) has demonstrated that there are slight differences in $\tau^*_{c_{ri}}$ values using the same data but differing definitions of

reference transport rate. Figure 1.5 is only a first-order categorization of τ^*_{c50} data and, strictly speaking, compatibility of τ^*_{c50} values is only assured when identical investigative methods are used. More clarity may also be achieved by using appropriate k_s values when calculating Re^*_c. There have been numerous k_s empiricisms proposed [cf. Einstein and Barbarossa (1952), Leopold et al. (1964), Kamphuis (1974), Hey (1979), Bray (1980), Whiting and Dietrich (1990)], most of which for heterogeneous bed surfaces are greater than D_{50s}. Whiting and Dietrich (1990), for example, suggest $k_s=3D_{84}$. Even for near-uniform sediments, $k_s=D_{50}$ may be inappropriate, as indicated by the discrepancy between boundary Reynolds Numbers for structurally similar portions of Shields' (1936) curve and that of Nikuradse (1933) [see discussion by Yalin and Karahan (1979)]. As is commonly done in engineering practice, k_s should be defined relative to Nikuradse's (1933) results as an equivalent (Nikuradse) sand grain roughness, providing a common reference frame amongst incipient motion studies.

Chapter 2: Investigation of the Threshold Channel Model and Examination of Textural Response to Sediment Supply

Application of Existing Data Sets to the General Model

In order to investigate the general validity of the bankfull threshold channel model a literature search was conducted to find all available paired data of median surface grain size and bankfull shear stress. Four hundred thirty six data points from 14 studies representing a wide range of channel sizes and types located throughout the United States, Britain, Ireland, India, and Canada are plotted in Figure 2.1. The data from sand-bedded channels ($D_{50s} < 2$ mm, circles) segregate from the gravel- and cobble-bedded streams (Fig. 2.1), due to basic differences between live-bed and threshold channels. Sand-bedded channels exhibit live-bed transport, with mobility occurring at most stages. As such, D_{50s} predicted from a bankfull threshold of mobility should be a considerable overestimation. Furthermore, sand-bedded channels typically have closer-spaced and multi-scale bedforms, causing potentially greater relative bedform roughness (e.g., τ_f/τ_0) than in gravel-bedded channels. Consequently, live-bed channels should have lower relative bed shear stress (e.g., τ'/τ_0) and hence smaller grain sizes. The strong separation of the sand-bedded data from both the coarse-grained data and the bankfull threshold prediction (Fig. 2.1) is thus likely due to a mobility threshold significantly less than bankfull, as well as potentially greater relative bedform roughness. This separation of data reinforces fundamental differences between live-bed and threshold channels.

The bankfull threshold channel prediction of D_{50s} using $\tau^*_{c50s} \approx 0.032$ is shown by the solid black line in Figure 2.1. According to the hypotheses presented in Chapter 1, the median surface grain sizes of coarse-grained channels should plot on or below the threshold prediction, depending on the degree of textural response. Median surface grain

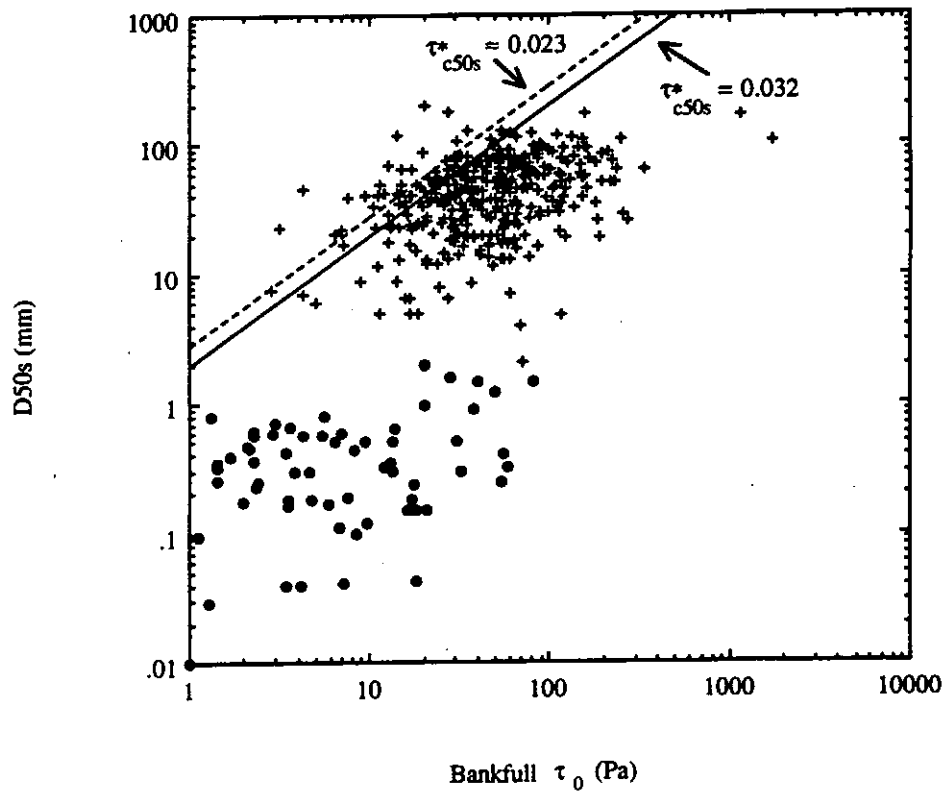

Figure 2.1 Published τ_0 and D_{50s} data compared with the threshold model prediction, assuming τ^*_{c50s}=0.032 (solid line). Channels with $D_{50s} \leq 2$ mm are defined as sand-bedded (i.e., live-bed) channels (•), distinguished from gravel- and cobble-bedded (i.e., threshold) streams (+). Data are from natural channels and irrigation canals studied by: Lane and Carlson (1953); Brush (1961); Simons and Albertson (1963); Chitale (1970); Thorne and Lewin (1979); Lisle (1979); Andrews (1984); Florsheim (1985); Hey and Thorne (1986); Higginson and Johnston (1988); Kinerson (1990); Lisle and Madej (1992); Smith and Buffington (in press); and present study.

sizes that plot above the threshold prediction imply sediment immobility at bankfull stages. While the bulk of the data lie on or below the solid prediction line, there are a fair number of points above it. Rather than being immobile, an alternative explanation for these upper data is that my choice of τ^*_{c50s} is too high. A lower τ^*_{c50s} value would raise the D_{50s} prediction line, capturing some of the upper data. These upper data exhibit a plateau, indicated by a decline in the density of points at larger grain sizes. A line fit by eye to this plateau corresponds with a τ^*_{c50s} value of about 0.023 (dashed line, Fig. 2.1). If these data are reliable, then $\tau^*_{c50s} \approx 0.023$ presumably represents the natural upper limit of competence for a given bankfull shear stress in coarse-grained channels. In other words, the least sorting and angularity, the greatest protrusion and sphericity, and the least amount of other hydraulic roughness found in natural, coarse-grained channels; consequently maximizing D_{50s} for a given bankfull shear stress.

Because the data presented in Figure 2.1 are synthesized from many different studies, potentially employing slightly different data collection methods, there is some danger in making this empirical fit. It is unlikely that slope is a significant source of error, because most of the studies measured slopes over reasonably long reaches. Admittedly, recognition of bankfull geometry can be problematic (Williams, 1978). Personal experience, however, suggests that field-oriented investigators are usually in agreement about bankfull location; thus, little error is attributed to reported shear stress values. The largest potential source of error is likely due to differences in grain size sampling techniques. Accurate representation of bed grain sizes depends on the sampling strategy employed; as will be seen in Chapter 3, a single sample of limited areal extent can be an extremely poor representation of reach-average grain size in natural coarse-grained streams, as such channels are typically composed of complex and diverse textural patches. Because the grain size sampling error is unknown for the data presented in Figure 2.1, $\tau^*_{c50s} \approx 0.032$, rather than $\tau^*_{c50s} \approx 0.023$, will be retained for the bankfull threshold channel

prediction of D_{50s}. The empirical plateau at $\tau^*_{c50s} \approx 0.023$ is nevertheless intriguing, warranting further, more carefully constrained research of the natural lower limit of τ^*_{c50s} and the upper limit of competence in coarse-grained channels.

Median surface grain sizes that plot on and just below the threshold channel prediction are hypothesized to represent low sediment supply, armored, plane-bed channels in which bed and banks provide all of the hydraulic roughness. Increased sediment supply or the introduction of other roughness elements is expected to cause textural fining and deviation from the prediction. Within this framework, Figure 2.1 indicates that textural response is common in coarse-grained channels; the data do not collapse into a single trend, but rather span about an order of magnitude of median surface grain sizes for a given shear stress.

Further examination of Figure 2.1 shows that beyond shear stresses of about 70 Pa in coarse-grained channels there is a decrease in the range of median surface grain sizes and a general lack of data around the threshold prediction line. Assuming that the plotted data for channels with depth-slope products in excess of 70 Pa are typical, then there is presumably some characteristic change in sediment supply or hydraulic roughness for these channels, as was suggested for the sand-bedded rivers. Since the magnitude of total boundary shear stress is generally dominated by slope, the channels with shear stresses in excess of 70 Pa are likely to be steep gradient plane-bed channels, approaching cascade and step-pool morphologies in the terminology of Montgomery and Buffington (1993). Although steep-gradient channels are characteristically high energy environments, much of the available shear stress is turbulently dissipated by tumbling or jet-and-wake flow caused by individual large grains or grain clusters. Consequently energy dissipation characteristic of steep-gradient channels may lead to smaller median surface grain sizes due to less available bed shear stress and may explain the leveling-off of median surface grain sizes observed in Figure 2.1.

TEXTURAL RESPONSE TO SEDIMENT SUPPLY

Several data sets exist that can be used to examine textural response to sediment supply within the framework of the bankfull threshold channel model. Flume experiments by Kuhnle and Southard (1988) and Dietrich et al. (1989) both document surface fining of laboratory plane-bed channels with increased sediment loads. Both studies found that low sediment supplies produced armored beds, while extreme sediment loading created surface textures similar to the size distribution of the supplied sediment ($q^*=1$). Within the threshold model framework the low sediment supply armored beds from these two studies plot close to the threshold channel prediction line and have lower q^* values (Fig. 2.2), while increasing sediment supply produces finer surface textures that progressively deviate from the threshold prediction and have higher q^* values. Thus with increasing sediment load there is a systematic surface textural fining and deviation from the bankfull threshold channel prediction.

As mentioned previously, textural response to sediment supply within the threshold model construct is simply another way to express the q^* theory. By definition a q^* of 0 corresponds with the threshold channel prediction. However, because the surface and subsurface critical shear stresses are back-calculated from Shields' equation [i.e., (2)] the resultant q^* values depend on the τ^*_{c50s} value used, as illustrated by Figures 2.2a and 2.2b. Furthermore, while the magnitude of q^* increases with deviation from a given threshold prediction, the gradient of q^* values with this deviation depends on the ratio of τ_0/τ_{c50ss} [i.e., (6)]. For example, because τ_0/τ_{c50ss} is different in the two flume studies (Dietrich et al., 1989), their q^* values are not necessarily the same for similar deviations from the threshold prediction; in the study by Dietrich et al. (1989) a q^* value of 1 is approached with significantly less deviation from the threshold prediction (Fig. 2.2). The

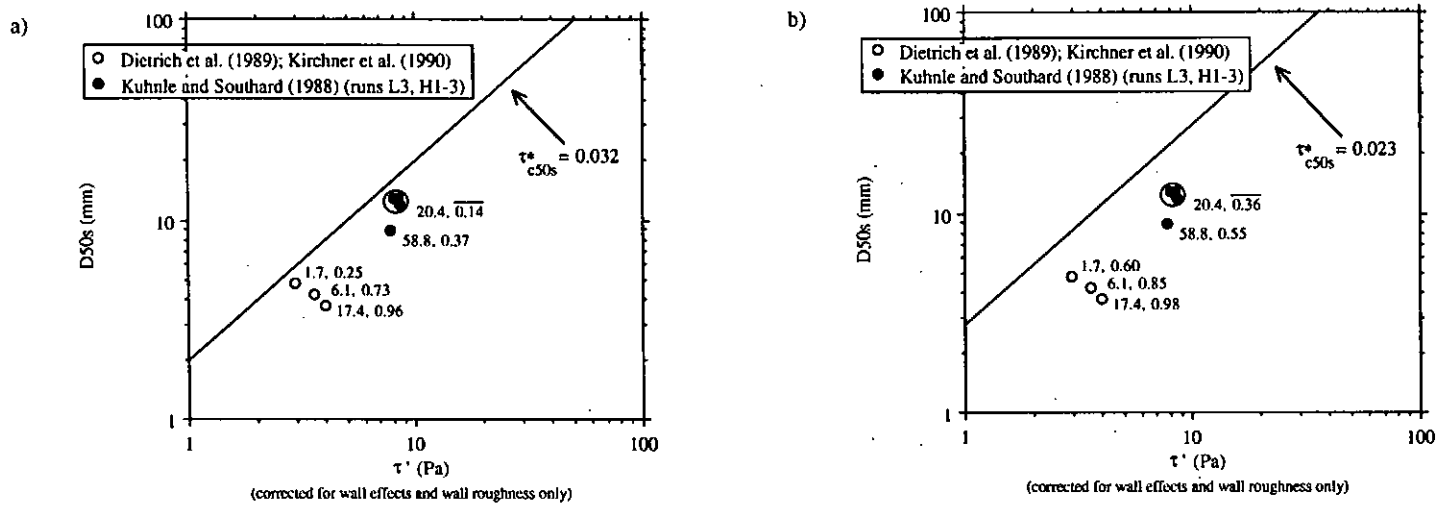

Figure 2.2 Systematic deviation of D_{50s} from the threshold model prediction [a) τ^*_{c50s}=0.032, b) τ^*_{c50s}=0.023] as a function of increasing sediment volume supplied to laboratory plane-bed channels. τ' is the cross-sectionally-averaged total boundary shear stress corrected for sidewall effects using the method of Shimizu (1989), assuming a bed roughness 100 times that of the flume walls (see also discussion of sidewall effects in Chapter 3 Methods and Fig. 3.4 caption). Numbers next to plotted points are sediment feed rates (g/min•cm) followed by q* values calculated from (6) with $\tau_0=\tau'$ and $\tau_{c50}=\tau^*_{c50s}(\rho_s-\rho)gD_{50}$, assuming ρ=1000 kg/m^3 and ρ_s=2650 kg/m^3; τ_{c50s} and τ_{c50ss} values are calculated using respective median grain sizes of the bed surface material and sediment feed as reported by Kirchner et al. (1990, Table 2) and Kuhnle and Southard (1988, Figs. 2 and 14). Only data from plane-bed morphologies are plotted; bedload sheets (Whiting et al., 1988) within plane-bed channels are considered unobtrusive "bedforms."

ratio of τ_0/τ_{c50ss} is the theoretical critical shear stress of a fully armored channel relative to that of a completely unarmored channel. As such, this ratio expresses the theoretical potential for textural response, with lower values indicating less response potential. For a given depth-slope product the ratio of τ_0/τ_{c50ss} is largely a function of the imposed sediment supply distribution. Consequently the gradient and lower limit of textural response (D_{50ss}) expressed by the q* theory cannot be predicted theoretically, because the input sediment supply distribution at any given point in a channel network is a stochastic function of basin geology, geomorphology, and climate; D_{50ss} and the ratio of τ_0/τ_{c50ss} must be determined by field investigation. While the ratio of τ_0/τ_{c50ss} provides an indication of a channel's overall potential for textural change, the current degree of textural response to sediment supply must be evaluated by other means, such as q*.

Once textural fining has occurred in response to increased sediment supply a channel no longer exhibits bankfull threshold mobility, as smaller D_{50s} values imply a lower threshold of mobility. It is hypothesized that extreme textural response to sediment supply can create mobility thresholds low enough that the channel begins to behave more like a live-bed channel (e.g., Reid and others' (1985) Turkey Brook site discussed in Chapter 1). However, extreme changes in sediment transport characteristics of this sort depend on the ratio of τ_0/τ_{c50ss}. For example, a low τ_0/τ_{c50ss} ratio limits the range of textural fining and thus the range of critical shear stresses, while for a high ratio of τ_0/τ_{c50ss} there is a much broader range of both potential textural fining and corresponding critical shear stresses. Consequently channels with high τ_0/τ_{c50ss} ratios are more likely to behave like live-bed channels in response to extreme sediment loading. High τ_0/τ_{c50ss} ratios can be natural or induced by management activities, such as road building and use, that increase the proportion of fine sediment supplied to a channel (e.g., Reid and Dunne, 1984), hence lowering D_{50ss} and τ_{c50ss}.

Kinerson (1990) documented sediment-induced textural fining in natural channels in northern California and validated the use of q* as an indicator of sediment loading. He examined channels with a variety of sediment loading conditions and chose sample sites in straight sections of the channel with low-amplitude bedforms and away from in-channel obstructions. Sample sites were chosen in this fashion so as to minimize hydraulic roughness other than grain roughness. He found that channels with low sediment supplies had low q* values, while sediment-impacted channels had q* values near 1. With the exception of one point, Kinerson's (1990) data show the same systematic deviation of surface textures from the threshold channel prediction with increasing q* and hence sediment supply (Fig. 2.3). However, the sediment loading conditions inferred from Kinerson's (1990) q* values were substantiated in some cases by fairly qualitative assessments of sediment supply.

Application of results from a study by Lisle and Madej (1993) imply that q* was not a good indicator of sediment loading in a comparison of aggrading (high sediment supply) and degrading (low supply) reaches of a northern California stream. Lisle and Madej's (1993) negative results may be due to neglecting differences in bedform roughness between the two study reaches.

With q* as a surrogate for sediment loading, the field and laboratory studies discussed above are combined in Figure 2.4 in order to emphasize the systematic textural fining and deviation from the threshold channel prediction of median surface grain size with increasing sediment supply. These data show that textural fining in response to sediment supply can be quite significant, resulting in a minimum ratio of observed-to-predicted D_{50s} of about 0.1, or a ten-fold decrease in D_{50s}. Figure 2.4 also demonstrates that similar q* values can correspond to different magnitudes of textural fining, where fining is expressed as the ratio of observed-to-predicted median surface grain size. At low sediment supplies

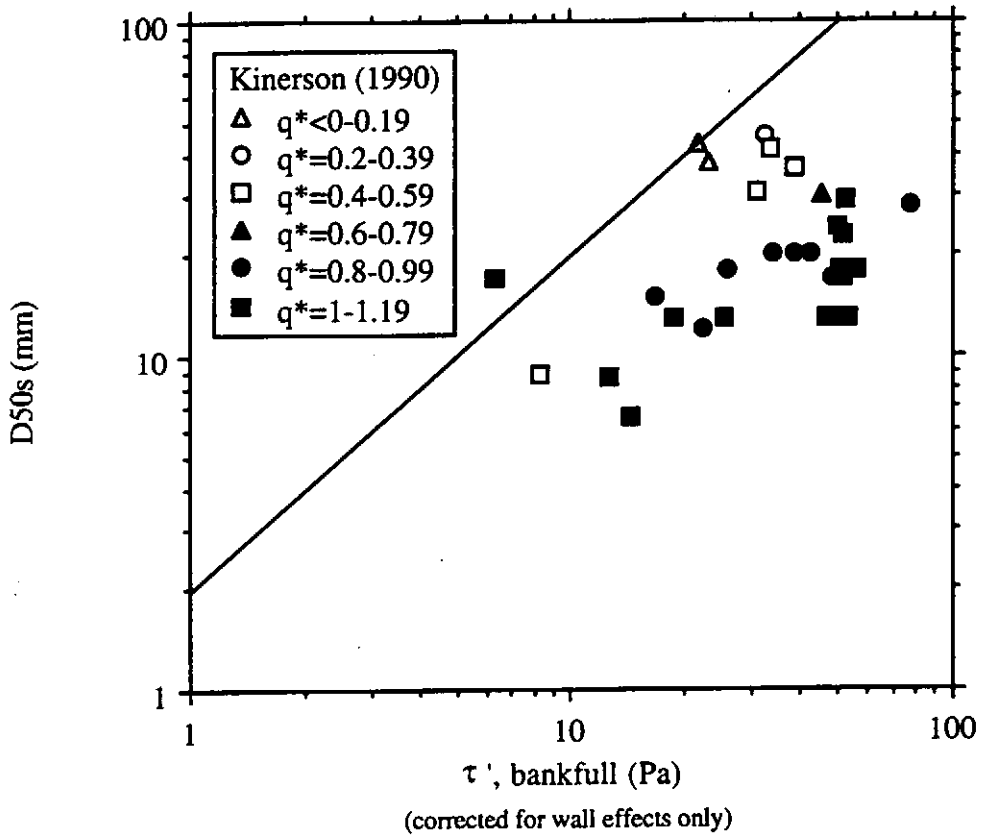

Figure 2.3 Textural fining and deviation of D_{50s} from the threshold model prediction as a function of increasing sediment supply in natural gravel-bedded channels. τ' is the cross-sectionally-averaged total boundary shear stress corrected for sidewall effects using the method of Shimizu (1989), assuming uniform bed and bank roughness length scales. q^* values are determined with τ^*_{c50s}=0.032 as per Figure 2.2 caption.

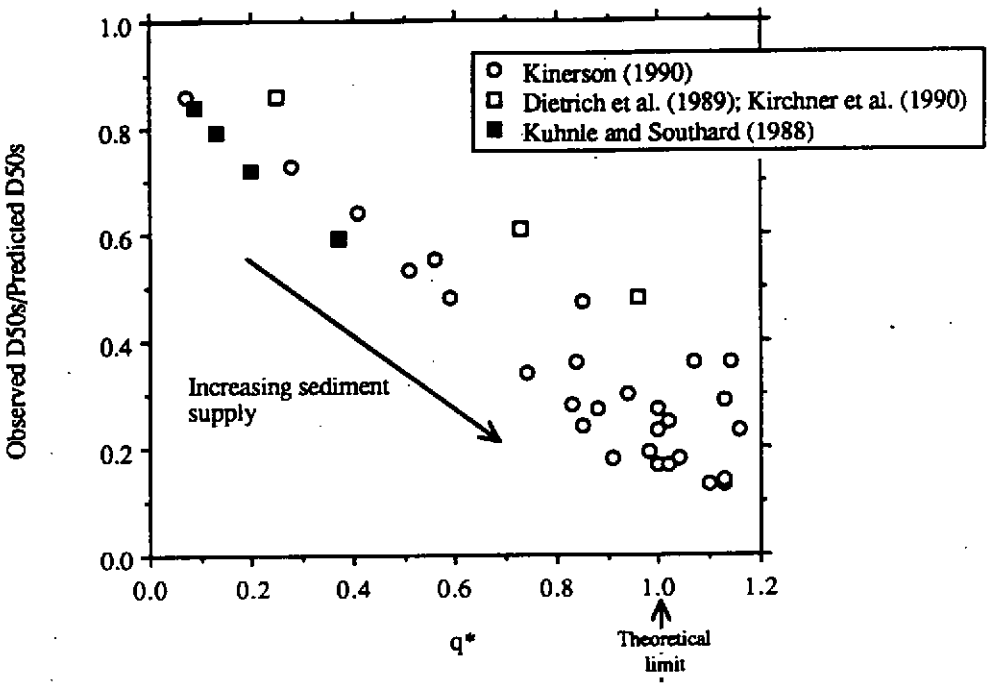

Figure 2.4 q* versus the ratio of observed-to-predicted D_{50s} in both natural and laboratory channels. The ratio of observed-to-predicted D_{50s} is inversely related to q*, and thus sediment supply. The D_{50s} ratio is not unique for specific q* values, having a range of up to 0.3 units for a given q*.

(i.e., q* near zero) the ratio of observed-to-predicted D_{50s} is close to one in natural channels, indicating that the bankfull threshold model accurately predicts the median grain size of a fully armored channel. The bankfull threshold model thus provides a significant contribution to the q* theory in that it defines the critical shear stress corresponding to the limit of textural coarsening in gravel-bedded channels. As originally proposed (Dietrich et al., 1989), the q* equation did not specify a characteristic boundary shear stress; that is, q* was expressed in terms of a generic boundary shear stress, rather than in terms of the bankfull boundary shear stress, τ_0, as in (6).

Although previous investigation of the q* theory has been limited, results from such studies generally validate its use as an indicator of sediment supply, provided that other roughness effects are accounted for. This later point is an important clause that Kinerson (1990) recognized, but that has not been fully explored. Surface textural response due to hydraulic roughness in forest gravel-bedded streams is examined in the next chapter and a preliminary analysis of relative magnitudes of influence caused by sediment supply and hydraulic roughness is presented. These results provide some insight into typical ranges of roughness correction necessary for q* analyses in forest channels.

Chapter 3: Field Study of the Effects of Hydraulic Roughness on Gravel-bed Surface Textures

A field study of forest gravel-bedded rivers was conducted in order to document textural response to other types and scales of hydraulic roughness. Detailed morphologic information was collected, but the principal intent was a reach-average comparison of textural response in channels characterized by distinctly different roughness elements. Investigation of in-channel roughness features was limited to roughness caused by bed surface particles, bedforms, and LWD. Three distinctly different channel types were examined that showed increasing complexity of roughness: plane-bed channels; pool-riffle channels with minimal amounts of LWD; and LWD-rich pool-riffle channels (Fig. 3.1). These three channel types represent a progressive cumulation of particle, bedform, and LWD roughness.

Forty-one gravel-bedded channels were studied in forest environments of northwestern Washington and southeast Alaska. Infrequent, catastrophic sediment inputs from hollow failures and resultant debris flows are characteristic of this steep, mountainous terrain. Although sediment loading of the study sites was not quantified, channels exhibiting evidence of recent catastrophic sediment impacts were avoided. Evidence for such impacts includes: recent landslide tracks entering a channel; fresh debris flow levees, and riparian vegetation inundated by debris flow deposits; in-channel LWD that is predominantly buried by alluvium; pools with low residual depths and largely filled by fine sediment (Lisle and Hilton, 1992); bar-riffle topography conspicuously lacking pools; wide, shallow channels with width-to-depth ratios anomalously larger than adjacent upstream and downstream reaches and in some instances accompanied by braiding; and riffles covered by extensive sand stripes and drapes (Lisle and Hilton, 1992). Evidence for

a1)

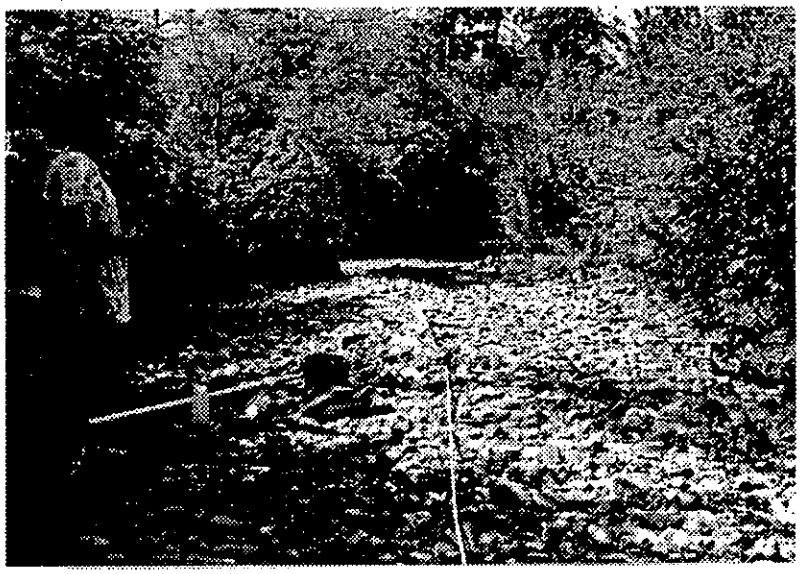

a2)

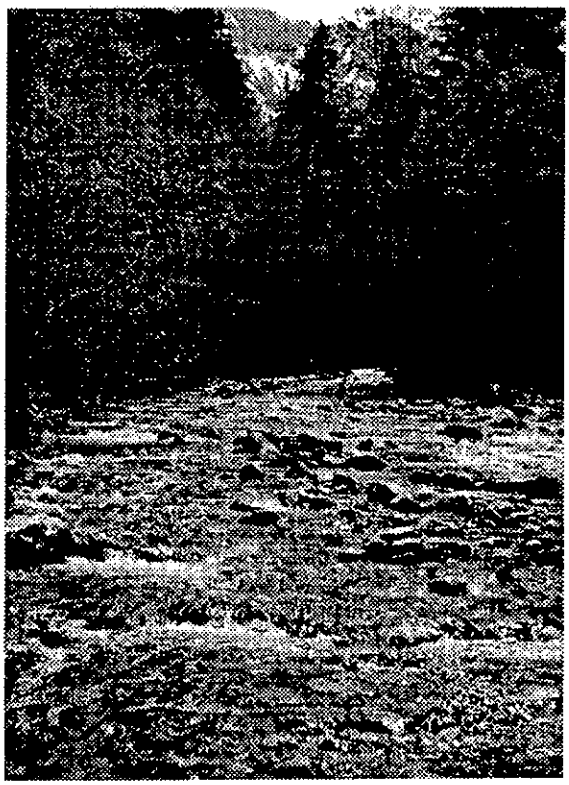

Figure 3.1 Photographs of typical a) plane-bed, b) LWD-poor pool-riffle, and c) LWD-rich pool-riffle forest channels of the Pacific Northwest and southeast Alaska.

b1)

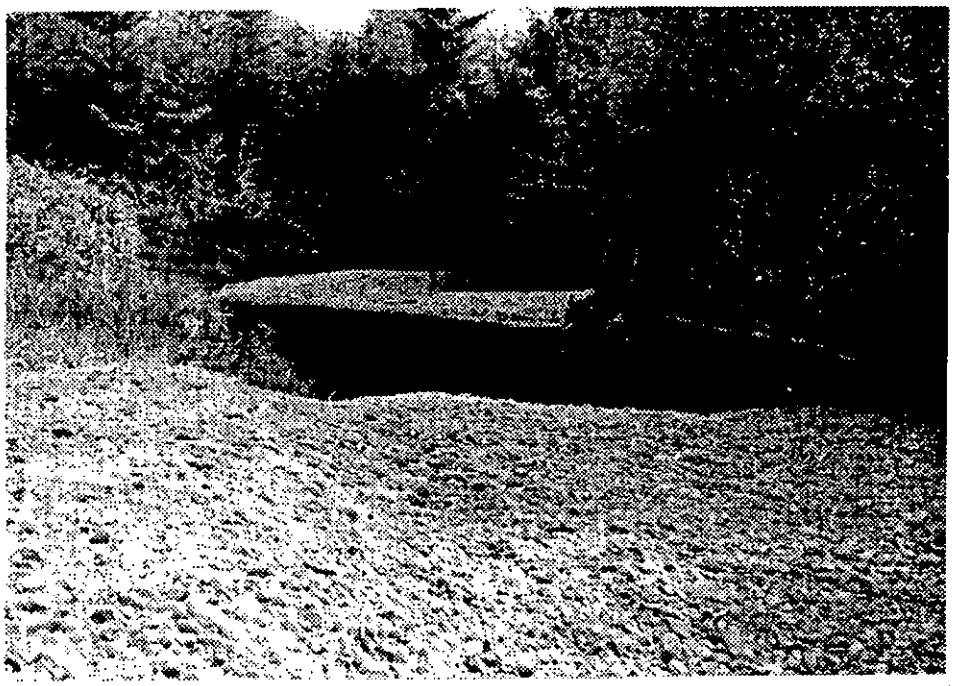

b2)

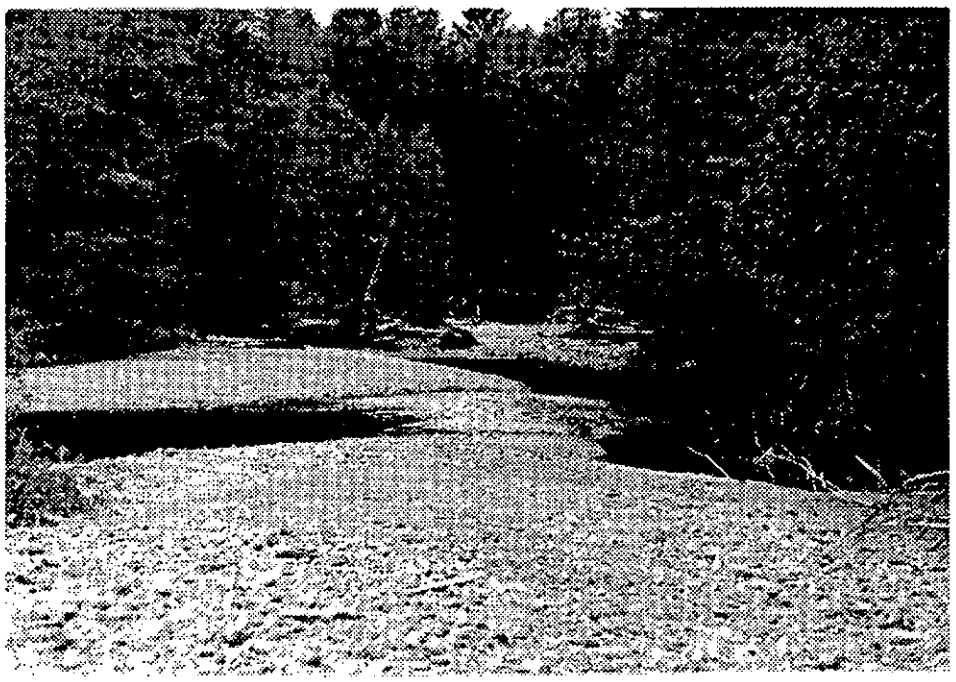

Fig. 3.1 cont.

c1)

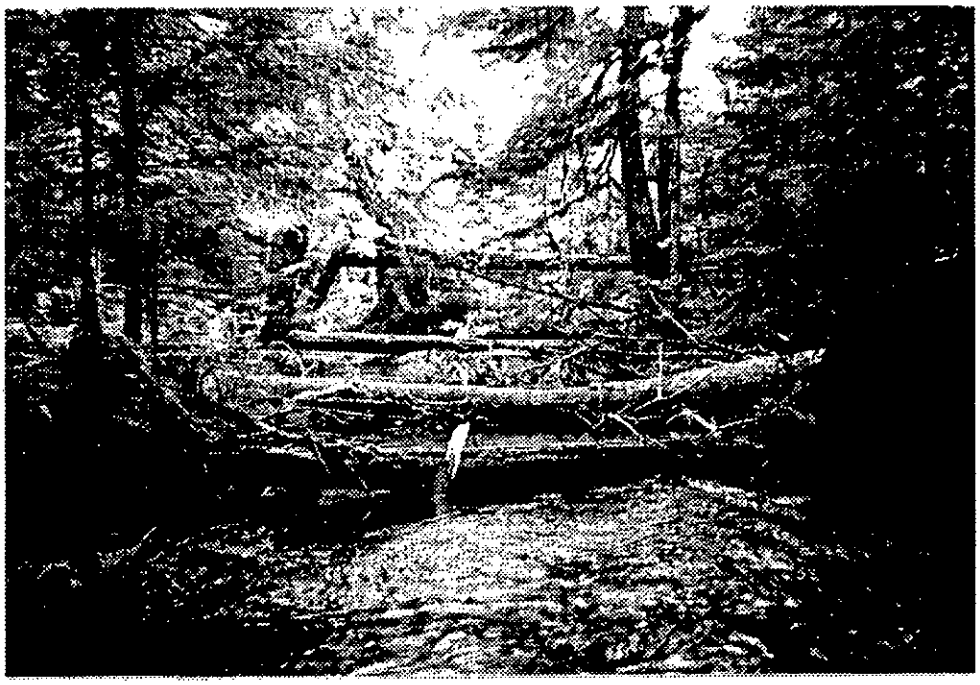

c2)

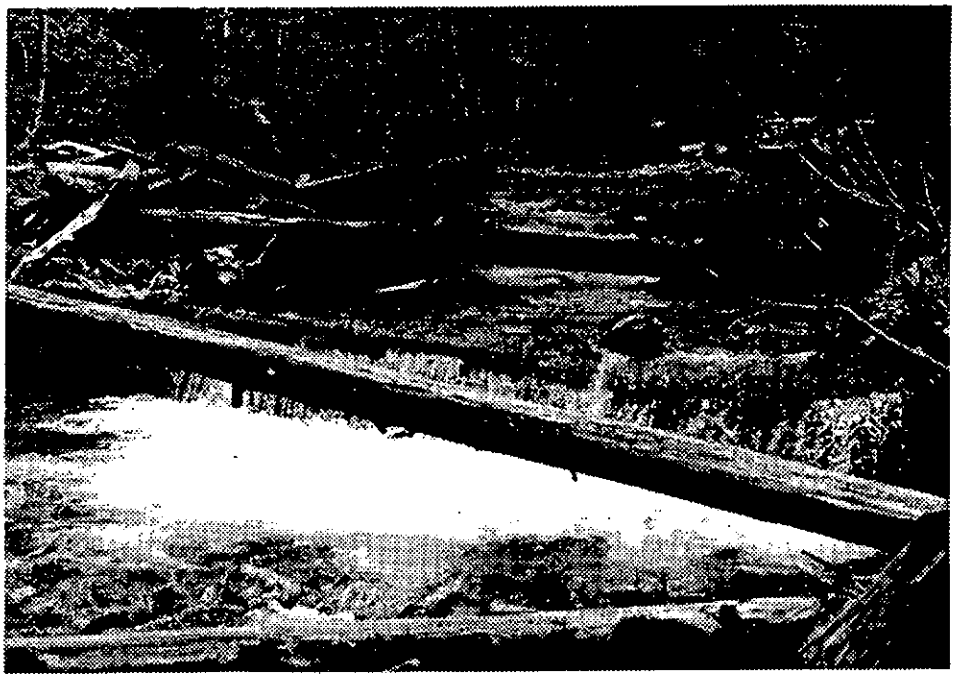

Figure 3.1 cont.

significant sediment impacts of this sort was only observed in five of the forty-one study sites. Levels of sediment loading at the remaining sites was likely variable, but not orders of magnitude different. The sediment-impacted channels, however, will be given special consideration in the following analysis:

STUDY SITES

Fourteen channels were studied on the Olympic Peninsula of northwestern Washington (Fig. 3.2). The Peninsula is characterized by mountainous terrain and a coastal rain forest of Sitka spruce (*Picea sitchensis*), western hemlock (*Tsuga heterophylla*), red cedar (*Thuja plicata*), and Douglas fir (*Pseudotsuga taxifolia*). Bedrock geology of the Peninsula is predominantly composed of marine basalts and sediments of Eocene to Miocene age accreted onto the North American plate (Tabor and Cady, 1978a; b). The Peninsula is divided into two terrains: the peripheral rocks, interlayered marine basalts and sediments forming an easterly concave arc believed to have resulted from subductive accretion pinned between older terrains of Vancouver Island and the Cascades (Tabor, 1975); and the core rocks, accreted lithic assemblages of predominantly marine sediments that have been sheared, folded, and metamorphosed to varying degrees within the confine of the basaltic peripheral rocks (Tabor and Cady, 1978a; b). All of the Olympic channels surveyed in the current study lie in watersheds influenced by Pleistocene glaciation (either alpine or continental) and are typically incised into fluvioglacial deposits. The northern study channels flow through an area exposed to repeated advances and retreats of continental ice. Lithologies associated with each channel are listed in Table 3.1, based on mapping by Tabor and Cady (1978a).

Logging activity on the Olympic Peninsula is generally intensive, with some forests on their third rotation. Due to recent progressive management practices most study sites

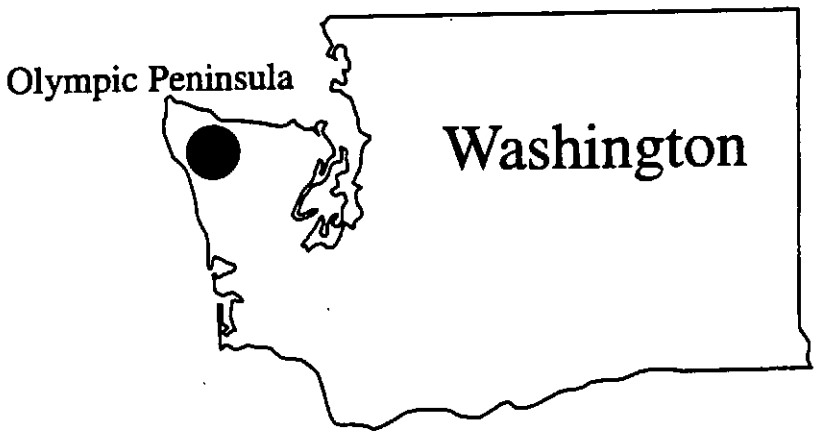

Figure 3.2 Location map of the Olympic study sites.

TABLE 3.1: Rock Types Associated with Olympic Study Sites

	Proximal to channel	Headwaters
Channel		
Lower Dry Creek	1	5
Upper Dry Creek	1	5
Alder Creek	1	4
Lower S Fork Hoh Slough	1	3, 4, 5
Upper S Fork Hoh Slough	1	3, 4, 5
Lower Pins Creek	1	1
Upper Pins Creek	1	1
Cedar Creek	1	1
Hoko River	2	4, 6, 7
Hoko Tributary	2	4
Lower Skunk Creek	2	4
Upper Skunk Creek	2	4
Flu Hardy Creek	2	4
Mill Creek	4	4

Key:

1) Pleistocene alpine glacial deposits of gravel, sand, silt, and clay.
2) Pleistocene glacial gravels, sand, silt, and clay deposited from continental ice sheets. Characterized by xenolithic clasts.
3) Sandstone and conglomerate [undifferentiated Tur unit of Tabor and Cady (1978a), Eocene(?) to Miocene (?)].
4) Sandstone and conglomerate [Tabor and Cady's (1978a) Two unit of Western Olympic Lithic Assemblage, Eocene to Oligocene].
5) Slate and Phylite (Tabor and Cady's (1978a) Twos unit of Western Olympic Lithic Assemblage).
6) Eocene sandstone and siltstone [unnamed Tusb unit of Tabor and Cady (1978a)].
7) Eocene basalt [Tcb unit of Crescent Formation (Tabor and Cady (1978a)].

had riparian buffers composed of mixed shrub and conifer, however some study sites had been clear cut to channel margins, resulting in riparian forests of mixed shrub and red alder (*Alnus rubra*). Coniferous buffers were typically not pristine old growth, indicating a long history of management disturbance. Hillslope failures are common in the Peninsula and are attributed to timber harvesting and subsequent reduction of root strength in topographic hollows. Relict debris flow deposits form channel-margin terraces in one of the pool-riffle channels studied and indicate both long runout paths and the potential for periodic large sediment inputs. A more recent debris flow disturbed one of the plane-bed channels, leaving riparian vegetation inundated with alluvium. Most of the channels studied had banks composed of fluvioglacial clays, silts, sands, and gravels, providing a readily accessible sediment source.

The Olympic data were further supplemented by data from 27 coastal channels of the southeast Alaskan Alexander Archipelago (Fig. 3.3). These data were collected by the US Forest Service as part of a morphologic comparison of pristine and heavily disturbed watersheds (Smith and Buffington, in press). An important difference between the two land use types investigated in southeast Alaska is that the pristine channels were characterized by high LWD loading, while the disturbed channels were generally clear cut to the stream banks and had most or all of their in-channel LWD removed. The Alaskan channels are of particular relevance to the current study because of the spectrum of LWD loading that they provide, and thus the potential range of textural response. The majority of the Alaskan channels are pool-riffle-type, but four of them are transitional between pool-riffle and plane-bed. Two of the study sites are downstream of recent large landslides. One other study site has also had recent landslide input, but of a lesser magnitude.

The southeast Alaskan study areas are characterized by steep glaciated terrain, maritime climate, and rain forests predominantly composed of Sitka spruce (*Picea*

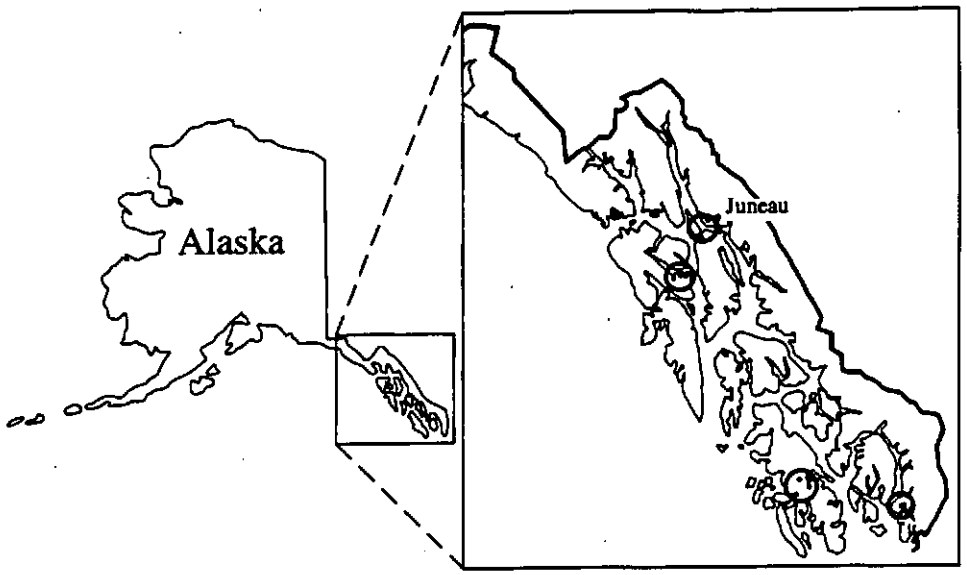

Figure 3.3 Location map of the southeast Alaskan study sites.

sitchensis) and western hemlock (*Tsuga heterophylla*). Hillslopes are commonly grooved by avalanche chutes and hollow failures. The geology of southeast Alaska is characterized by all major rock types of ages ranging from Proterozoic(?) to Quaternary (Gehrels and Berg, 1992), largely accreted during the Cretaceous to Eocene (Goldfarb et al., 1988; Gehrels et al., 1990). Lithologies associated with study sites are listed in Table 3.2, based on generalized mapping by Gehrels and Berg (1992) and personal observation. Many of the waterways of the Alexander Archipelago are fault controlled and were previously occupied by massive glaciers. The entire Archipelago was profoundly influenced by Pleistocene glaciation, with only the highest peaks exposed during the glacial maximum (Reed, 1958). Isostatic rebound following glacial retreat continues today and emergent marine terraces are common. Unlike the Olympic channels, however, the Alaskan study sites are devoid of glacial deposits.

METHODS

Olympic Study Sites

Bankfull channel widths were measured at 10 m intervals in order to iteratively establish reaches that were ten channel widths long. Average bankfull geometries were determined from surveys of three cross sections per reach, and a center-line survey of bed topography was used to approximate the energy slope. For each of the study sites detailed topographic, textural, and LWD maps were constructed using a total station digital theodolite. Bed topography was contoured with Surfer®; various contouring techniques, search patterns, and search radii were tested, with the most accurate representation of channel topography produced from a Kriging technique. Mapped surface textures were used to determine spatially averaged grain size characteristics of each reach and to relate textural patterns to bed topography and LWD.

TABLE 3.2: Rock Types Associated with Southeast Alaskan Study Sites

Channel	*Basin Geology*
12 Mile Creek 1	pre-Ordovician metasediments and metavolcanics
12 Mile Creek 2	"
Maybeso Creek 1	Silurian to Ordovician sediments and volcanics
Maybeso Creek 2	"
Maybeso Creek 3	"
Maybeso Creek 4	"
Cable Creek	Silurian to Ordovician volcanics
Fubar Creek 1	Silurian to Ordovician sediments and volcanics
Fubar Creek 2	"
Indian Creek	Silurian to Ordovician volcanics
Muri Creek	Devonian volcanics and (?) Silurian syenite and trondhjemite
Bambi Creek	Cretacious granodiorite and Devonian and Ordovician sediments and volcanics
Upper Weasel Creek 2	Cretacious to Permian sediments and volcanics
Lower Greens Creek	Triassic to Ordovician sediments and volcanics
Hook Creek	Devonian to Ordovician sediments and volcanics (dacite with phenocrysts of cruciform amphibole) and (?) Silurian syenite and trondhjemite
Trap Creek 1	Silurian carbonates
Trap Creek 2	"
Trap Creek 3	"
Trap Creek 4	"
Trap Creek 5	"
Trap Creek 6	"
East Fork Trap Creek 1	"
East Fork Trap Creek 2	"
Fowler Creek 1	Cretacious to Jurassic sediments
Fowler Creek 2	"
Lower Fish Creek	Cretacious to Jurassic sediments and volcanics
Upper Fish Creek	"

Initial reconnaissance of each stream was conducted to visually identify and partition surface textures. Textures were differentiated according to the method used by Kinerson (1990) and Collins (unpub.), which involves identifying the characteristic grain size(s) of a given patch according to approximate standard grain size divisions [i.e., Wentworth (1922) as modified by Church et al. (1987)]. For example, patches might be distinguished as: sand and gravel; gravel and small boulder; cobble, gravel, and sand; etc. In my particular application the order of the adjectives used to describe a patch indicates the visual abundance. Transitions between textures are often quite subtle, but resultant mapping error is believed to be small. After surface textures were visually partitioned a random pebble count of 100 grains (Wolman, 1954) was conducted over one or more of each identified textural type. Sampling of every textural patch was prohibitive due to complexity of their spatial distribution within a given channel. Consequently a single pebble count was generally conducted for each textural type and assumed representative of other visually similar textural patches. Error associated with this assumption was examined in some channels by sampling several textural patches of the same type. Sampled patches were chosen randomly, and the entire area of a given patch was covered in the sampling.

Subsurface sampling was also conducted in order to establish theoretical limits of textural fining as expressed by the q* theory. Samples were collected from a 1 m^2 area within textural patches that had been pebble counted. The surface layer was excavated by hand and shovel to a depth equal to or greater than the surface D_{84} (Church et al., 1987), and the underlying material was dry sieved to determine the subsurface grain size distribution. It is commonly accepted that subsurface bulk sieving is a sampling technique equivalent to pebble counting (Kellerhals and Bray, 1971; Diplas and Sutherland, 1988), allowing direct comparison of surface and subsurface samples.

Several studies have been conducted to determine the volume of material needed to adequately represent the subsurface grain size distribution (Church et al., 1987; Diplas and

Fripp, 1992; Wolcott and Church, 1991), with the common statistical requisite that the sample should be large enough to capture the relatively fewer coarse grains, but not be biased by those large grains. Church et al. (1987) proposed that a good representation of the subsurface grain size distribution was achieved when the largest clast comprised 0.1% of the sample weight; however, they recognized that for coarse material the requisite sample volume would be enormous and suggested a 1% criterion. Because a field scale was unavailable I employed a sampling technique using fixed volumes in which 1 to 3 10 ℓ buckets were sampled depending on the maximum surface grain size, D_{maxs}, of a given textural patch. Assuming equivalence of surface and subsurface grain size ranges, D_{maxs} was used to estimate the requisite subsurface sample volume using the following ranges:

10 ℓ: $D_{maxs} \leq 58$ mm
20 ℓ: 58 mm $< D_{maxs} \leq 73$ mm
30 ℓ: $D_{maxs} > 73$ mm

where D_{maxs} values of 58 and 73 mm respectively represent 1% of the weight of 10 and 20 ℓ volumes assuming spherical grains of ρ_s=2650 kg/m^3 and a voidless sample volume. For ideal samples of this sort, the weight percent of D_{maxs} is ≤1%, but >1% for 30 ℓ samples with D_{maxs}>83 mm, as 30 ℓ was the maximum sample volume collected regardless of D_{maxs}. The 1 m^2 sample area was divided into three strips perpendicular to channel flow and one strip was randomly sampled for the first 10 ℓ bucket. Subsequent 10 ℓ volumes for a given sample were collected in an analogous fashion but from progressively greater depths. Each 10 ℓ sample was analyzed separately to examine grain size variation with depth.

Initially each 10 ℓ volume was field sieved by hand using standard, square-mesh, 8" diameter sieves. Samples were sieved in half phi intervals and grain sizes less than 8 mm were split according to ASTM (1985) standards and taken for further laboratory

sieving. Grain weights of clasts between 8 and 45 mm were determined in the field by volume displacement in a graduated cylinder, assuming ρ_s=2650 kg/m^3. This method is based on a technique developed by Booth et al. (1991). Samples of grains weighed in this fashion were taken for laboratory analysis to determine true densities in order to correct field estimates of weight. Weights of grains larger than 45 mm were calculated from intermediate diameter measures, assuming a spherical grain shape with ρ_s=2650 kg/m^3. Subsurface sampling conducted later in the field season involved collection of whole 10 ℓ samples for subsequent laboratory analysis. In the laboratory, grains larger than 45 mm were separated by hand and binned at half phi intervals based on intermediate diameter measures. The remaining sample was dry sieved at half phi intervals using a Ro-Tap® shaker. All grain weights were measured to 0.1 g using a standard, pad-sensor, laboratory scale.

Reach-average depth-slope products of both the Olympic and Alaskan sites were corrected for wall effects using theoretical findings of Shimizu (1989). Wall effects are examined in the current analysis purely as a function of channel geometry, assuming a uniform roughness of bank and bed material. Channel geometry significantly affects boundary shear stress distribution and average flow velocity (Lundgren and Jonsson, 1964; Williams, 1970; Hey, 1979; Knight, 1981; Knight et al., 1984; Flintham and Carling, 1988; Shimizu, 1989). For obstruction-free, straight, plane-bed channels with large width-to-depth ratios, flow is commonly assumed to be two dimensional and shear stress at the bed is well approximated by the total depth-slope product. Turbulence caused by momentum differences between the channel center and margins causes flow to become progressively more three dimensional for increasingly lower width-to-depth ratios, effectively transferring a portion of the total boundary shear stress to the channel walls (Parker, 1978b) and reducing the accuracy of the depth-slope product to approximate bed

shear stress. In practice, wall effects are assumed negligible for W/h ≥ 11-13, for which case bed shear stresses are approximately 90% of the depth-slope product (Flintham and Carling, 1988). Wall effects are more formally assessed in this analysis through graphical determination (Fig. 3.4) based on results of Shimizu's (1989) theoretical calculations. Shimizu's (1989) estimates of τ_w are preferred as they are based on theoretical reasoning, as opposed to other more empirical methods (e.g., Williams, 1970; Knight, 1981; Flintham and Carling, 1988).

Because the bankfull threshold model examines mobility of bedload material, the suspended load component must be removed from measured surface and subsurface grain size distributions. To this end a modified version of the approach taken by Kinerson (1990) in examining the q* theory was employed. The largest suspendable grain size at bankfull flow, D_{sus}, was calculated from results of Dietrich's (1982) settling velocity study (Fig. 3.5), assuming a Corey shape factor (CSF) of 0.7 for natural sediments (Dietrich, 1982), ρ_s=2650 kg/m^3, ρ=1000 kg/m^3, ν=10^{-6} m^2/s, and w_s=u*, where w_s is the grain fall velocity; in Figure 3.5 w* and D* are dimensionless values of grain fall velocity and size. Shear velocities are calculated here from wall-corrected total shear stresses as $u^*=\sqrt{(\tau_0-\tau_w)/\rho}$. With calculated values of w*, D* values were read from Figure 3.5, allowing determination of $D_{sus}=D_n$. Grain sizes less than or equal to D_{sus} were removed from grain size measurements and distributions were recalculated. Examination of textural response to other hydraulic roughness elements using grain size distributions corrected in this fashion is, however, paradoxical, as accurate calculation of D_{sus} requires use of τ' and thus knowledge of shear stress dissipation caused by hydraulic roughness features. Because D_{sus} is calculated here using $\tau'=\tau_0-\tau_w$ (neglecting τ_f, τ_l, and any other sources of shear stress dissipation), D_{sus} values are likely overestimated for all but the plane-bed channels. The resultant magnitude of error in determining D_{50s} and D_{50ss} cannot be predicted as the

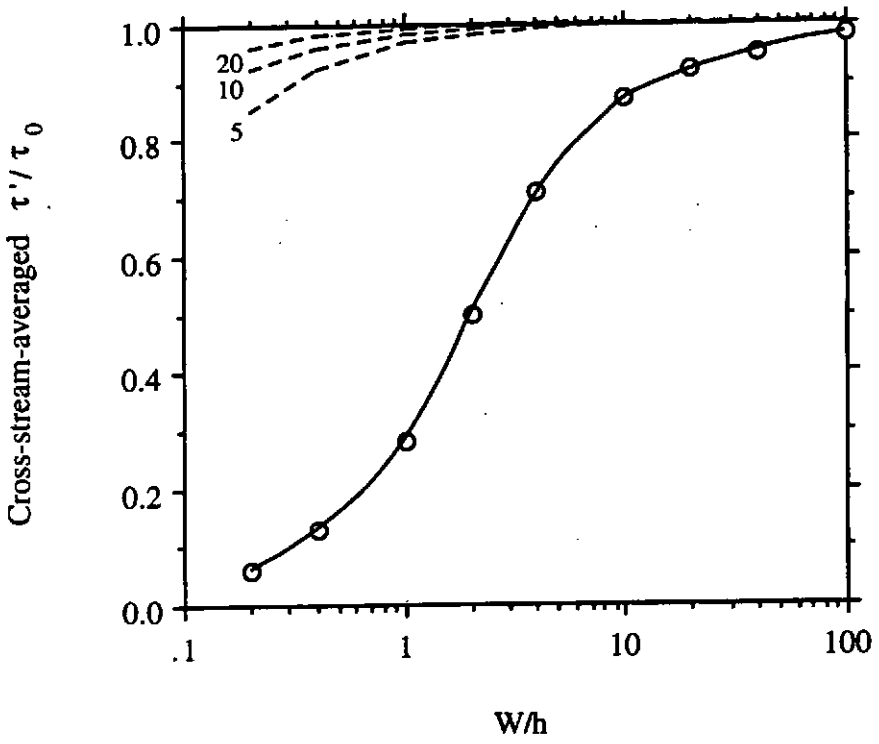

Figure 3.4 Calculated cross-stream-averaged ratio of effective shear stress to total shear stress (i.e., τ'/τ_0) as a function of channel width-to-depth ratio in a straight, unobstructed, rectangular, plane-bed channel. Re-drawn from Shimizu's (1989) Figure 8c for uniform bed and wall roughness length scales. Williams' (1970) sidewall correction factor is also shown (dashed lines, with numbers indicating channel width) and is seen to be trivial compared to Shimizu's (1989). Williams' (1970) correction factor applies to centerline shear stress (as opposed to cross-sectionally-averaged) and was measured under conditions in which sidewalls were considerably smoother than the bed surface; both of which result in smaller sidewall correction factors [cf. Shimizu's (1989) Fig. 8a-c] that are inappropriate for cross-sectionally-averaged shear stresses of channels with significant wall roughness.

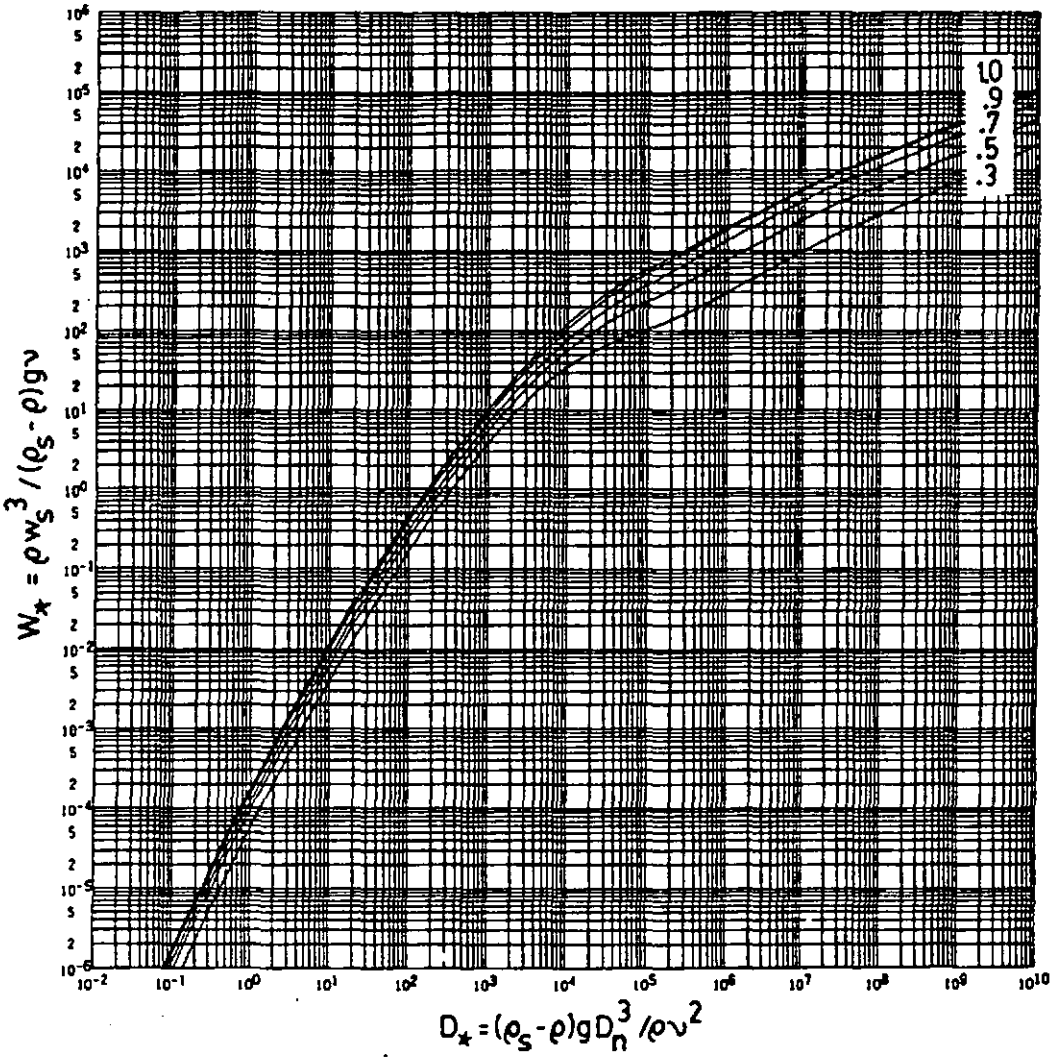

Figure 3.5 Dimensionless grain settling velocity versus dimensionless grain diameter. Taken from Dietrich (1982).

error is dependent on the specific character (i.e., range, skew, and kurtosis) of a given grain size distribution. Nevertheless, potential overestimations of D_{sus} will have a conservative effect on assessment of textural response to sediment supply and hydraulic roughness elements, as overestimated D_{sus} values will increase D_{50s} and D_{50ss}, reducing the magnitude of grain size deviation from model predictions.

Alaskan Study Sites

A variety of information was collected in the Alaskan field study and is detailed elsewhere (Smith and Buffington, 1990; in press), while the information relevant to the current investigation is briefly reported here. Five cross sections and a center-line bed profile were surveyed with an engineer's level over study reaches that were generally 20 channel widths long. At each cross section a bank-to-bank random pebble count of 100 grains was conducted. Because the Forest Service data were collected for study purposes other than the current investigation there are differences in the way reach-average grain sizes were determined; spatial averaging of mapped textures (Olympic) versus averaging discrete cross-channel areas sampled at fixed intervals (Alaskan). It is assumed, however, that the two sampling techniques are comparable. This assumption will be further examined later in the chapter.

Channels were segregated by land use history in the Forest Service study (Smith and Buffington, in press). Here, however, I am more interested in differences in wood loading and subsequent potential influences on surface textures. Although pristine and managed land use types can be discriminated based on wood loading (Smith and Buffington, in press), on the whole the Alaskan channels exhibit a continuum of LWD loading. Figure 3.6 illustrates this continuum and is used to segregate debris-poor from

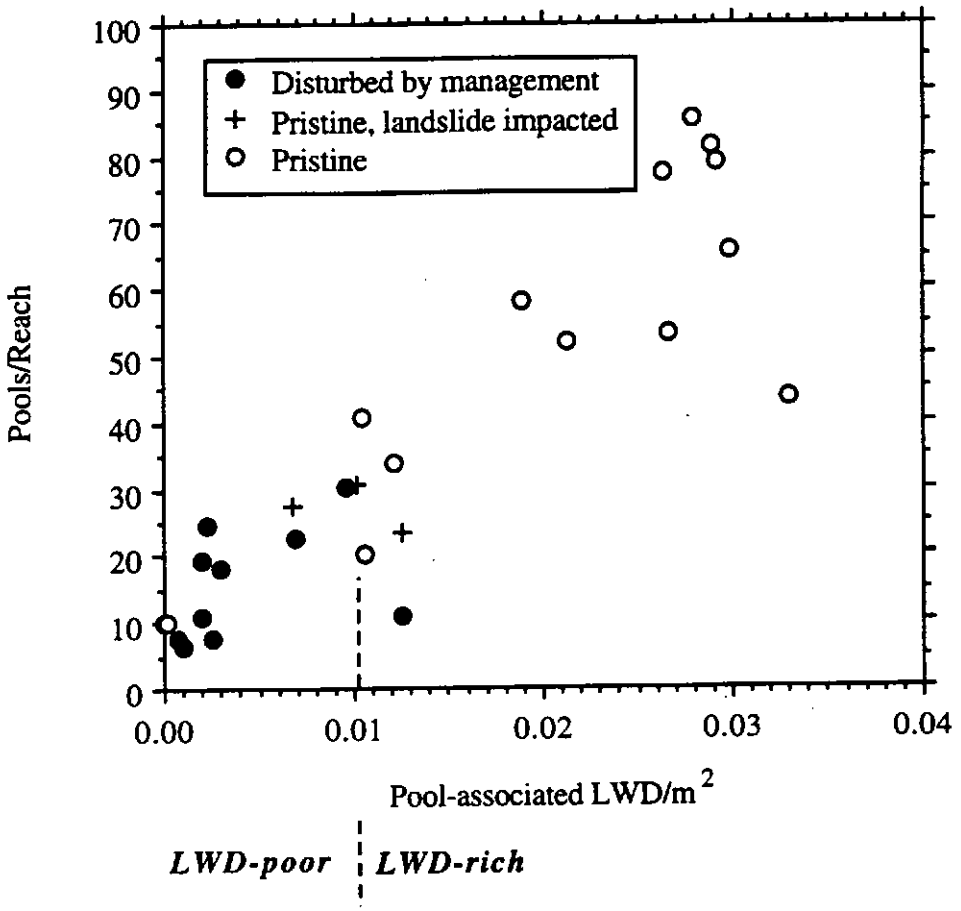

Figure 3.6 Pool frequency (number/reach, where a reach is twenty bankfull channel widths long) versus pool-associated LWD loading (pieces/m^2) in pristine and managed channels of southeast Alaska. Channels are empirically divided into LWD-poor and LWD-rich categories at the median value of pool-associated LWD loading (0.0103 pieces/m^2).

debris-rich pool-riffle channels by a simple division of the channels at the median of the LWD loading spectrum (0.0103 pieces/m^2). This division correlates well with land use history; further explanation of a similar figure and other morphologic distinctions of land use type are discussed by Smith and Buffington (in press). The direct correlation of numbers of pools with LWD loading seen in Figure 3.6 demonstrates the morphologic significance of LWD in forest gravel-bedded streams [see also Montgomery et al. (in press)].

Because all in-channel LWD was inventoried in the Olympic streams, while only pool-associated LWD was recorded in the Forest Service study, it was necessary to derive a conversion factor for the two types of LWD measurement before the data sets could be combined. Using data collected during Montgomery and others' (in press) pool spacing study, a reasonably good correlation is observed between pool-associated LWD/m^2 and all in-channel LWD/m^2 (Fig. 3.7); the plotted data are from southeast Alaskan channels, some of which are the same reaches studied by Smith and Buffington (in press) and used in the current analysis. Based on the correlation shown in Figure 3.7 the median value of pool-associated wood loading given in Figure 3.6 is equivalent to a total wood loading of about 0.0328 pieces/m^2; this value was used to separate the Olympic pool-riffle channels into debris-rich and debris-poor categories, providing a common definition of channel type for the Olympic and Alaskan sites.

RESULTS AND DISCUSSION

Channel Geometry and LWD Loading

Reach-average bankfull geometries for the Olympic and Alaskan study sites are shown in Table 3.3. Overall, the data represent a broad range of slopes (0.0017-0.0371), bankfull widths (4.0-28.1 m), depths (0.33-1.16 m), width-to-depth ratios (W/h, 7.26-

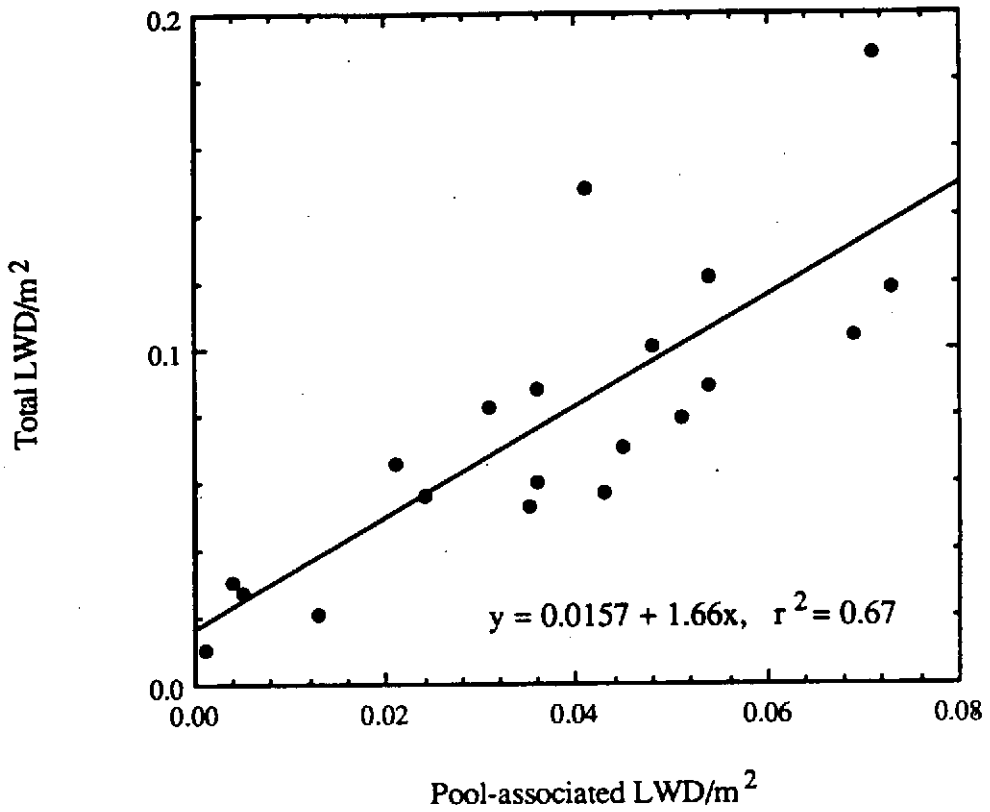

Figure 3.7 Relationship between pool-associated LWD/m^2 and total LWD/m^2 for Alaskan sites studied by Montgomery et al. (in press).

TABLE 3.3: Reach-Average Bankfull Hydraulic Geometry, D_{50s}, and τ_w/τ_0

Channel	Slope	Width (m)	Depth (m)	Width/Depth	D_{50s} (mm)†	τ_w/τ_0
Olympic Channels						
Plane-bed						
Upper Dry Creek	0.0122	6.84	0.59	11.59	67.1 (68.7)	0.122
Alder Creek*	0.0257	8.37	0.62	13.50	56.4 (61.0)	0.113
Hoko Tributary	0.0160	5.02	0.35	14.34	54.8 (55.2)	0.108
Lower Hoh Slough	0.0059	11.53	0.51	22.61	19.3 (41.8)	0.072
Upper Hoh Slough	0.0114	10.65	0.56	19.02	56.8 (61.2)	0.085
LWD-poor Pool-riffle						
Upper Skunk Creek	0.0126	7.02	0.97	7.24	39.2 (44.2)	0.204
Hoko River	0.0085	13.41	0.81	16.56	35.0 (36.9)	0.097
Lower Pins Creek	0.0071	6.39	0.48	13.31	31.4 (33.0)	0.113
LWD-rich Pool-riffle						
Upper Pins Creek	0.0133	6.17	0.50	12.34	36.0 (39.3)	0.118
Flu Hardy Creek	0.0105	6.83	0.62	11.02	24.4 (29.2)	0.125
Mill Creek	0.0143	8.72	0.88	9.91	19.4 (24.0)	0.132
Lower Dry Creek*	0.0222	7.90	0.59	13.39	53.4 (55.9)	0.113
Lower Skunk Creek	0.0040	13.36	0.80	16.70	19.8 (23.8)	0.097
Cedar Creek	0.0046	11.51	0.62	18.56	27.2¥	0.087
Southeast Alaskan Channels						
LWD-poor Pool-riffle						
12 Mile Creek 1	0.0021	23.34	0.95	24.57	24.1¥	0.073
12 Mile Creek 2	0.0028	23.35	1.09	21.42	21.7 (24.9)	0.078
Maybeso Creek 1	0.0071	22.31	1.13	19.74	49.4 (53.2)	0.081
Maybeso Creek 2	0.0065	28.10	0.84	33.45	36.1 (38.0)	0.060
Maybeso Creek 3£	0.0023	26.95	0.93	28.98	36.2¥	0.067
Maybeso Creek 4£	0.0036	24.48	1.06	23.09	46.2 (47.7)	0.075
Cable Creek	0.0017	16.89	0.88	19.19	13.1¥	0.084
Fubar Creek 1	0.0106	17.64	0.62	28.45	42.9 (47.4)	0.055
Fubar Creek 2	0.0127	16.32	0.79	20.66	56.8 (60.8)	0.079
Indian Creek£	0.0121	24.37	1.16	21.01	79.3 (82.9)	0.078
Muri Creek£	0.0149	14.29	0.59	24.22	44.1 (53.5)	0.074
Bambi Creek	0.0091	4.0	0.33	12.12	17.4 (18.8)	0.119
Upper Weasel Creek 2*	0.0023	15.10	0.92	16.41	25.4¥	0.098
Lower Greens Creek*	0.0371	12.90	0.66	19.55	47.0 (53.6)	0.082
LWD-rich Pool-riffle						
Hook Creek*	0.0109	17.33	0.76	22.80	27.2 (32.2)	0.076
Trap Creek 1	0.0055	12.63	0.86	14.69	16.7 (17.8)	0.107
Trap Creek 2	0.0067	15.29	0.62	24.66	15.1 (15.8)	0.073
Trap Creek 3	0.0077	11.78	0.58	20.30	14.8 (17.2)	0.079
Trap Creek 4	0.0071	9.54	0.69	13.83	11.6 (16.2)	0.111
Trap Creek 5	0.0101	13.73	0.66	20.80	15.9 (20.3)	0.079
Trap Creek 6	0.0120	14.60	0.65	22.46	13.4 (18.7)	0.073
East Fork Trap Creek 1	0.0126	14.61	0.59	24.76	14.5 (23.5)	0.066
East Fork Trap Creek 2	0.0125	11.20	0.55	20.36	24.2 (27.4)	0.079
Fowler Creek 1	0.0062	18.39	0.67	27.45	13.9 (18.5)	0.058
Fowler Creek 2	0.0055	12.20	0.65	18.77	18.9 (24.5)	0.086
Lower Fish Creek	0.0270	19.03	1.02	18.66	25.7 (32.3)	0.087
Upper Fish Creek	0.0224	12.88	0.56	23.00	45.6 (48.5)	0.076

† Values in parentheses are derived from grain size distributions truncated at D_{sus} and are thus indicative of bedload material only.

¥ Bedload and suspended load material could not be differentiated as the calculated D_{sus} value is < 2 mm, the minimum resolution used for surface pebble counts; all grain sizes ≤ 2 mm were lumped into one category and are consequently undifferentiable.

* Evidence of catastrophic sediment inputs.

£ Transitional between pool-riffle and plane-bed morphology.

33.45), and median surface grain sizes (10.6-79.3 mm). The Alaskan channels typically have larger W/h, with the debris-poor channels having higher ratios on average than the debris-rich channels; greater W/h ratios are attributed to larger drainage areas for the debris-poor channels compared to those of the debris-rich (Smith and Buffington, in press). The ratio of τ_w to τ_0 for each channel is also given in Table 3.3, with values ranging from 0.055-0.204.

Composite distributions of LWD loading (pieces/m^2) for the three channel types studied are presented in Figure 3.8. Debris loading for the Alaskan sites was calculated from the relation given in Figure 3.7. The plane-bed channels are virtually debris-free, while the pool-riffle channels have variable loading (Fig. 3.8). By definition the debris-poor channels have loadings less than 0.0328 pieces/m^2. The bulk of the debris-poor channels have a small, narrow range of loadings (0.0158-0.0323 pieces/m^2) with a median of 0.0200 pieces/m^2. In contrast, the majority of the LWD-rich channels have a much broader and higher range (0.0339-0.0688 pieces/m^2), with a median value nearly three times greater than the pool-riffle channels classified as debris-poor.

Surface Textures of the Olympic Channels

Mapped surface textures of the Olympic channels are summarized in Table 3.4 by channel type. Examples of topographic, textural, and LWD maps for each channel type are also provided (Maps 1-5); because the pool-riffle channel types are quite variable, two maps of each of these types are presented. Numbers of textures observed in a reach varied from one to seven and were composed of grain sizes ranging from silt to small boulders. No formal grain size analysis was done for textural patches formed completely of either sand or silt, instead an approximate median grain size was assigned (2 or 0.0625 mm, respectively). Cumulative grain size distributions of sampled textures are shown in Figure 3.9. Except for T4 of Upper Hoh Slough, pebble counts of visually identical textures

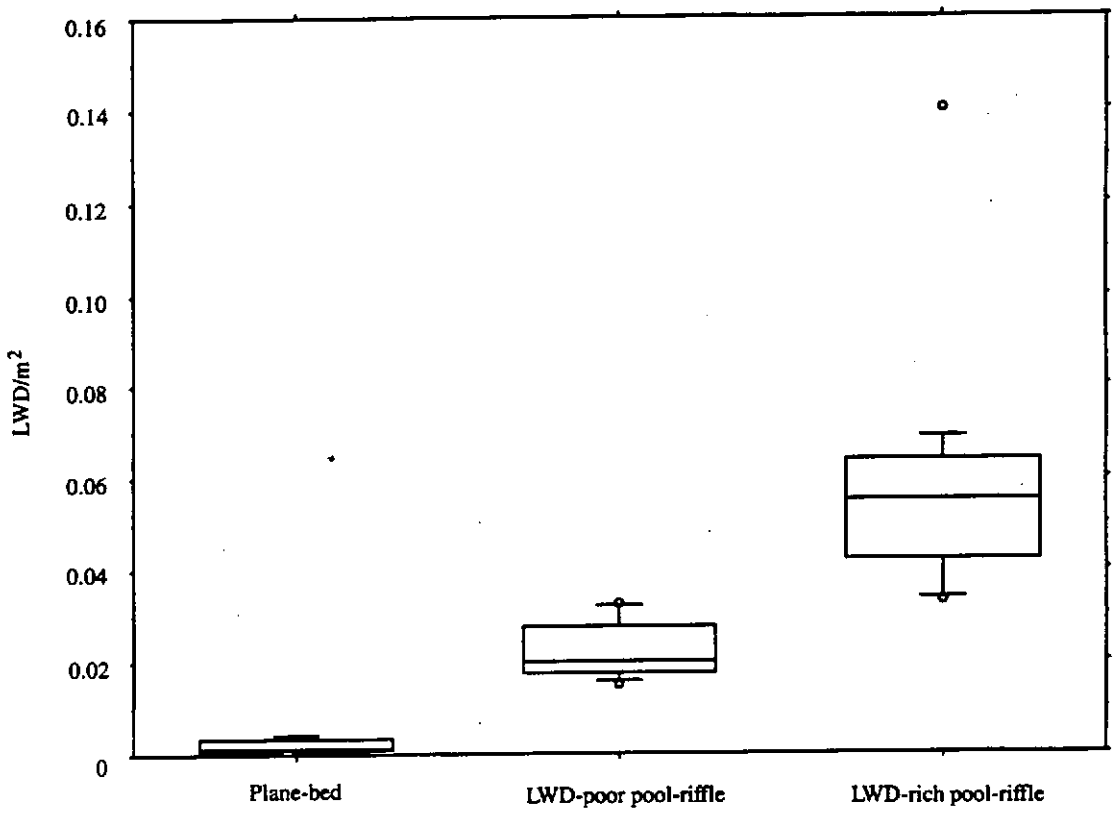

Figure 3.8 Composite LWD loading (pieces/m^2) distributions for the three channel types studied. Line within each box plot represents the median value of the distribution, box ends are the inner and outer quartiles, whiskers are the inner and outer tenths, and circles are extrema.

TABLE 3.4: Surface Textural Composition of the Olympic Channels

Channel	Reach D_{50s} (mm)†	Texture	% of Bed	Patch Frequency (#/reach)‡	D_{50s} (mm)†	$\lvert\sigma_{gs}\rvert$ (ϕ)†
Plane-bed						
Upper Dry Creek	67.1 (68.7)					
		T1: cobble, gravel	100	1	67.1 (68.7)	1.24 (1.19)
Alder Creek	56.4 (61.0)					
		T1: cobble, boulder, gravel	100	1	56.4 (61.0)	1.58 (1.28)
Hoko Tributary	54.8 (55.2)					
		T1: cobble, gravel	100	1	54.8 (55.2)	1.34 (1.31)
Lower Hoh Slough	19.3 (41.8)					
		T1: sand, gravel	63	3	9.0 (42.7)	2.76 (1.26)
		T2: gravel, cobble	35	3	38.9 (40.3)	1.10 (1.05)
		T3: sand	2	2	~2.0 (na)	
Upper Hoh Slough	56.8 (61.2)					
		T1: sand, gravel	4	1	9.0 (42.7)	2.76 (1.26)
		T2: gravel, cobble	0.5	1	38.9 (40.3)	1.10 (1.05)
		T3: sand	4	2	~2.0 (na)	
		T4: cobble, gravel, boulder	91.5	1	61.4 (63.6)	1.54 (1.48)
LWD-poor Pool-riffle						
Upper Skunk Creek	39.2 (44.2)					
		T1: cobble, gravel	71.24	2	50.4 (51.1)	1.10 (1.07)
		T2: gravel	8.22	4	25.0 (27.8)	1.37 (0.98)
		T3: fine gravel, coarse gravel, cobble	11.19	9	9.9 (12.8)	1.41 (1.06)
		T4: sand	9.33	9	~2.0 (na)	
Hoko River	35.0 (36.9)					
		T1: gravel, cobble	61.58	4	38.4 (38.8)	1.24 (1.22)
		T2: fine gravel	5.10	7	~6.0 (?)	
		T3: gravel	13.87	9	13.1 (13.5)	0.98 (0.91)
		T4: cobble, gravel	19.45	3	47.4 (47.7)	0.92 (0.92)
Lower Pins Creek	31.4 (33.0)					
		T1: medium/coarse gravel	2.58	3	12.7 (13.3)	1.15 (1.10)
		T2: gravel, cobble	92.11	1	33.3 (34.6)	1.57 (1.37)
		T3: fine/medium gravel	4.15	6	9.2 (9.8)	1.32 (1.19)
		T4: sand	1.16	3	~2.0 (na)	

† Values in parentheses are derived from grain size distributions truncated at D_{sus} and are thus indicative of bedload material only. D_{sus} values for each channel are shown in Figure 3.7. Textures with assigned/estimated D_{50s} values (i.e., T3 and T4 of Flu Hardy, etc.) less than D_{sus} are completely suspendable at bankfull and are given a bedload D_{50s} designation of 'na'; for such cases, reach-average D_{50s} values of bedload material were calculated from re-proportioned areal extents of the remaining textural patches.

‡ Reach length is ten channel widths.

¥ Bedload and suspended load material could not be differentiated as the calculated D_{sus} value is < 2 mm, the minimum resolution used for surface pebble counts; all grain sizes ≤ 2 mm were lumped into one category and are consequently undifferentiable.

TABLE 3.4 cont.

Channel	Reach D_{50s} (mm)†	Texture	% of Bed	Patch Frequency (#/reach)	D_{50s} (mm)†	$\lvert\sigma_{gs}\rvert$ (ϕ)†
LWD-rich Pool-riffle						
Upper Pins Creek	36.0 (39.3)					
		T1: gravel, cobble	40.61	7	52.4 (52.8)	1.01 (1.00)
		T2: coarse gravel	48.47	3	29.6 (30.0)	0.93 (0.91)
		T3: fine gravel	3.22	3	7.1 (8.0)	0.92 (0.52)
		T4: sand	7.71	4	~2.0 (na)	
Flu Hardy Creek	24.4 (29.2)					
		T1: coarse/medium gravel	80.53	1	29.5 (30.0)	0.89 (0.88)
		T2: medium/fine gravel	3.70	6	11.7 (12.0)	0.92 (0.90)
		T3: sand	11.79	9	~2.0 (na)	
		T4: silt	3.98	2	~0.06 (na)	
Mill Creek	19.4 (24.0)					
		T1: coarse gravel, cobble	8.15	5	39.6 (39.6)	0.58 (0.58)
		T2: medium/coarse gravel	62.57	2	23.7 (24.5)	1.04 (0.94)
		T3: fine gravel	11.77	25	8.4 (10.4)	0.93 (0.68)
		T4: sand	15.89	21	~2.0 (na)	
		T5: silt	1.63	2	~0.06 (na)	
Lower Dry Creek	53.4 (55.9)					
		T1: cobble, gravel	47.48	8	77.0 (77.4)	0.66 (0.66)
		T2: gravel, cobble	39.28	3	39.1 (39.6)	1.12 (1.09)
		T3: gravel	7.52	5	13.8 (15.7)	1.09 (0.87)
		T4: fine gravel, cobble	4.79	2	9.3 (38.8)	2.34 (1.85)
		T5: sand	0.94	3	~2.0 (na)	
Lower Skunk Creek	19.8 (23.8)					
		T1: gravel, cobble	21.54	4	29.2 (29.2)	0.91 (0.91)
		T2: gravel	62.31	6	21.2 (22.0)	0.96 (0.84)
		T3: sand	16.15	32	~2.0 (na)	
Cedar Creek¥	27.2					
		T1: cobble, gravel	7.53	3	74.4	0.89
		T2: medium gravel, cobble	64.19	1	26.6	0.70
		T3: coarse gravel, cobble	6.15	1	35.3	0.82
		T4: gravel	12.80	11	17.6	0.65
		T5: sand	2.64	3	~2.0	
		T6: fine gravel	1.08	6	6.6	0.98
		T7: silt	5.61	2	~0.06	

† Values in parentheses are derived from grain size distributions truncated at D_{sus} and are thus indicative of bedload material only. D_{sus} values for each channel are shown in Figure 3.7. Textures with assigned/estimated D_{50s} values (i.e., T3 and T4 of Flu Hardy, etc.) less than D_{sus} are completely suspendable at bankfull and are given a bedload D_{50s} designation of 'na'; for such cases, reach-average D_{50s} values of bedload material were calculated from re-proportioned areal extents of the remaining textural patches.

‡ Reach length is ten channel widths.

¥ Bedload and suspended load material could not be differentiated as the calculated D_{sus} value is < 2 mm, the minimum resolution used for surface pebble counts; all grain sizes ≤ 2 mm were lumped into one category and are consequently undifferentiable.

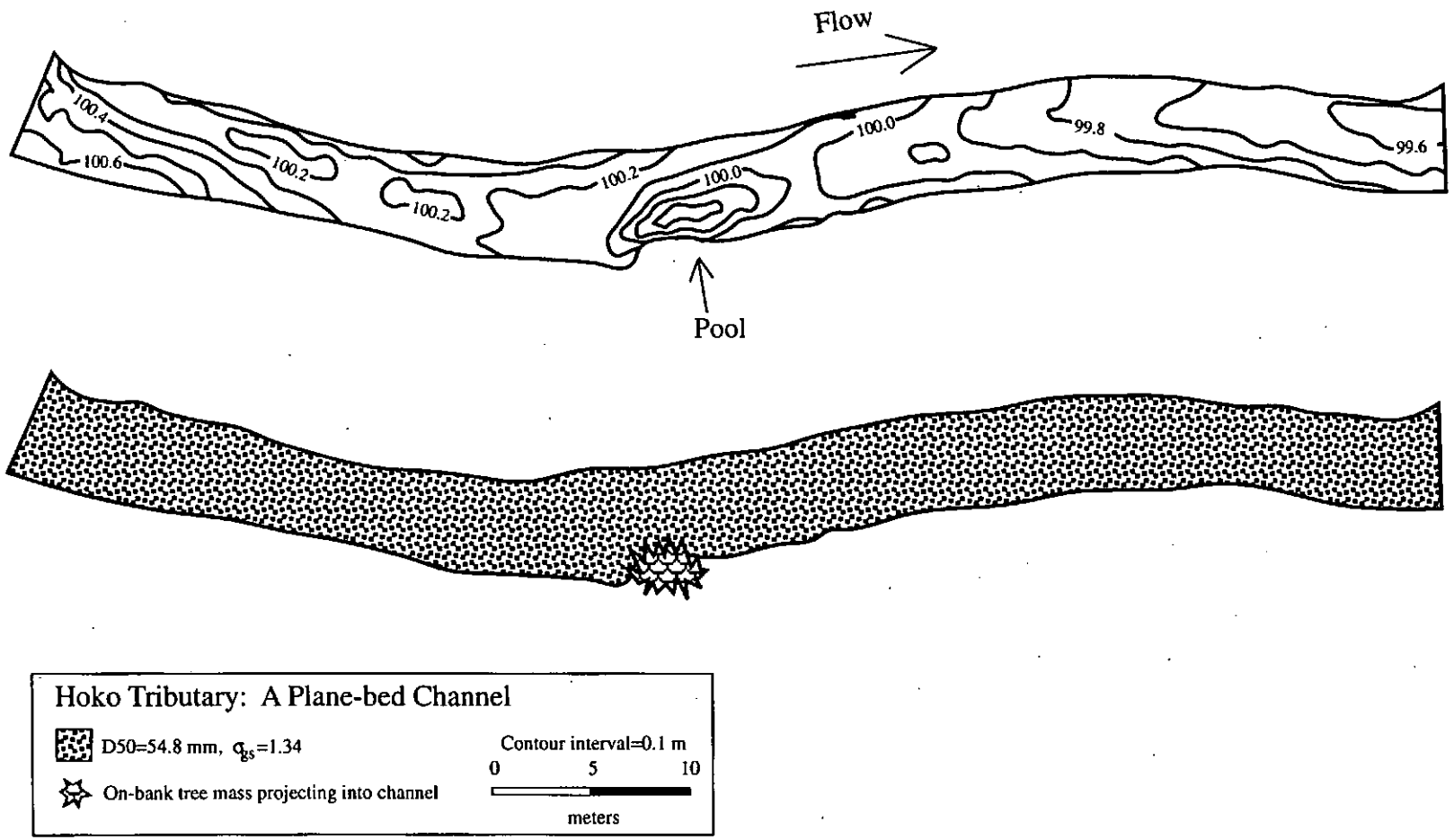

Map 1: Hoko Tributary, a plane-bed channel. Reach shown is ten channel widths long.

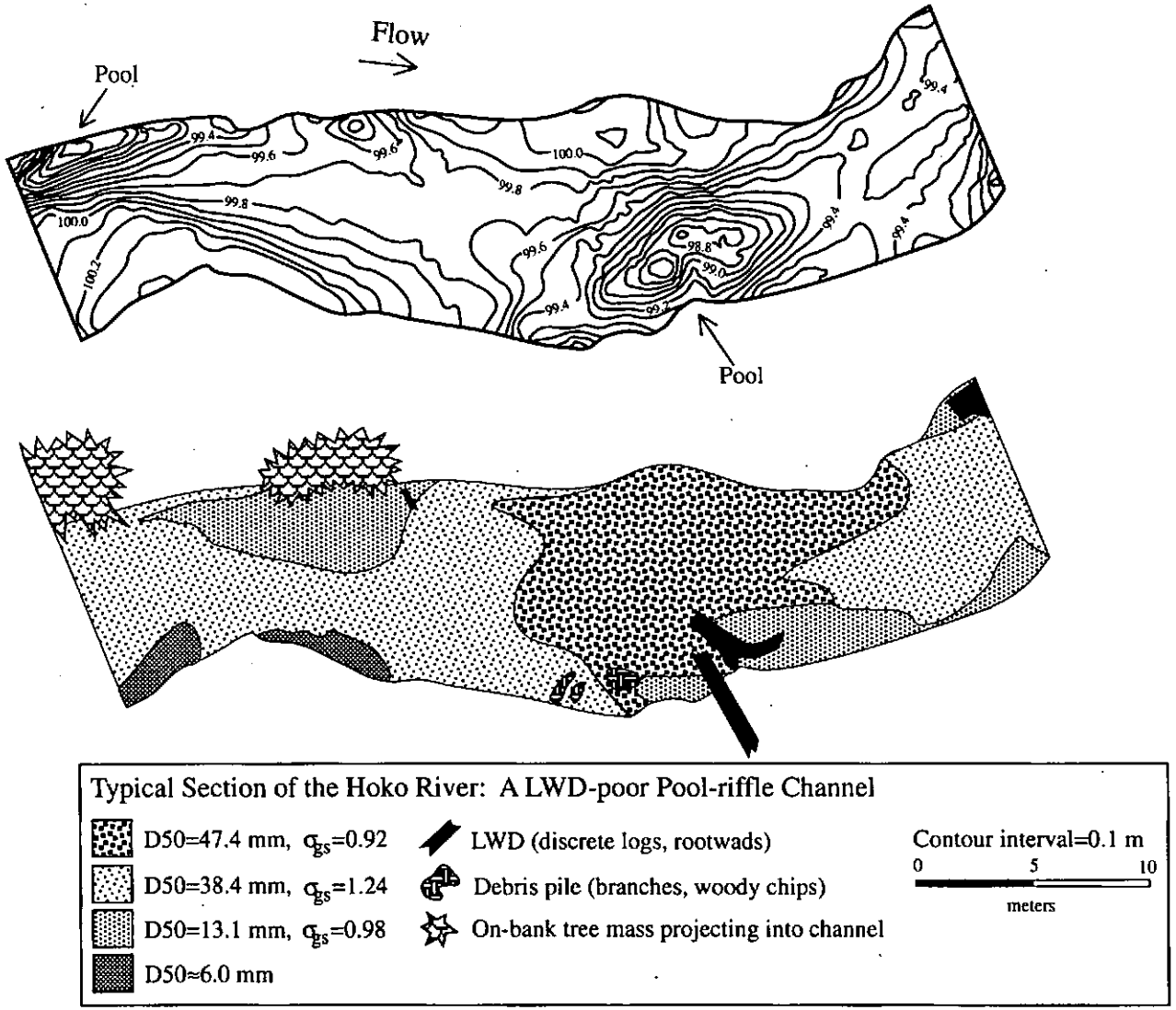

Map 2: Typical section of the Hoko River, a LWD-poor pool-riffle channel. Section shown is three channel widths long.

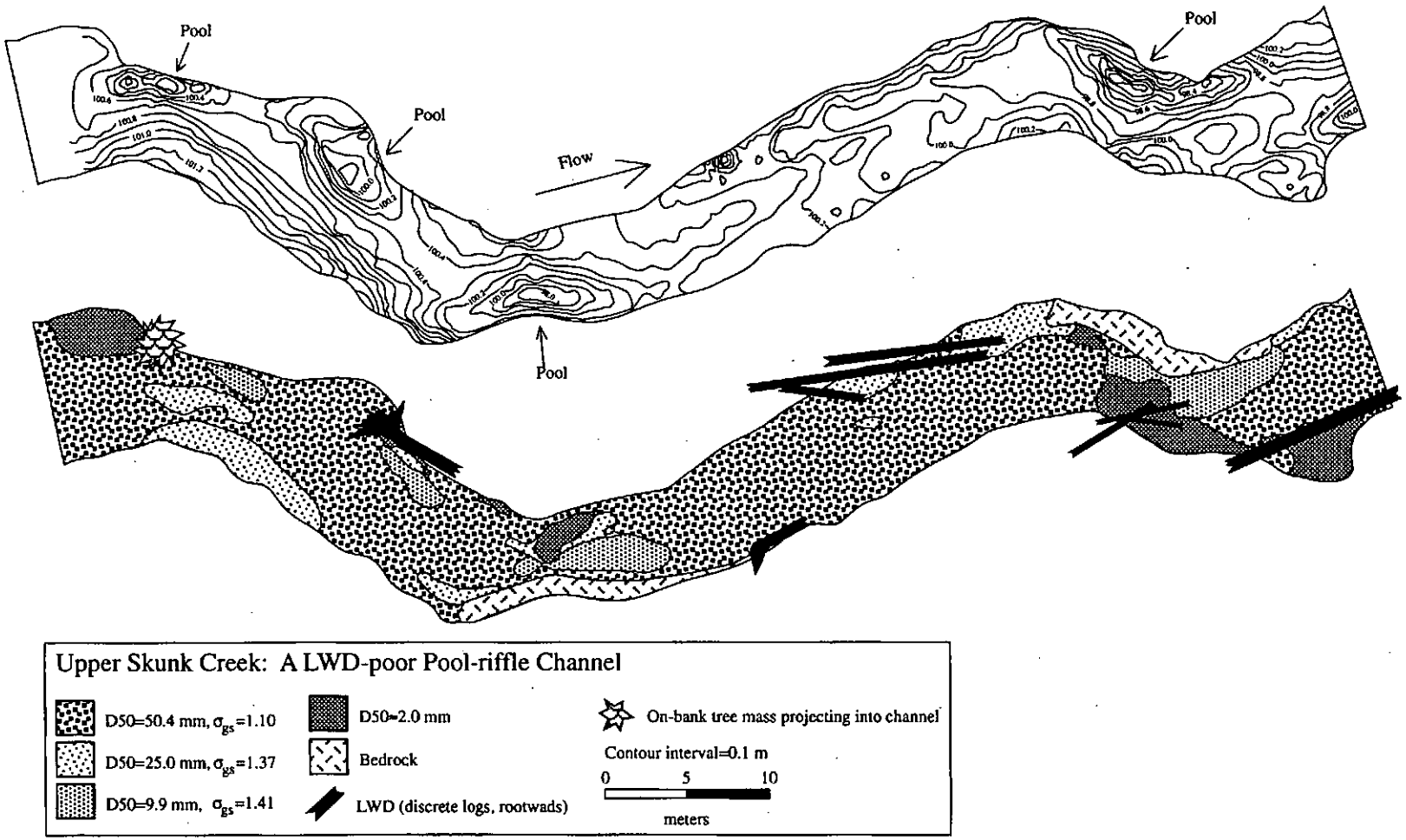

Map 3: Upper Skunk Creek, a LWD-poor pool-riffle channel. Reach shown is ten channel widths long.

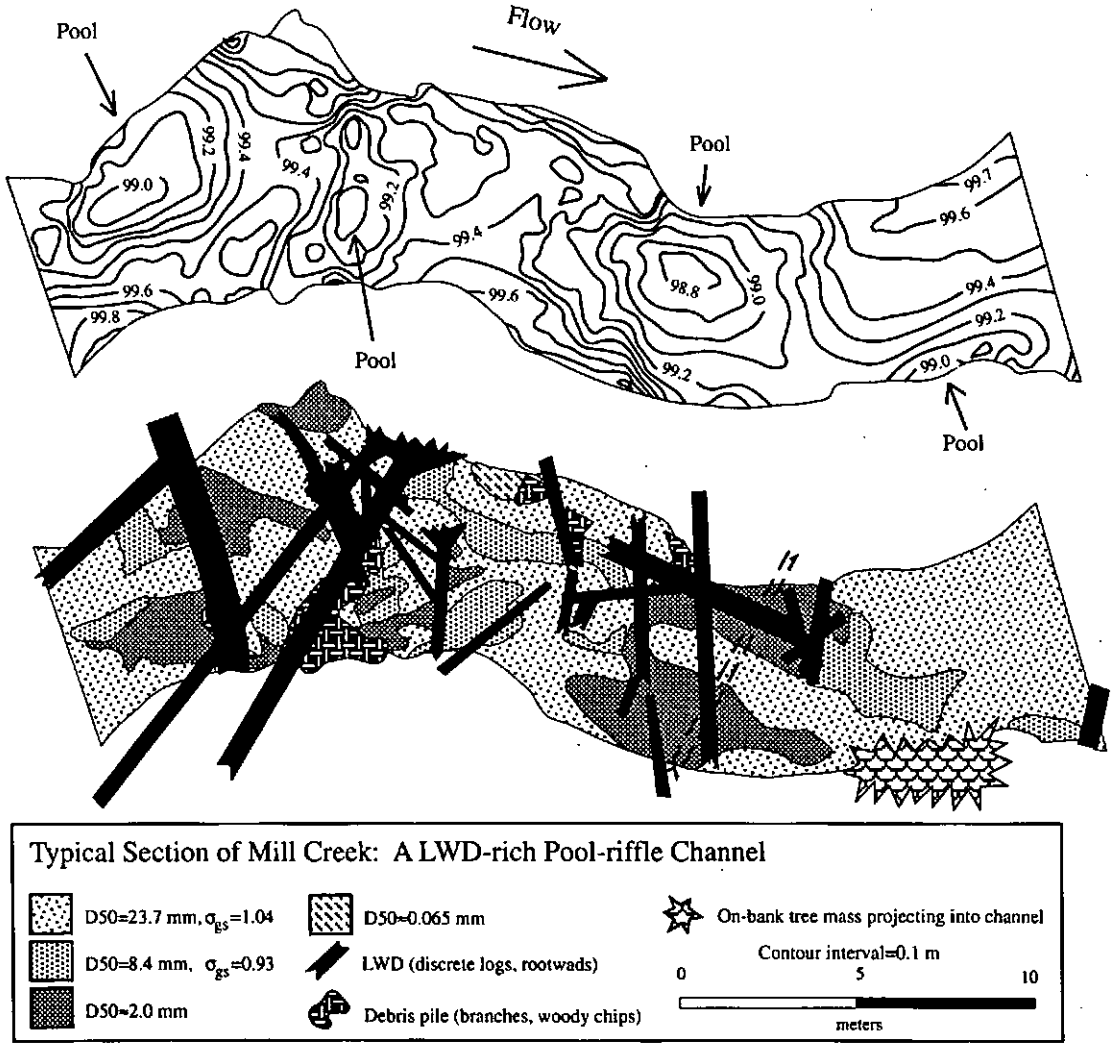

Map 4: Typical section of Mill Creek, a LWD-rich pool-riffle channel. Section shown is 3.4 channel widths long.

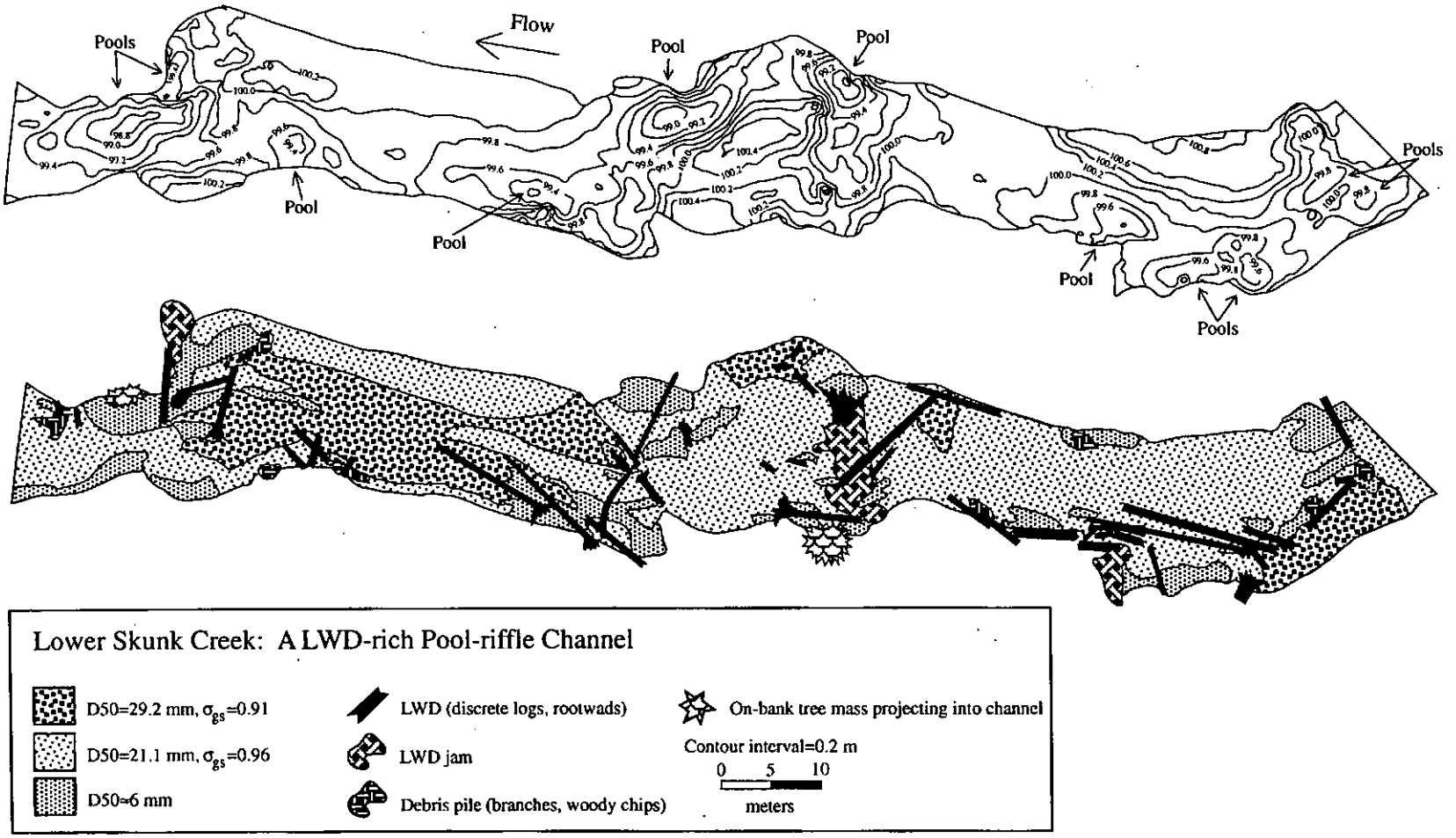

Map 5: Lower Skunk Creek, a LWD-rich pool-riffle channel. Reach shown is ten channel widths long.

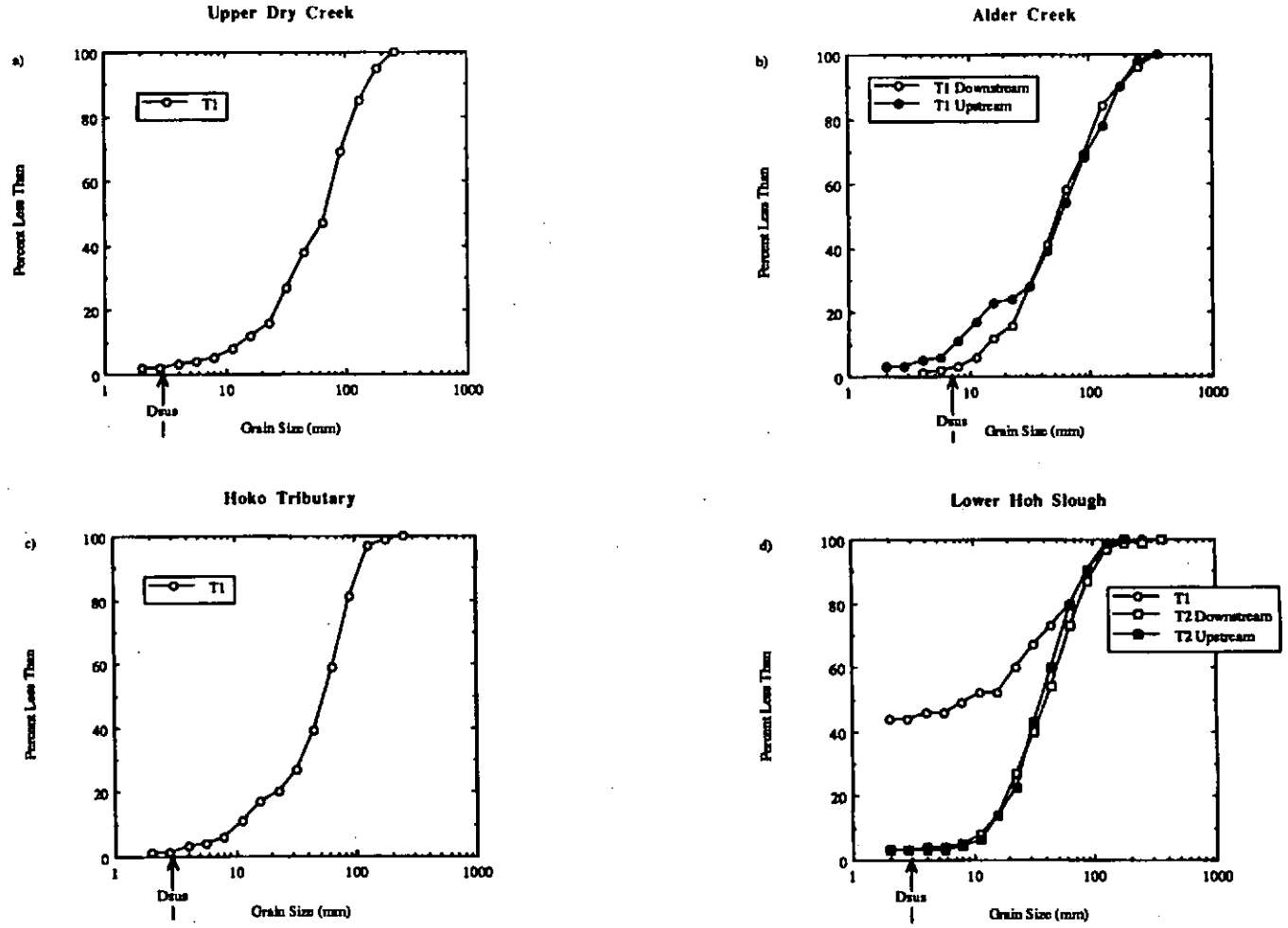

Figure 3.9 Surface grain size distributions of textures mapped in the Olympic study sites. Abscissa arrow indicates calculated reach-average D_{sus} value.

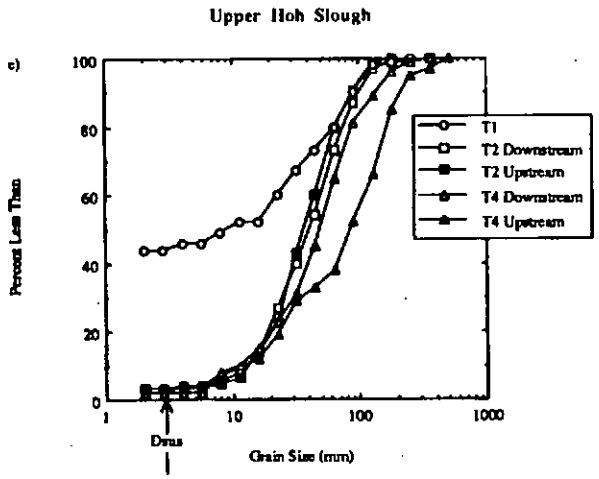

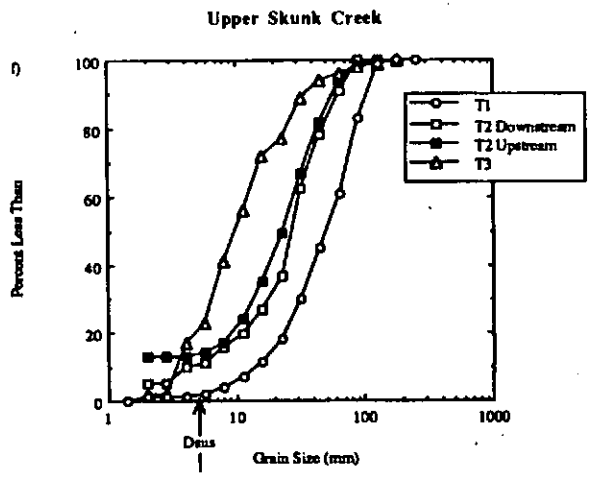

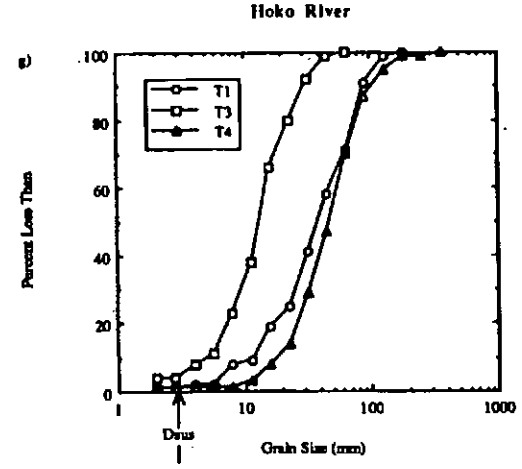

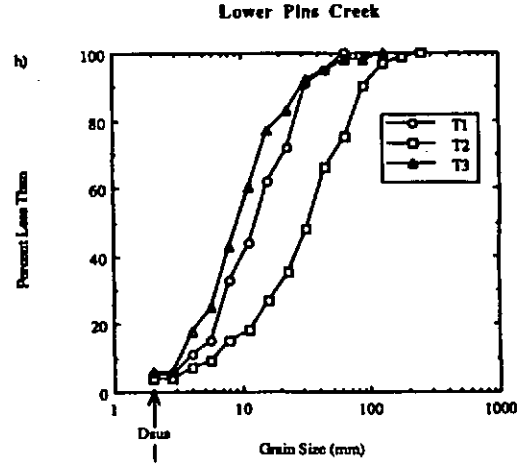

Figure 3.9 cont.

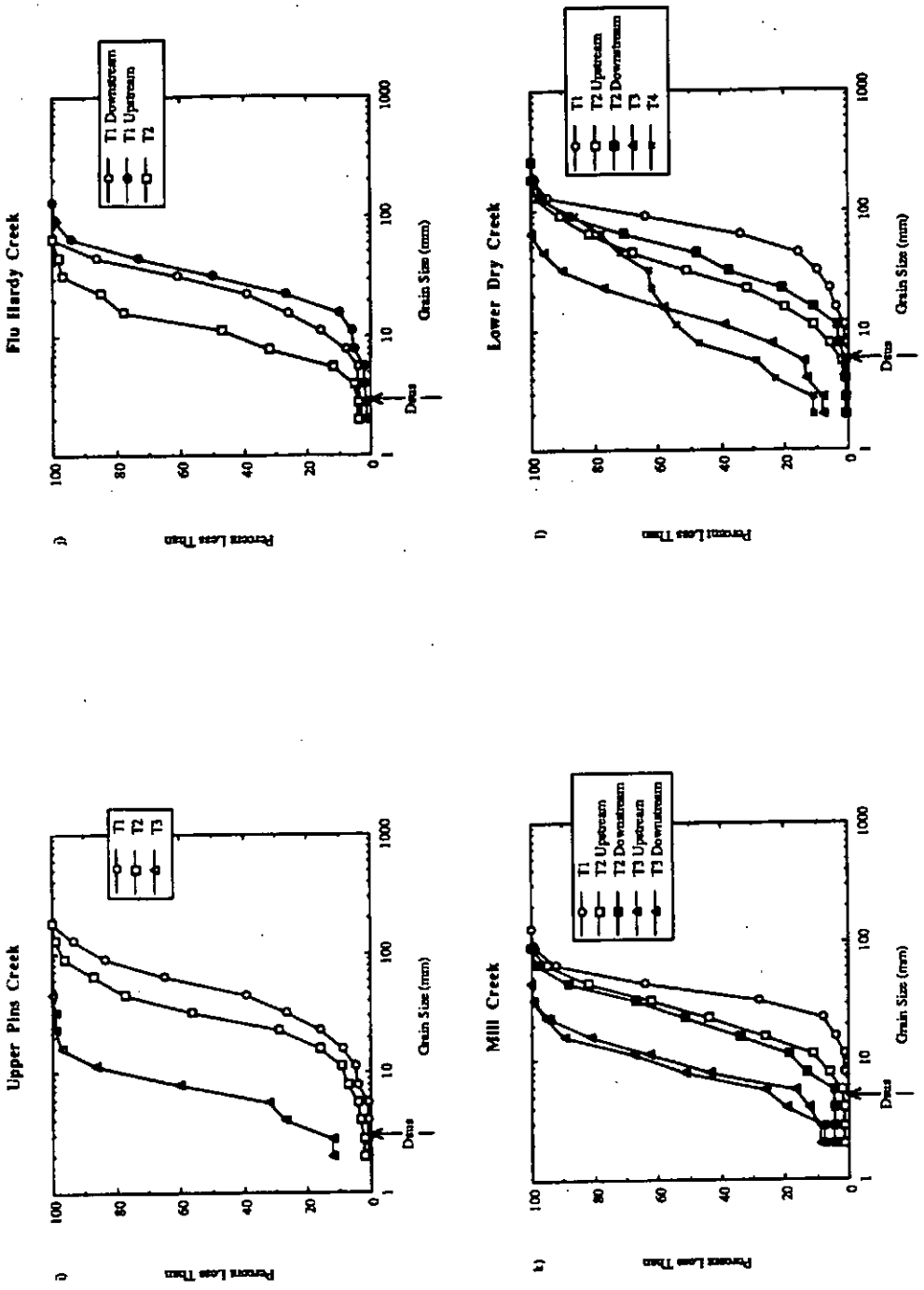

Figure 3.9 cont.

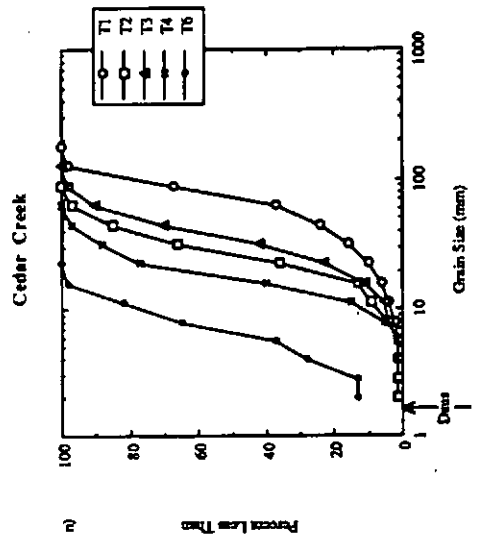

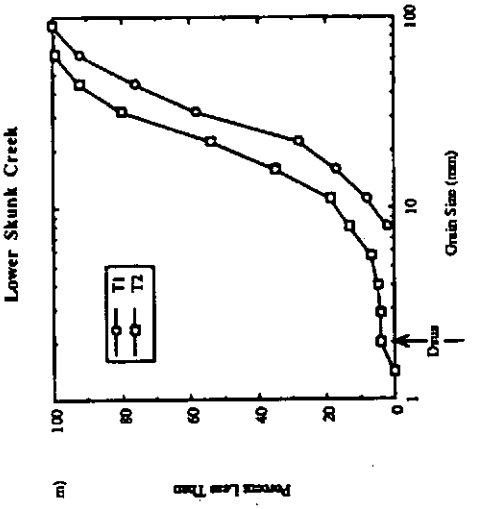

Figure 3.9 cont.

located in different portions of a reach yield similar grain size distributions (Fig. 3.9b, d, f, j, k, l), generally validating the procedure of characterizing textures by sampling a single patch. In contrast, some facies identified in the field as visually distinctive show fairly similar grain size distributions [e.g., Fig. 3.9g (T1,T4)]; however, differences in sorting coefficients lend credence to the field partitioning of these textures as different from one another (Table 3.4). Partitioning similar textures as different does not significantly affect reach-average evaluations of D_{50s}. While facies mapping accurately characterizes spatial distributions of textures, the reach-average D_{50s} values reported here should be viewed as first-order estimates (as opposed to zero-order) due to the small number of textural patches sampled per reach.

Facies mapping demonstrates that the number and spatial distribution of surface textures is strongly influenced by channel type. Plane-bed channels exhibit one to four grain-size facies, but are typically mono-textural (Table 3.4). Each of the LWD-poor pool-riffle channels are composed of four textures, while LWD-rich pool-riffle channels exhibit three to seven facies per reach. Thus, the number of textures increases with greater complexity of channel roughness. Furthermore, complexity of the spatial distribution of textures increases with complexity of channel roughness (Maps 1-5). The total frequency of textural patches within a reach ranges from 1-8 in plane-bed channels, but increases to 13-24 in LWD-poor pool-riffle channels and 17-55 in LWD-rich pool-riffle streams (Table 3.4). The data also show a slight increase in sorting (i.e., lower σ_{gs} values) with increasing channel roughness (Table 3.4); bedload-material surface textures in plane-bed channels are poorly sorted, while LWD-rich pool-riffle streams tend to have moderately sorted textures.

An increase in textural complexity from plane-bed to pool-riffle channels is not surprising, given previous observations of textural variation in sinuous pool-riffle channels. Systematic downstream and cross-channel variation in shear stress can be

caused by channel curvature and topographically-induced convective accelerations (Dietrich and Smith, 1983; 1984a; 1984b; Dietrich et al., 1979). In a meander bend it is commonly observed that surface grains fine both downstream along the point bar and cross-stream from the pool to the bar. These textural variations reflect the shifting of the high velocity core across the bar toward the pool, causing flow convergence in the pool and divergence along the bar (Dietrich and Smith, 1983; 1984a; 1984b; Dietrich et al., 1979). Mechanics of topographically-induced shear stress and textural variation are essentially similar in both sinuous and straight channels (Nelson and Smith, 1989a). Predictable textural variations of this sort occur in some of the pool-riffle sequences of the Olympic channels, but are by no means ubiquitous and tend to be less common in the LWD-rich streams (Maps 2-5). In-channel obstructions complicate flow patterns and modify local shear stresses, causing spatially complex textural arrangements that are not as readily predictable as in obstruction-free pool-riffle channels. Differences in textural patch frequency and the finer scale of textural partitioning noted above result from a progressively greater frequency of LWD obstructions in the sequence of channel types examined (Fig. 3.10). Patch frequency is a power function of LWD loading.

Despite the observed complexity of textural sequences, some general patterns of channel unit textural composition can be identified from the field maps; channel units are basic morphologic components of a stream reach (i.e., pools, bars, etc.) (Bisson et al., 1982; Sullivan, 1986; Grant et al., 1990; Church, 1992; Smith and Buffington, in press). Figure 3.11 shows the relative areal extent of facies within pool, bar, and riffle channel units; surface textures are divided here into reach-specific, relative categories of coarse, intermediate and fine grain sizes. Of the facies present in each channel, coarse and intermediate textures comprise the majority of bar-forming grains in both debris-rich and debris-poor streams (Fig. 3.11). Fine textures are almost always present on bar surfaces, but usually in relatively small quantities. In contrast to similar barform textural

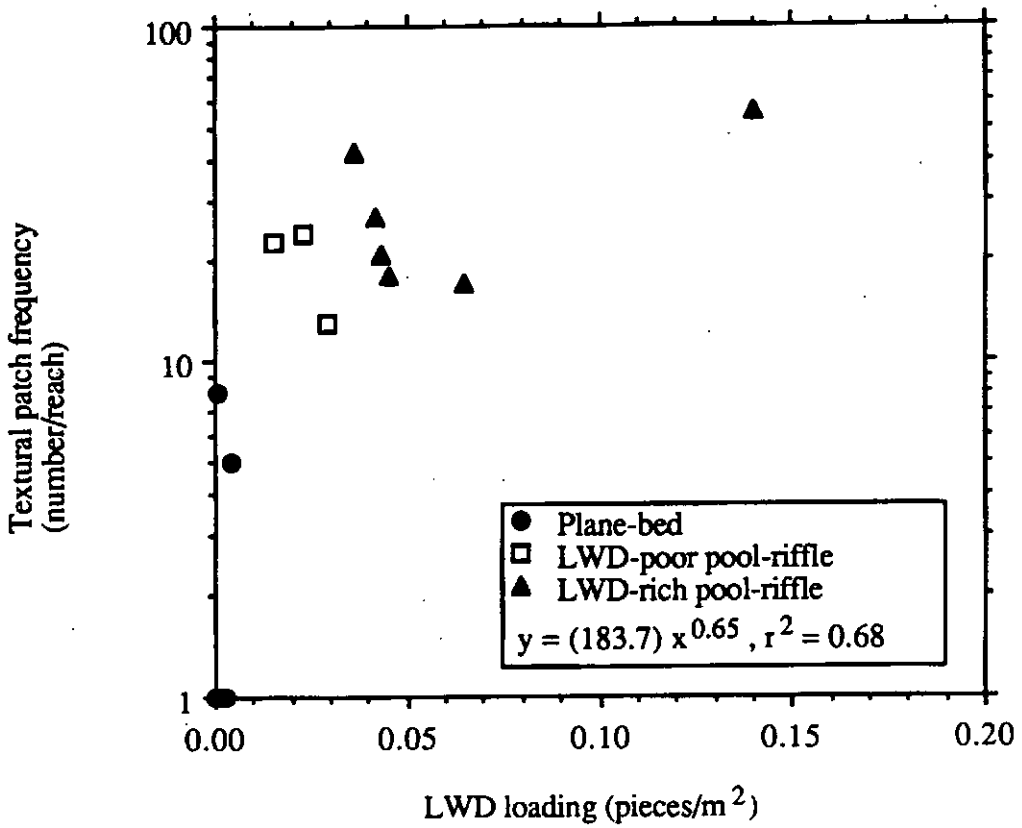

Figure 3.10 Textural patch frequency (number/reach) versus LWD loading (pieces/m^2) stratified by channel type.

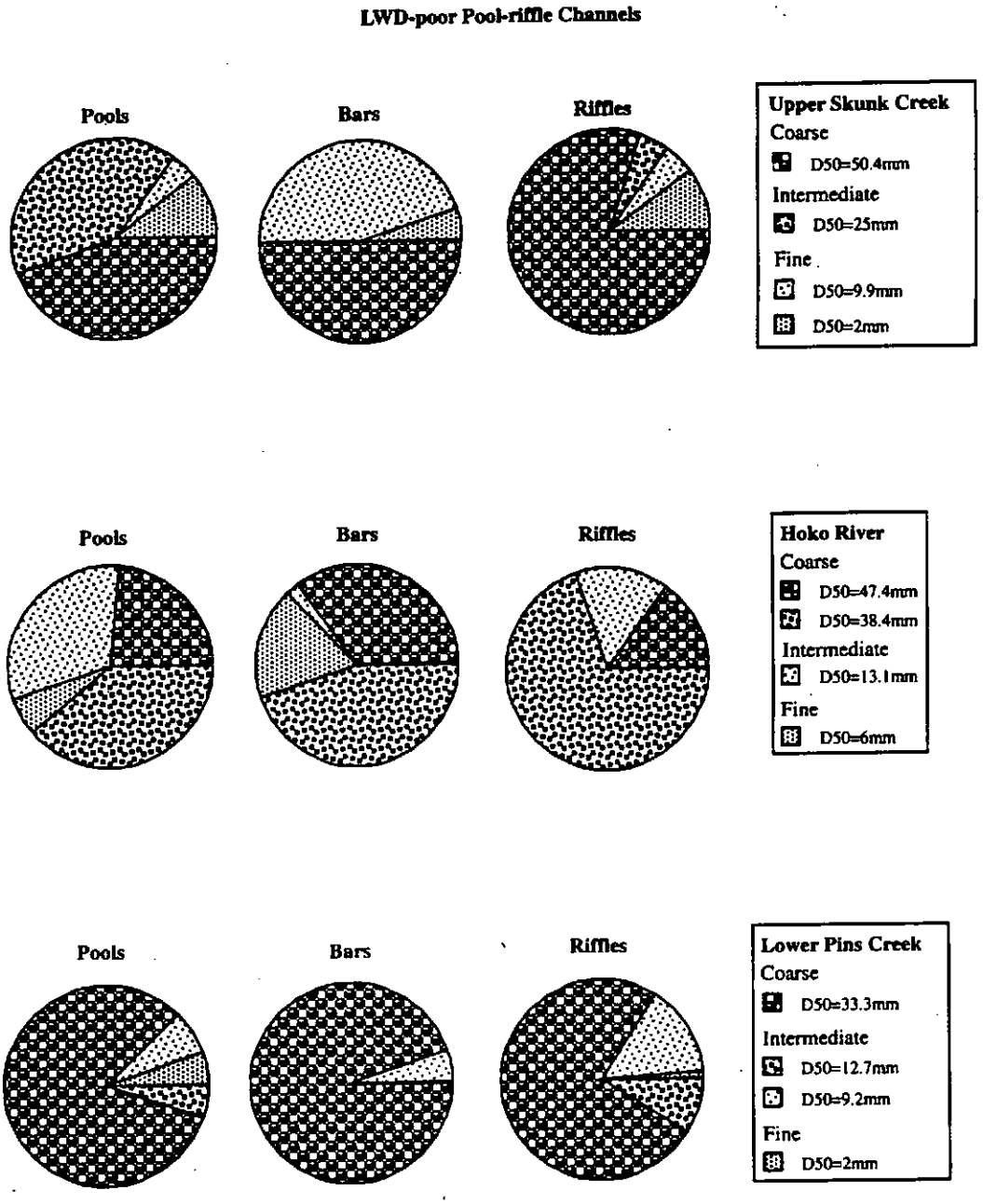

Figure 3.11 Textural composition of pool, bar, and riffle channel units expressed as relative areal extents. Grain size divisions of coarse, intermediate, and fine are based on reach-specific relative sizes observed in the field and quantified by Figure 3.9.

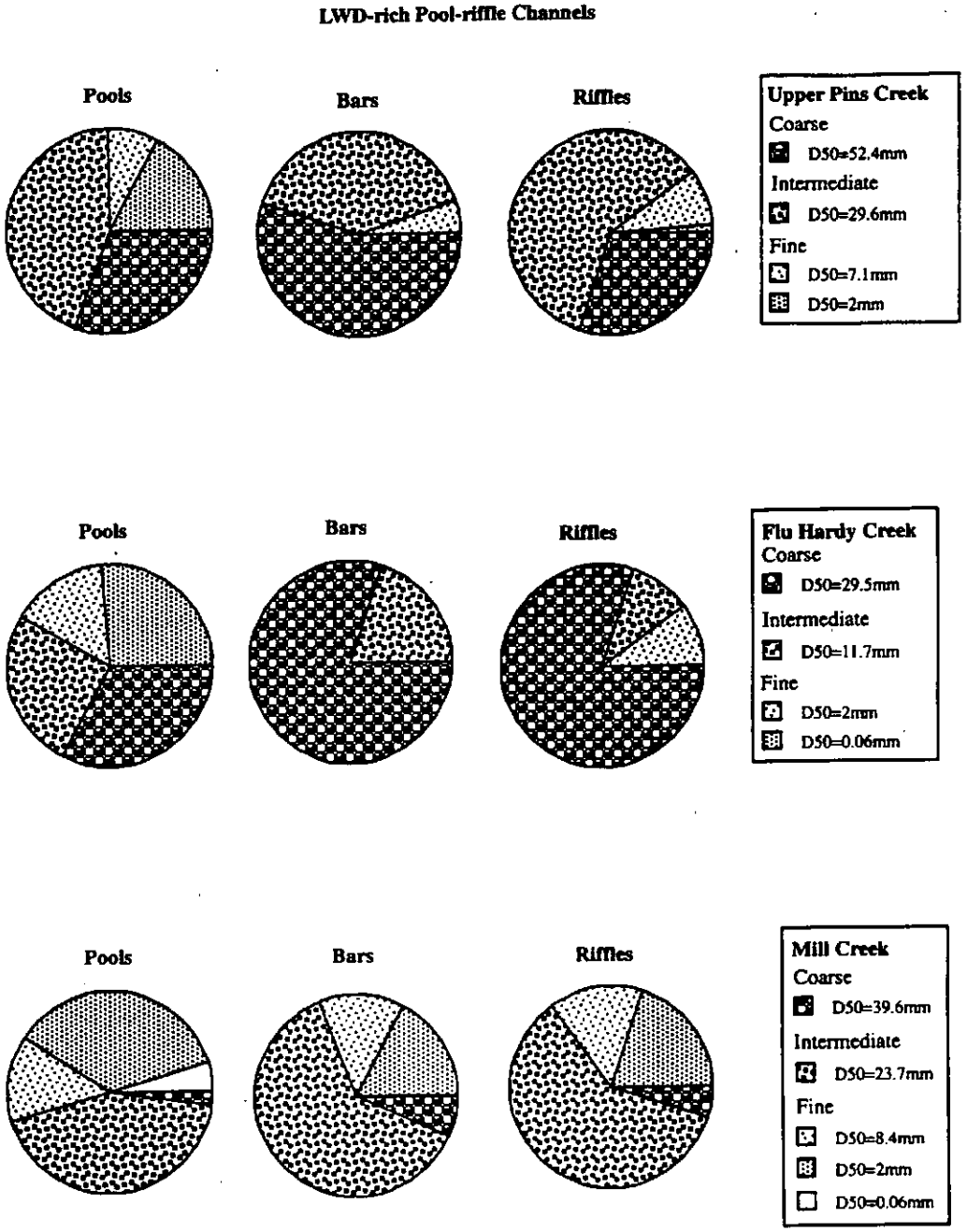

Figure 3.11 cont.

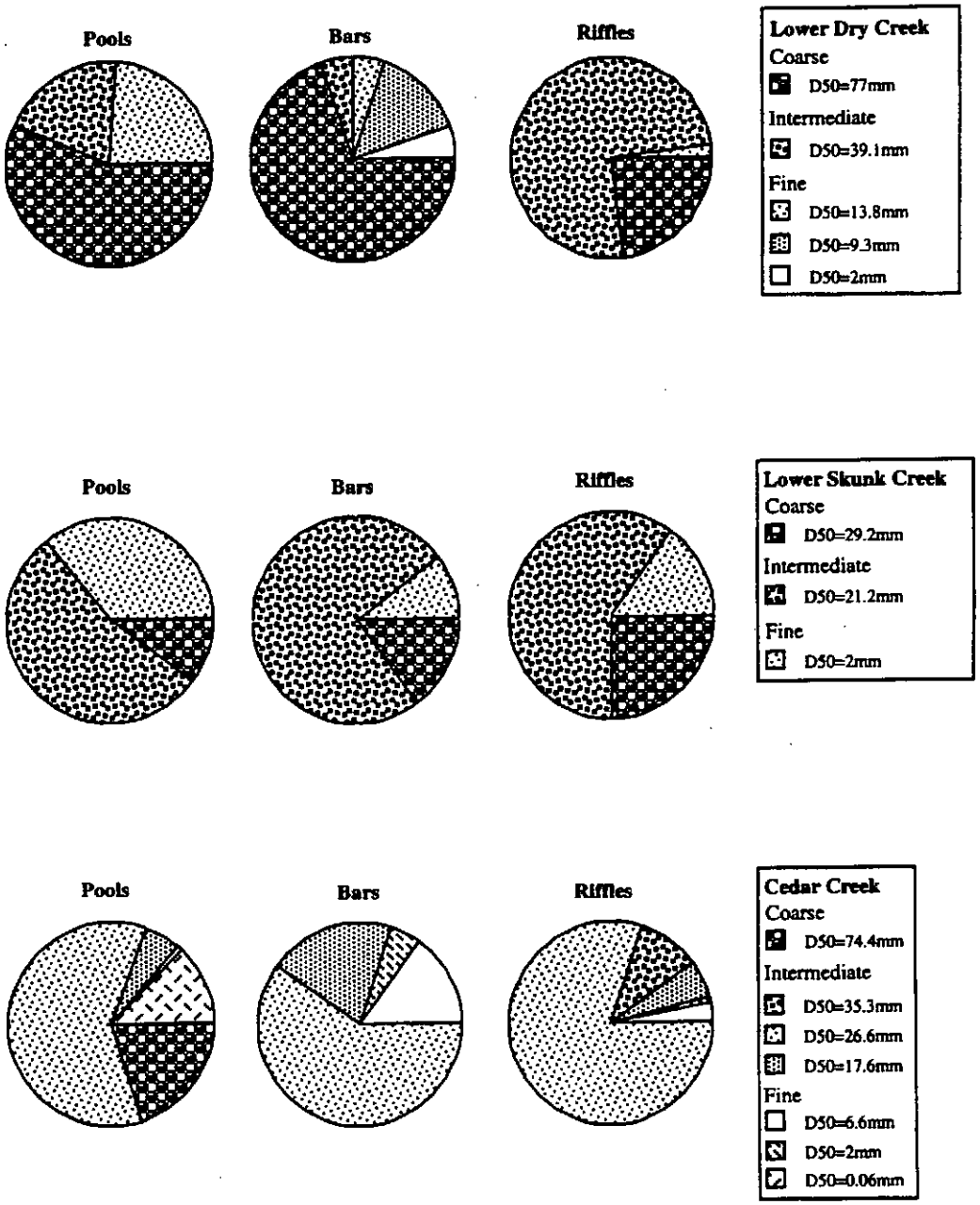

Figure 3.11 cont.

associations, patterns of pool-forming textures differ between the two channel types. Pools are dominantly composed of coarse textures in debris-poor channels, while the majority of pool-forming textures are fine- and intermediate-grained in LWD-rich channels. Furthermore, while nearly all of the pools in LWD-poor channels contain coarse grains (found as expected on pool bottoms), the percentage of pools containing coarse grains in LWD-rich streams averages about 63% and can be as low as 13%. Riffles are texturally transitional between pools and bars in both channel types (Fig. 3.11).

For practical reasons, textural mapping was conducted during summer low flow, and because of this it is possible that the finer textures in pools may represent seasonal storage. Fine material is commonly stored in pools between pool-scouring events that are characterized by bankfull velocity reversals (Keller, 1971; Lisle, 1979). In such channels the underlying pool bottom is typically coarse-grained, reflecting high bankfull shear stresses. During lesser stages, pools are typically low energy environments in which fine sediment is deposited by waning floods or by low flows capable of mobilizing small exposed grains. Whether fine-grained pool facies are seasonal or not, the contrast in pool-forming substrate in the two pool-riffle channel types is of more importance, as it suggests fundamental differences in either sediment loading or hydraulic roughness. Lisle and Hilton (1992) found a positive correlation between estimates of sediment supply and the volume of fine-sediment stored in pools, and they proposed an index of this volume, V*, as an indicator of sediment load. Deposition, however, can occur either due to an increase in sediment supply that exceeds the channel transport capacity or due to a decrease in transport capacity relative to the sediment load. As such, decreased transport capacity due to LWD roughness may also induce deposition. Given that it is the LWD-rich channels that exhibit finer pool textures, this later explanation is more plausible.

Rather than just being representative of seasonal storage, fine-grained pool textures may alternatively be a characteristic feature of all stages, including bankfull, in debris-

dominated channels. In other words, textural fining in pools may simply be a result of a reduction of transport capacity, rather than an exceedence of capacity and consequent deposition, as in the first scenario. Although woody debris is effective at causing flow convergence and constriction that lead to forced pool scour, the resistance created by a pool-forming LWD obstruction must simultaneously cause significant momentum extraction at all stages. Consequently, while accelerations around LWD may cause scour and local surface coarsening, it is expected that proximal zones of low shear stress characterized by finer textures would also be associated with LWD-forced pools due to debris form drag. This concept is supported by the observation that many of the pools in the debris-rich channels have coarse or intermediate pool bottoms (zone of highest shear stress) and fine-textured pool tails or sidewalls, while the surrounding riffles are typically of intermediate grain size.

A third possible explanation of fine-grained pool textures is suggested by flume studies of Lisle et al. (1993) and Dietrich et al. (1989). They found that for conditions of low sediment supply, the active transporting zone of the bed is confined to a narrow corridor of fine-grained material surrounded by coarser textures. These textural distinctions result from differential spatial patterns of sediment supply (Dietrich et al., 1993; Lisle et al, 1993). Mobile grains are essentially mined from exposed positions on the bed and concentrated into a high sediment supply, fine-textured, transporting zone. Lisle et al. (1993) found that for a pool-riffle morphology this transporting zone coincided with the thalweg, producing fine-textured pools. Because continuous, recognizable, fine-grained corridors were not observed in the Olympic sites this scenario is not considered relevant to the study reaches.

Given that it is the LWD-rich channels that exhibit finer pool textures, it seems likely that regardless of whether the finer-grained textures are seasonal or not they are a response to increased momentum extraction caused by woody debris. Repeated textural

mapping throughout the year and during different flow stages would be needed to assess whether finer-grained pool textures are seasonal or not.

Further examination of the reach maps shows a consistent local response of surface textural fining near most LWD, regardless of morphologic association of the debris (Maps 2-5). A section of Flu Hardy Creek (Fig. 3.12) exemplifies the local influence of LWD on surface textures. The dominant surface texture (D_{50}=29.5 mm) fines to intermediate (D_{50}=11.7 mm) and small (D_{50}=2 mm) textures near in-channel LWD. Mechanisms of LWD momentum extraction that cause textural fining include form drag, skin friction, hydraulic jumps, and physical blockage resulting in back-water and decreased energy slope. Logs and old-growth rootwads with low angles of attack also effectively steer flow, forcing local flow convergence and divergence in a fashion analogous to topographic steering (e.g., Dietrich and Smith, 1983). Momentum fluxes associated with flow steering alter channel shear stresses, which are in turn reflected by changing textural patterns (e.g., Dietrich and Smith, 1984a; Dietrich et al., 1979). The fluid accelerations and decelerations resulting from these momentum fluxes implicitly indicate energy loss from the system. Form drag calculations are an engineering approach that approximates the energy lost via these processes, as well as the more abrupt and violent energy dissipation caused by obstructions with near-perpendicular attack angles. As such, when I speak of LWD form drag it should be recognized that I am invoking a broad variety of styles of energy dissipation.

Effectiveness of LWD as an energy dissipater depends on its size, orientation, and position within the flow column. For example, although the farthest downstream log in Figure 3.12 is significantly larger than the next two upstream ones, the orientation of the upstream logs perpendicular to flow causes a stronger textural and morphologic response. Flow constriction around the perpendicular logs forces the formation of a channel-spanning underscour pool, but also results in proximal textural fining due to the high form drag of

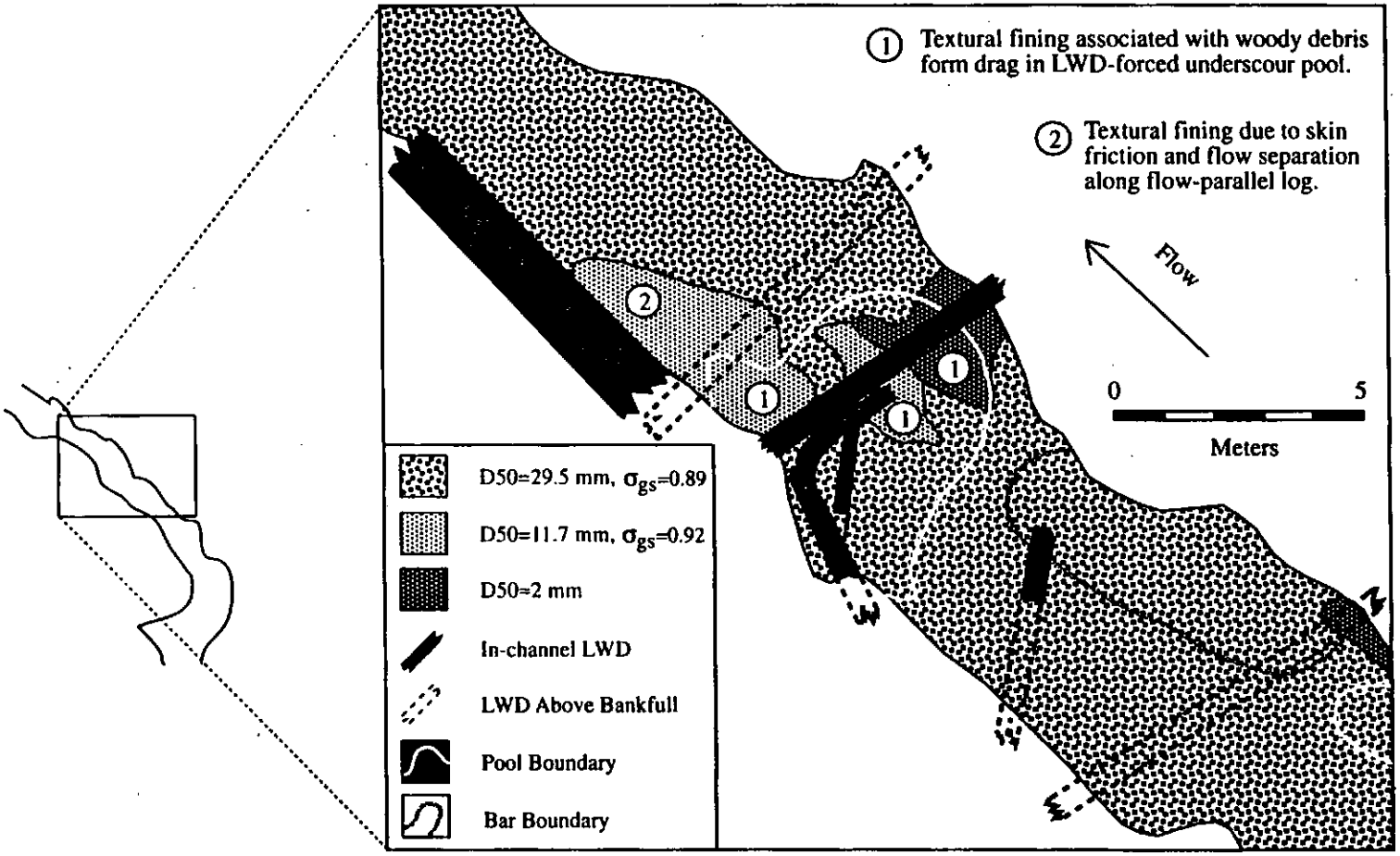

Figure 3.12 Section of Flu Hardy Creek showing mapped surface textures, LWD, and channel units. Surface textures are locally responsive to in-channel LWD (see numbered notes in the figure).

the LWD. The other two logs in this pool play a subordinate role to both textural and morphologic response (see discussion in Montgomery et al. (in press) regarding classification and identification of LWD morphologic function). Skin friction and flow separation along the large, downstream, flow-parallel log also induce textural fining, however persistence of fining to the downstream end of the log may be inhibited by channel narrowing and flow constriction, as well as by a local steepening of slope associated with a morphologic transition from pool to riffle (Fig. 3.12). The farthest upstream in-channel log has no textural effect, because of a much greater pitch than the other in-channel pieces, resulting in only a small portion of the log interacting with the flow.

Textural response to channel-spanning LWD jams has been documented by Rice (1990; 1994) in channels on the Queen Charlotte Islands of British Columbia. Rice (1994) proposed a cycle of textural response due to LWD regulation of sediment supply. As a LWD jam becomes established there is a progressive upstream damming and fining of sediment and a downstream deprivation and coarsening. Failure of the jam over time releases the upstream stored fines, completing the cycle by causing a progressive downstream fining and upstream coarsening. No effective wood jams were present at the Olympic study sites and so this style of textural response was not observed; rather, textural response occurred locally due to energy dissipation associated with relatively discrete LWD obstructions.

In addition to affecting local surface textures, LWD provides a significant control on channel morphology in forest streams (Zimmerman et al., 1967; Keller and Swanson, 1979; Lisle, 1986b; Smith and Buffington, in press; Montgomery et al., in press). The Olympic data agree quite well with the findings of Montgomery et al. (in press), which show that pool spacing in forest channels is inversely related to LWD frequency (pieces/m) (Fig. 3.13). The LWD-poor pool-riffle channels straddle Montgomery et al.'s (in press)

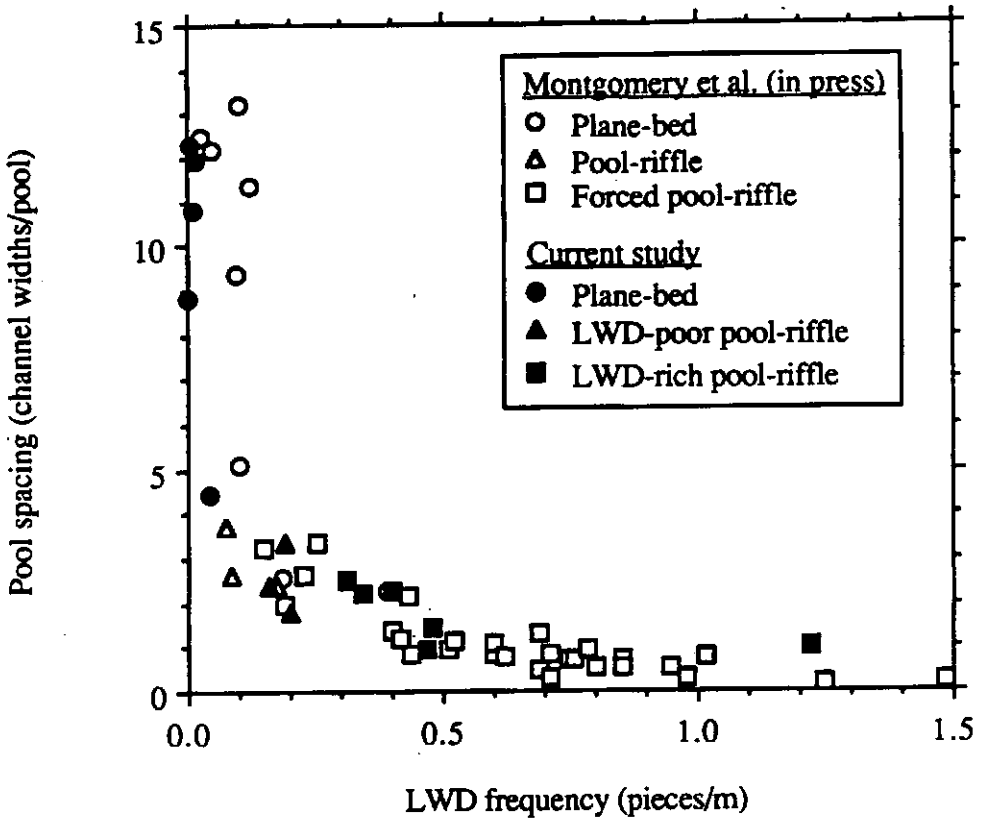

Figure 3.13 Pool spacing (number/channel width of stream length) as a function of LWD frequency (pieces/m). The Olympic data are typical of other Pacific Northwest and southeast Alaskan channels, all exhibiting similar morphologic response to LWD frequency. Montgomery et al. (in press) further detail the controls on pool spacing in forest channels.

TABLE 3.5: Pool Characteristics and LWD Abundance of the Olympic Channels

Channel	Pool Type			Pool Spacing (channel widths/pool)	LWD/m^2	LWD/m
	Self-formed (#)	LWD-forced (#)	Boulder-forced (#)			
Plane-bed						
Upper Dry Creek				>8.8	0.000	0.00
Alder Creek				>10.8	0.001	0.01
Hoko Tributary		1		12.0	0.003	0.02
Lower Hoh Slough	1			12.3	0.001	0.01
Upper Hoh Slough		1	1	4.5	0.004	0.04
LWD-poor Pool-riffle						
Upper Skunk Creek	2	3		2.4	0.023	0.16
Hoko River	3	4		1.4	0.015	0.20
Lower Pins Creek	2	1		3.3	0.029	0.19
LWD-rich Pool-riffle						
Upper Pins Creek		5		2.3	0.065	0.40
Flu Hardy Creek	2	2		2.5	0.045	0.31
Mill Creek	2	6		1.0	0.140	1.22
Lower Dry Creek		4		2.2	0.043	0.34
Lower Skunk Creek	2	9		1.0	0.036	0.47
Cedar Creek	2	4		1.5	0.042	0.48

self-formed and LWD-forced pool-riffle data, while the debris-rich pool-riffle channels plot with their LWD-forced data. Table 3.5 shows that most pools in the Olympic pool-riffle channels are LWD-forced, even in the debris-poor streams. Given this last observation it is not readily clear why the pools in debris-poor channels do not behave analogously to those of LWD-rich channels and exhibit a majority of fine and intermediate pool-forming textures. It may be that there are more pieces of LWD per pool, and thus more local energy dissipation, in the debris-rich channels, or it may be that higher wood loading provides greater reach-wide energy dissipation and a higher probability of significant textural response at pool-forming obstructions.

Differences in patterns and morphologic associations of textures emphasize process distinctions between obstruction-free and debris-loaded pool-riffle channels. Textural patterns in free-formed pool-riffle channels reflect topographically-induced spatial distributions of shear stress. Surface textures in debris-loaded pool-riffle channels additionally indicate LWD-induced redistribution and dissipation of channel shear stresses.

Subsurface Textures of the Olympic Channels

Subsurface grain size distributions for each layer (i.e., 10 ℓ volume) sampled below pebble-counted textural patches are presented in Figure 3.14, and Table 3.6 lists the corresponding D_{50ss} and σ_{gss} values. Subsurface samples were analyzed by layer in order to investigate textural variation with depth. Grain size distributions of textures were similar with depth in some channels (Fig. 3.14g, i, p, q, s, t), but in others were highly variable (Fig. 3.14b, d, h). Textures with variable subsurface distributions at depth demonstrate the need to sample a sufficient volume of sediment if a representative census is to be obtained, reinforcing the sampling criterion of Church et al. (1987).

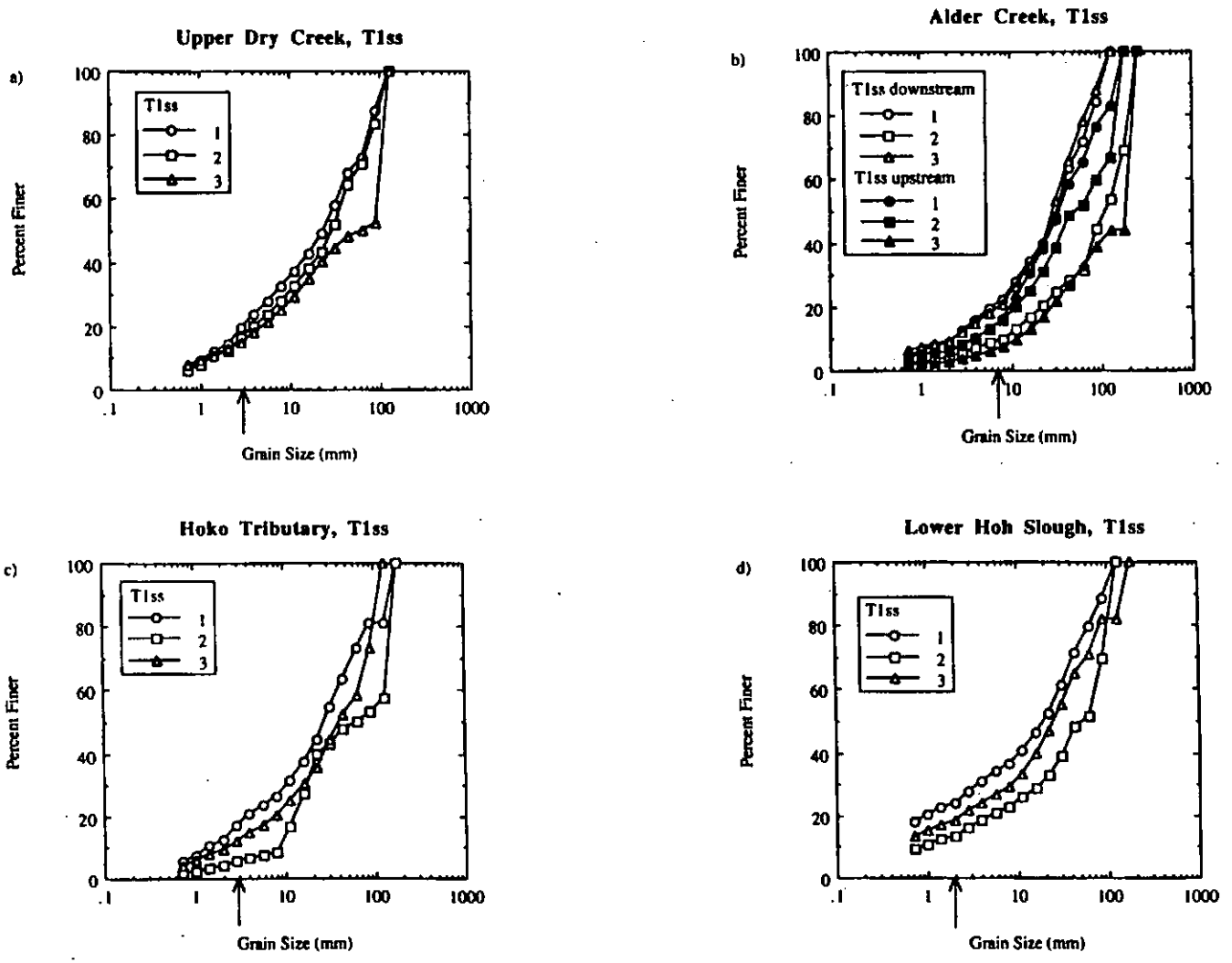

Figure 3.14 Subsurface grain size distributions of textures sampled in the Olympic channels. Grain size distributions are shown for each layer (10 ℓ bucket) sampled. Abscissa arrow indicates calculated reach-average D_{sus} value.

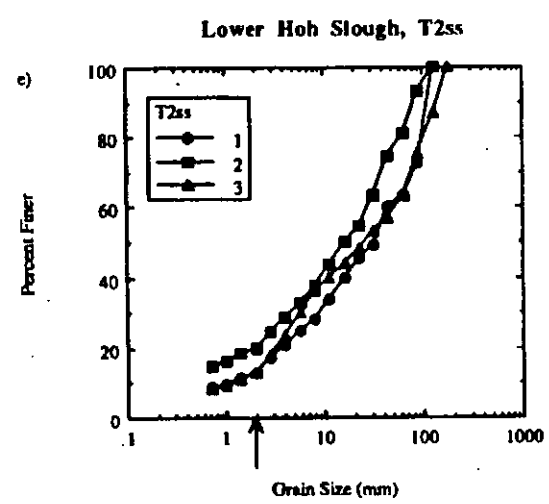

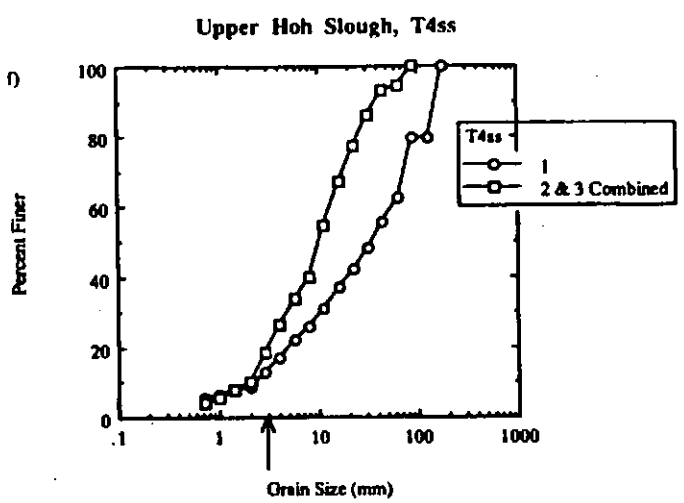

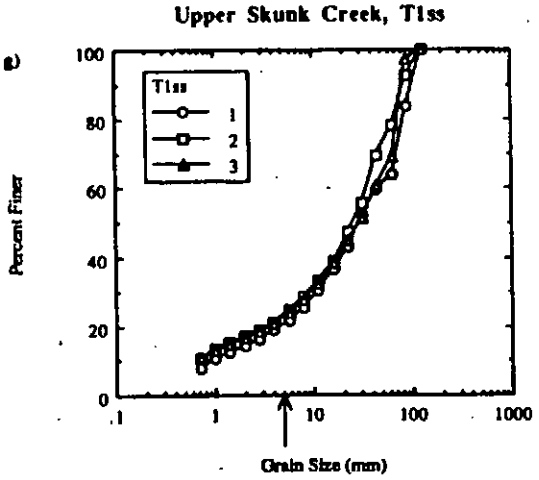

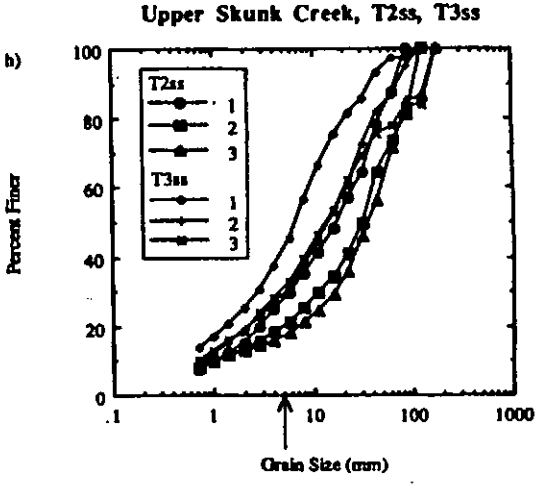

Figure 3.14 cont.

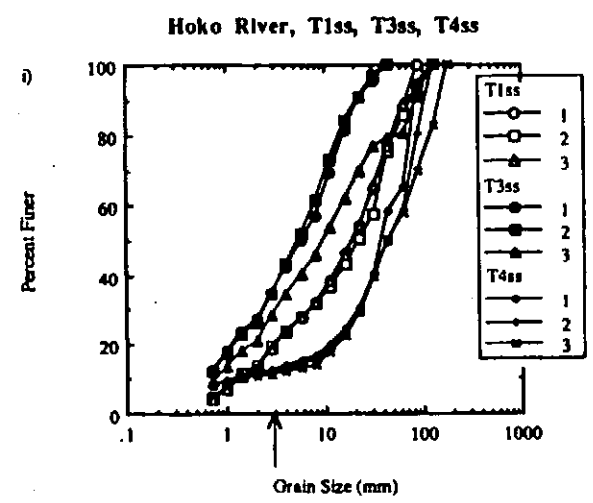

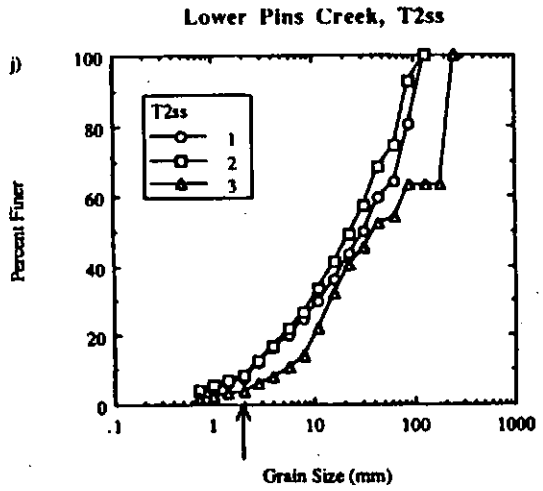

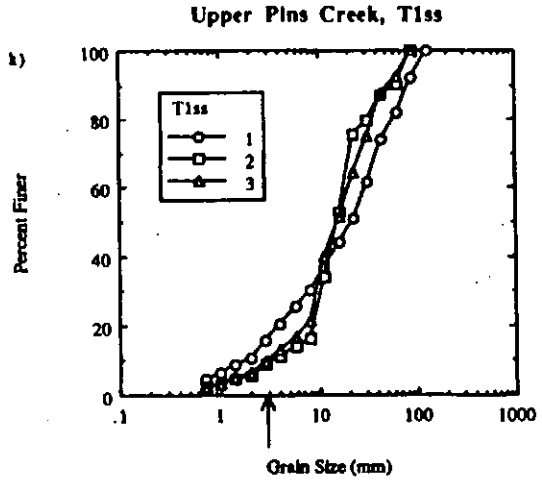

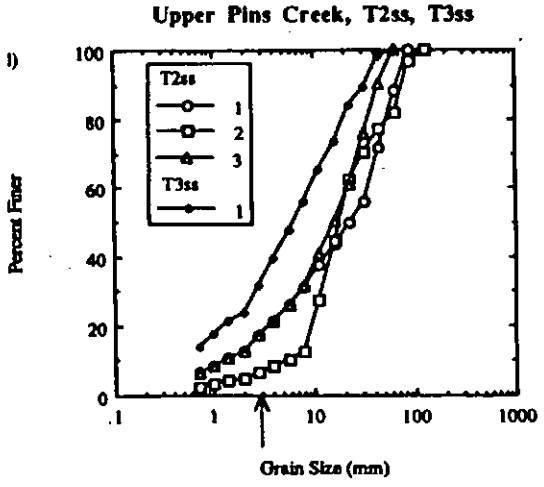

Figure 3.14 cont.

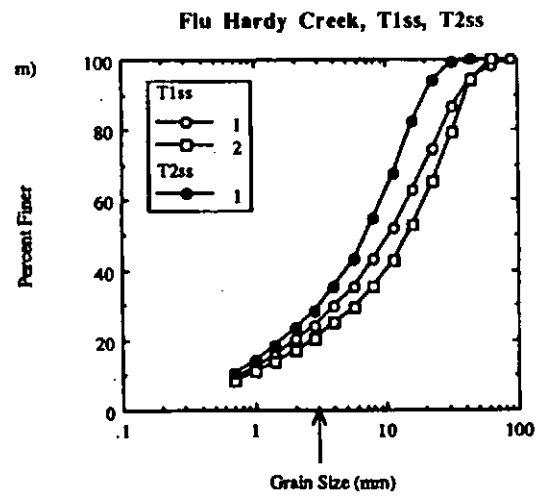

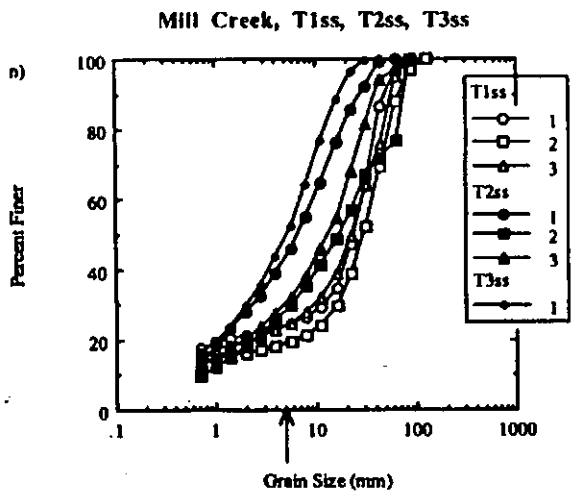

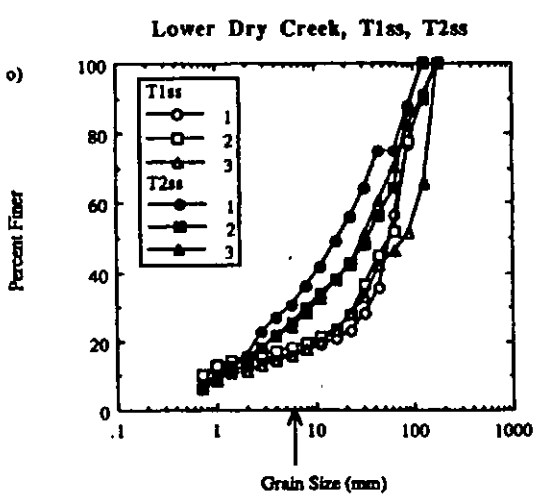

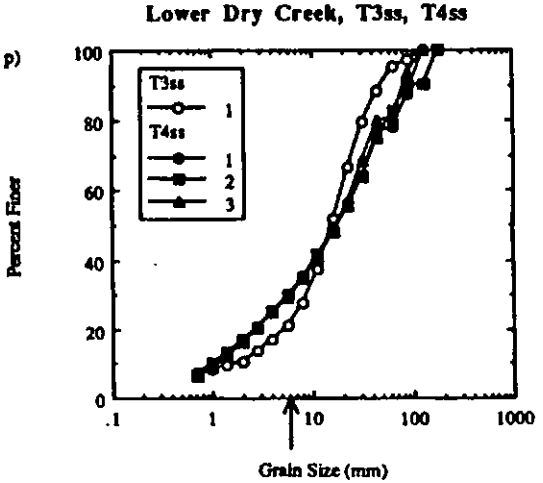

Figure 3.14 cont.

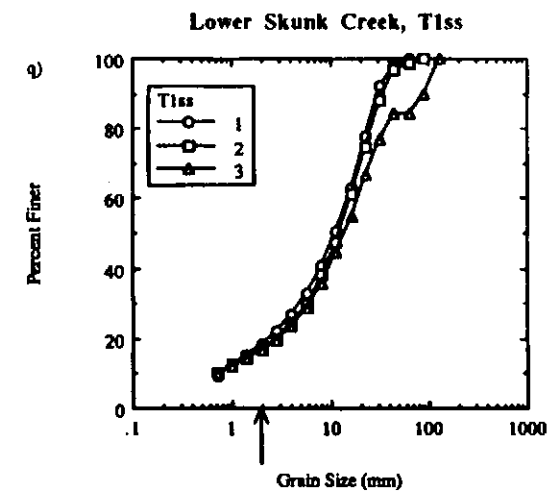

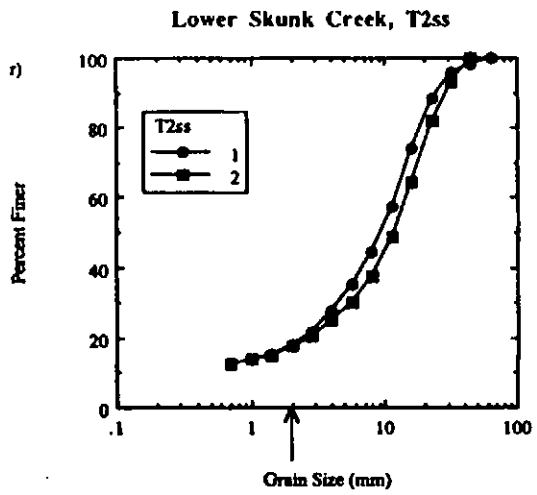

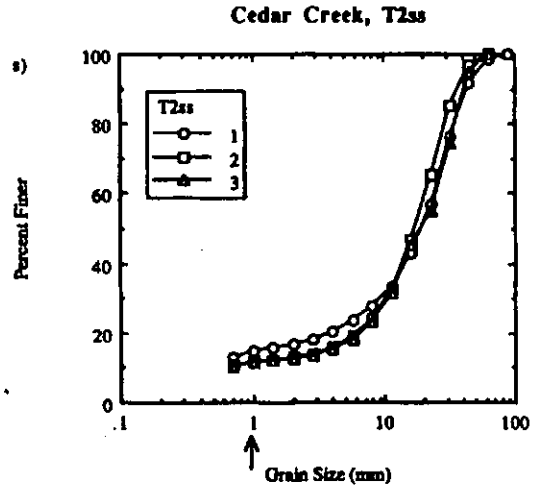

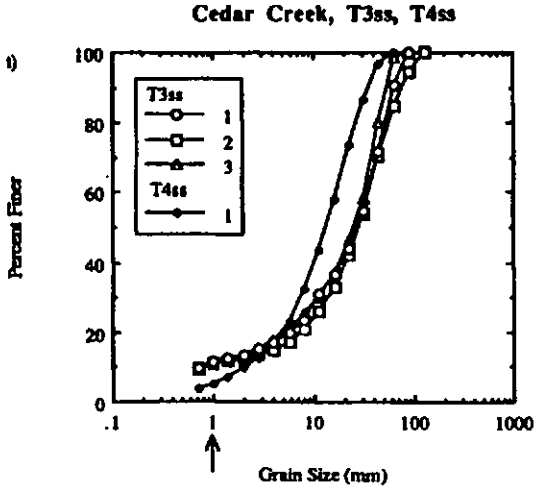

Figure 3.14 cont.

TABLE 3.6: Olympic Subsurface Grain Sizes By Sample Layer

Channel	Texture[$]	D_{50ss} (mm)[†]	$\lvert\sigma_{gss}\rvert$ (ϕ)
Plane-bed			
Upper Dry Creek	T1.1	23.4	2.60
	T1.2	29.8	2.54
	T1.3	62.6	2.58
Alder Creek	T1ds.1	33.4	2.23
	T1ds.2	111.6	1.91
	T1ds.3	29.5	2.06
	T1us.1	34.9	2.06
	T1us.2	51.9	2.11
	T1us.3	188	1.72
Hoko Tributary	T1.1	27.2	2.86
	T1.2	62.3	1.93
	T1.3	41.2	2.23
Lower Hoh Slough	T1.1	19.6	----
	T1.2	55.8	2.64
	T1.3	25.84	3.42
	T2.1	32.7	2.68
	T2.2	15.8	3.02
	T2.3	25.6	2.79
Upper Hoh Slough	T1, same as lower Hoh slough T1		
	T2, same as lower Hoh slough T2		
	T4.1	35.1	2.63
	T4.2 & 3	10.2	1.77
LWD-poor Pool-riffle			
Upper Skunk Creek	T1.1	29.3	2.55
	T1.2	25.2	2.75
	T1.3	29.6	2.72
	T2.1	17.3	2.37
	T2.2	32.3	2.51
	T2.3	36.7	2.24
	T3.1	6.6	2.49
	T3.2	13.6	3.26
	T3.3.	14.3	2.57
Hoko River	T1.1	18.8	2.28
	T1.2	22.3	2.38
	T1.3	19.1	2.26
	T3.1	5.7	1.98
	T3.2	5.2	1.94
	T3.3	9.6	2.94
	T4.1	38.7	1.78
	T4.2	46.4	1.77
	T4.3	45.5	1.87
Lower Pins Creek	T2.1	31.8	2.30
	T2.2	23.5	2.18
	T2.3	40.5	2.32
LWD-rich Pool-riffle			
Upper Pins Creek	T1.1	21.5	2.30
	T1.2	15.2	1.18
	T1.3	15.4	2.45

[$]Textures correspond with those given in Table 3.4. Number after decimal signifies sample layer relative to the surface. ds=downstream, us=upstream.

[†] Grain size distributions are untruncated.

TABLE 3.6 cont.

Channel	Texture[$]	D_{50ss} (mm)[†]	$\lvert\sigma_{gss}\rvert$ (ϕ)
	T2.1	22.7	2.24
	T2.2	17.7	1.48
	T2.3	15.7	3.91
	T3.1	6.2	2.35
Flu Hardy Creek	T1.1	10.5	2.19
	T1.2	14.6	2.18
	T2.1	7.0	1.94
Mill Creek	T1.1	23.9	---
	T1.2	30.2	2.56
	T1.3	22.8	2.66
	T2.1	6.7	---
	T2.2	17.0	2.74
	T2.3	13.2	2.43
	T3.1	5.2	2.01
Lower Dry Creek	T1.1	57.5	2.21
	T1.2	58.0	2.67
	T1.3	82.1	2.35
	T2.1	16.9	2.67
	T2.2	34.5	2.57
	T2.3	30.7	2.73
	T3.1	15.3	1.71
Lower Skunk Creek	T1.1	11.1	2.05
	T1.2	12.1	2.05
	T1.3	13.7	2.31
	T2.1	9.2	1.87
	T2.2	11.6	1.95
Cedar Creek	T2.1	19.0	2.32
	T2.2	16.9	1.48
	T2.3	19.0	1.55
	T3.1	27.6	2.06
	T3.2	56.5	3.27
	T3.3	28.7	1.86
	T4.1	13.2	1.50

[$]Textures correspond with those given in Table 3.4. Number after decimal signifies sample layer relative to the surface. ds=downstream, us=upstream.

[†] Grain size distributions are untruncated.

TABLE 3.7: Subsurface Textural Composition of the Olympic Channels

Channel	Reach D_{50ss} (mm)‡	Texture	% of Bed	Bulk Textural D_{50ss} (mm)‡	σ_{gss} (ϕ)‡
Plane-bed					
Upper Dry Creek	30.2 (42.5)				
		T1	100	30.2 (42.5)	2.65 (1.77)
Alder Creek	60.2 (75.8)				
		T1	100	60.2 (75.8)	2.19 (1.70)
Hoko Tributary	38.2 (47.4)				
		T1	100	38.2 (47.4)	2.18 (1.87)
Lower Hoh Slough	28.1 (39.7)				
		T1	63	31.1 (42.3)	3.20 (1.80)
		T2	35	24.2 (35.0)	2.76 (2.21)
		T3	2	~2.0† (na)	
Upper Hoh Slough	14.0 (22.4)				
		T1	4	31.1 (46.2)	3.20 (1.58)
		T2	0.5	24.2 (40.1)	2.76 (1.95)
		T3	4	~2.0† (na)	
		T4	91.5	13.7 (21.3)	2.33 (1.64)
LWD-poor Pool-riffle					
Upper Skunk Creek	23.5 (37.9)				
		T1	71.24	27.8 (40.6)	2.68 (1.40)
		T2	8.22	28.5 (38.3)	2.45 (1.43)
		T3	11.19	10.6 (20.7)	2.67 (1.70)
		T4	9.33	~2.0† (na)	
Hoko River	21.7 (29.8)				
		T1	61.58	19.9† (28.6)	2.3 (1.49)
		T2	5.10	~6.0† (?)	
		T3	13.87	6.5 (11.9)	2.30 (1.41)
		T4	19.45	42.3 (52.7)	1.76 (1.23)
Lower Pins Creek	30.3 (34.3)				
		T1	2.58	12.7† (13.3)	1.15 (1.10)
		T2	92.11	32.1 (36.0)	2.52 (2.24)
		T3	4.15	9.2† (9.8)	1.32 (1.19)
		T4	1.16	~2.0† (na)	
LWD-rich Pool-riffle					
Upper Pins Creek	15.5 (19.4)				
		T1	40.61	16.0 (18.1)	1.65 (1.29)
		T2	48.47	17.9 (21.0)	1.81 (1.35)
		T3	3.22	6.2 (11.5)	2.15 (1.40)
		T4	7.71	~2.0† (na)	
Flu Hardy Creek	10.6 (17.5)				
		T1	80.53	12.5 (17.8)	2.20 (1.26)
		T2	3.70	7.0 (10.4)	1.94 (0.98)
		T3	11.79	~2.0† (na)	
		T4	3.98	~0.06† (na)	
Mill Creek	10.1 (19.5)				
		T1	8.15	25.4 (32.4)	2.69 (0.92)
		T2	62.57	11.3 (19.6)	2.58 (1.42)
		T3	11.77	5.2 (9.8)	1.81 (0.83)
		T4	15.89	~2.0† (na)	
		T5	1.63	~0.06† (na)	

‡ Values in parentheses are derived from grain size distributions truncated at D_{sus} and are thus indicative of bedload material only.

†D_{50ss} assumed equal to D_{50s}.

¥ Bedload and suspended load material could not be differentiated as the calculated D_{sus} value is < 2 mm, the minimum resolution used for surface pebble counts; all grain sizes ≤ 2 mm were lumped into one category and are consequently undifferentiable.

TABLE 3.7 cont.

Channel	Reach D_{50ss} (mm)‡	Texture	% of Bed	Bulk Textural D_{50ss} (mm)‡	$\lvert\sigma_{gss}\rvert$ (ϕ)‡
Lower Dry Creek	41.1 (55.7)				
		T1	47.48	60.9 (73.5)	2.42 (1.17)
		T2	39.28	26.0 (44.0)	2.66 (1.45)
		T3	7.52	15.3 (19.7)	1.71 (1.06)
		T4	4.79	17.2 (31.4)	2.63 (1.46)
		T5	0.94	~2.0† (na)	
Lower Skunk Creek	9.4 (13.6)				
		T1	21.54	12.2 (15.8)	2.11 (1.30)
		T2	62.31	10.3 (12.8)	1.90 (1.11)
		T3	16.15	~2.0† (na)	
Cedar Creek	20.6 (24.6)				
		T1	7.53	74.4†¥	0.89
		T2	64.19	18.0 (21.3)	1.75 (1.05)
		T3	6.15	27.1 (32.0)	1.97 (1.33)
		T4	12.80	13.2 (14.4)	1.50 (1.28)
		T5	2.64	~2.0†¥	
		T6	1.08	6.6†¥	0.98
		T7	5.61	~0.06† (na)	

‡ Values in parentheses are derived from grain size distributions truncated at D_{sus} and are thus indicative of bedload material only.

†D_{50ss} assumed equal to D_{50s}.

¥ Bedload and suspended load material could not be differentiated as the calculated D_{sus} value is < 2 mm, the minimum resolution used for surface pebble counts; all grain sizes ≤ 2 mm were lumped into one category and are consequently undifferentiable.

Median subsurface grain sizes for each bulk subsurface sample are shown in Table 3.7. Sand and silt-sized patches were not sampled, as it was assumed that surface and subsurface grain sizes would be negligibly different. Several other textures were not sampled, because of insufficient dry exposure; these samples were also assumed to have equivalent surface and subsurface distributions. Of those textures sampled the weight percent of the largest subsurface grain varied from 0.5 to 16.1% of the total weight, with a median value of 3.6%. Consequently, the sampling technique employed generally underestimated the volume of material necessary to produce the intended D_{maxss} weight percent of ≤1. Because of the particular sampling technique used, D_{maxss} values less than 1% of the total weight may result from $D_{maxss}>D_{maxs}$, $D_{maxss}>83$ mm, or samples with significant porosity. While a median D_{maxss} weight percent of 3.6 is acceptable, traditional field weighing of samples is recommended to avoid potentially erroneous assumptions and yield samples with uniform D_{maxss} weight percents.

As expected, reach average D_{50ss} values (Table 3.7) are less than the corresponding surface median grain sizes (Table 3.4), except for two channels; Alder and Lower Hoh have composite bedload and suspended load values of $D_{50s}<D_{50ss}$, while Alder and Lower Pins have bedload values of $D_{50s}<D_{50ss}$. As with the reach-average results, most of the individual bulk samples show $D_{50ss}<D_{50s}$ (cf. Tables 3.7 and 3.4). However, about 18% of the bedload textures and 14% of the composite textures (i.e., bedload and suspended load) exhibit subsurface median grain sizes greater than that of the surface. Kinerson (1990) also found cases of D_{50ss} larger than D_{50s}. Such results may represent insufficient sampling of either of the textural domains, or may occur due to erroneously sampling buried, relict, surface horizons at depth. Bed stratigraphy was not characterized in this analysis, but is a real concern for investigators conducting subsurface sampling; stratigraphy is largely ignored in the subsurface sampling literature, the present study included.

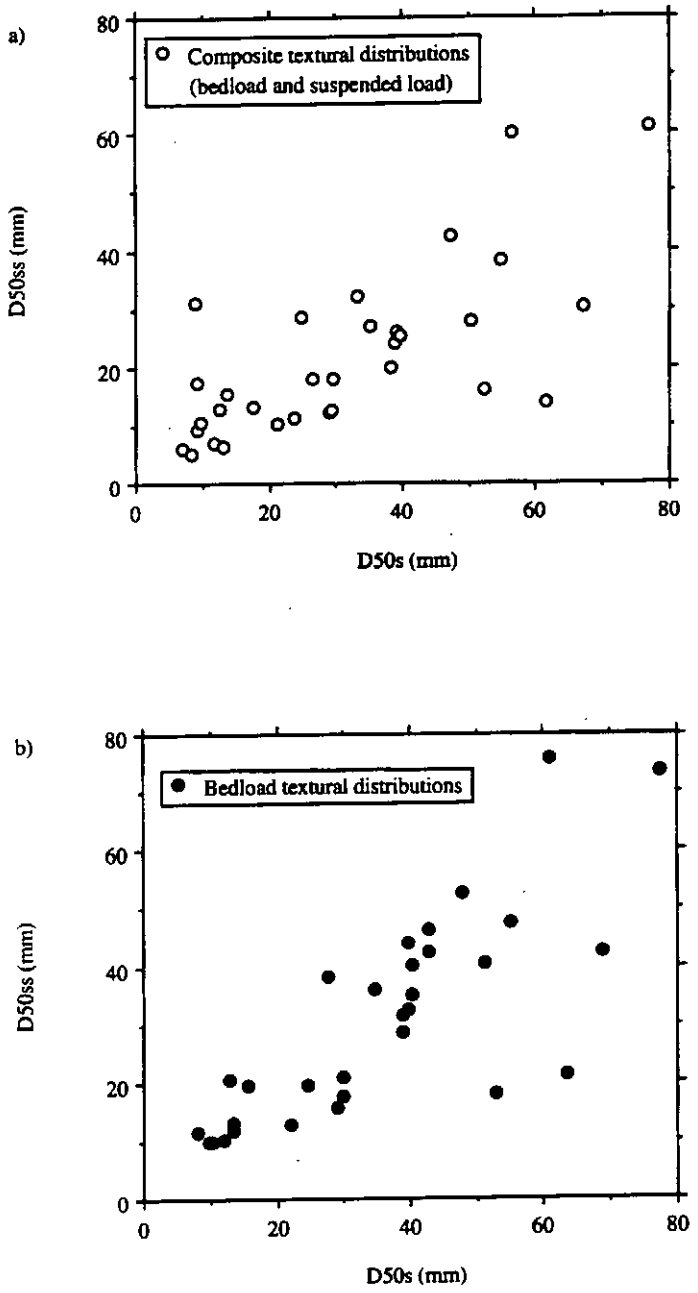

Figure 3.15 Correlation of D_{50s} and D_{50ss} for a) composite and b) bedload material of textures surveyed in the Olympic channels.

Although there is considerable scatter in the data, Figure 3.15 shows that D_{50ss} values are roughly correlated with surface median grain sizes. For a given reach, surface textural patches with larger median grain sizes have correspondingly larger subsurface median grain sizes (Table 3.7). One might intuitively expect this result. Bedload material moving through a reach will be sorted by differential shear stresses (e.g., Dietrich and Smith, 1984a; Dietrich et al., 1979), provided that grain sizes representative of a particular shear stress are available; a higher local shear stress will not have a correspondingly larger bedload grain size if larger sizes are not available in the supplied bedload distribution. As such, subsurface grain sizes [which approximate those of the bedload (Milhous, 1973; Kuhnle, 1993)] should parallel surface grain sizes in expressing the spatial pattern of shear stresses within a reach.

It is commonly assumed that in armored channels the surface grain size distribution results from winnowing of the parent subsurface distribution (Carling and Reader, 1982; Andrews and Parker, 1987). For this to be true the surface and subsurface grain size distributions would share the same range of values. With the lower end of grain size distributions truncated uniformly by reach-specific D_{sus} values, comparison of surface and subsurface D_{max} values indicates that 30% of the textures sampled have equivalent upper grain sizes, while 50% have $D_{maxss}<D_{maxs}$ and 20% have $D_{maxss}>D_{maxs}$. Consequently, the majority (80%) of truncated subsurface grain size distributions are equal to or narrower than their surface counterparts. Kinetic sieving (Sallenger, 1979; Rosato et al., 1987; Haff, 1991) may also be a mechanism for creating armored beds through concentration of coarse material at the surface. This mechanism for armor generation would deplete the subsurface of coarse material, resulting in grain size distributions narrower than that of the surface, which is the most common condition observed at the Olympic study sites.

Reach-Average Textural Response Within the Threshold Model Framework: Empirical Results and Preliminary Analysis of Relative Magnitudes of Influence

The bankfull threshold model is based on reach-average characterization of channel attributes. While examination of local textural response is important for understanding process mechanics, individual textural patches are indicative of particular site-specific conditions that are not easily predicted. As such, a reach-average focus is necessary for prediction of surface grain size and examination of textural response. Although mapped surface textures show locally intensive response to flow obstructions, it is likely that turbulent mixing characteristic of natural rivers and accentuated by LWD is sufficient to cause momentum exchange across textural patches, resulting in a range of obstruction influence broader than the obvious proximal textural responses. Turbulent mixing thus provides a mechanism for integrating local effects into a reach-wide channel response to roughness elements, providing a conceptual linkage between local and reach-scale channel processes.

Reach-average Olympic and Alaskan field data analyzed within the threshold model framework agree well with the hypothesized trends of textural response expressed by Figure 1.1. Within the model construct, study sites segregate by channel type into distinct zones of reach-average textural response (Fig. 3.16). As expected, increasing hydraulic roughness produces a systematic textural fining and decrease in reach-average D_{50s}. Plane-bed channels are characterized by grain roughness only and generally plot closest to the threshold channel prediction, while debris-poor pool-riffle channels with grain, bedform, and minimal LWD roughness cluster below the plane-bed streams. LWD-rich pool-riffle channels characterized by grain, bedform, and abundant woody debris roughness show the strongest textural response and cluster at the bottom of Figure 3.16. Four of the Alaskan channels have morphologies transitional between plane-bed and pool-riffle channel types.

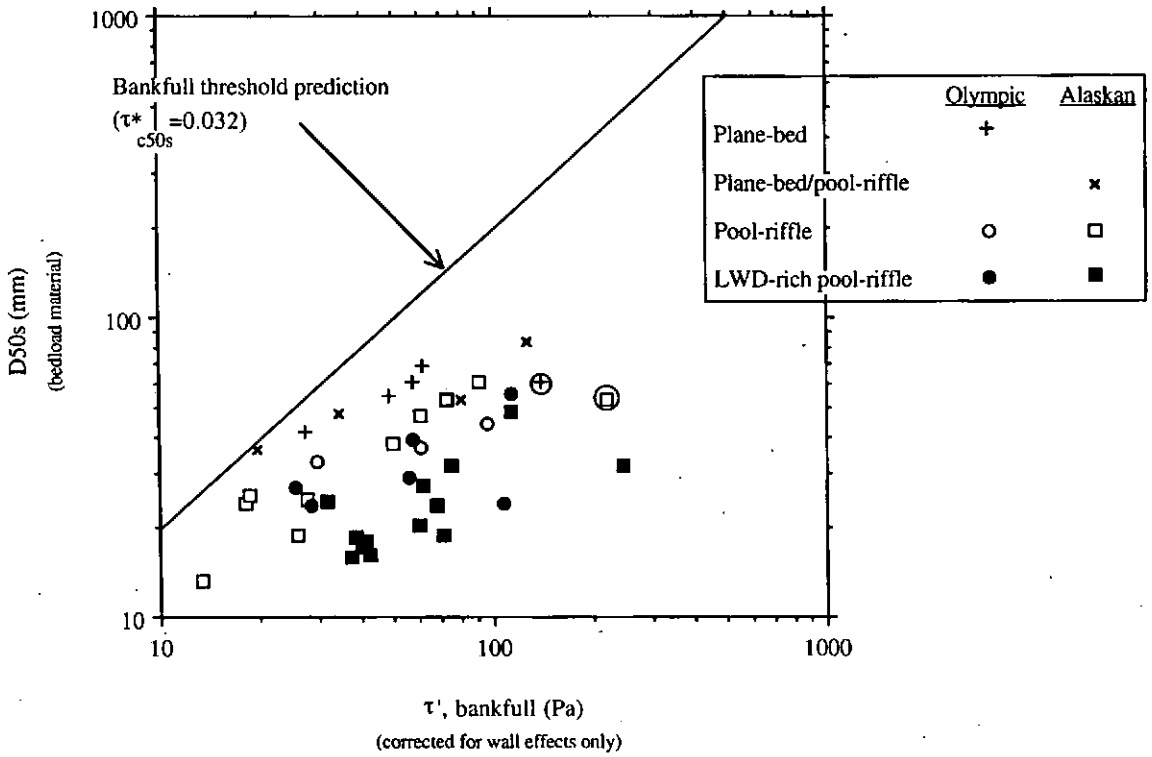

Figure 3.16 Reach-average D_{50s} values (bedload material only) of the Olympic and Alaskan study sites relative to the bankfull threshold prediction of median surface grain size. Abscissa values of τ' are corrected for τ_W only. Note the distinct zones of textural response for plane-bed, LWD-poor pool-riffle, and LWD-rich pool-riffle channels. These zones represent a progressive textural fining and deviation from the model predictions with increasing channel roughness embodied by the channel types examined. Circled data points are channels most recently impacted by catastrophic sediment inputs.

Two of these transitional channels behave like plane-bed streams and plot close to the bankfull threshold prediction (Fig. 3.16).

Of the five channels showing field evidence of catastrophic sediment inputs, only Alder Creek and Lower Greens Creek (circled points, Fig. 3.16) deviate from the textural response ranges of their respective channel types. Alder Creek, an Olympic plane-bed channel, has riparian margins inundated by recent debris flow deposits and shows a stronger magnitude of textural fining than the other plane-bed channels (Fig. 3.16). This larger degree of fining may be due to elevated sediment loads as a result of debris flow disturbance; field observation indicates that the Alder Creek debris flow deposited a short distance downstream of the study reach. The morphology of Alder Creek may also be responsible for an anomalously low reach-average D_{50s}. Alder Creek is a high-gradient, bouldery stream with a morphology verging on that of a cascade channel [definition of Montgomery and Buffington (1993)], evidenced by tumbling and tortuous flow over and around individual boulders. This style of turbulent, tumbling, jet-and-wake flow, different from the other plane-bed channels examined, significantly increases downstream energy dissipation (Chin, 1989) and may explain the low observed D_{50s}. The study reach of Lower Greens Creek, an Alaskan LWD-poor pool-riffle channel, lies just downstream of a recent, large landslide that entered and dammed the channel; the failure was initiated downslope of a mining road. The Lower Greens Creek data used here were collected a short time after the landslide dam was breached. Stored sediment liberated by the dam failure would have led to increased downstream sediment loading and may explain the larger magnitude of fining in this channel compared to the other LWD-poor pool-riffle channels. However, about 25% of Lower Greens Creek is composed of step-pool channel units containing two 1-1.5 m bedrock steps (falls); turbulent energy dissipation associated with these channel units may contribute to the low D_{50s} observed in this channel.

Of the landslide-affected channels, only the two most recently impacted ones show textural fining of greater magnitude than channels of similar morphologic type, suggesting a transient nature of textural response to catastrophic changes in sediment supply. For example, Lower Dry Creek, an Olympic LWD-rich pool-riffle channel, is characterized by relict (now vegetated) channel-margin debris flow terraces, indicating past catastrophic changes in sediment loading. However, Lower Dry Creek has a relatively high reach-average D_{50s} compared to the other LWD-rich pool-riffle channels, suggesting little residual influence of any past increases in sediment loading.

While showing no evidence of recent catastrophic sediment impacts, the other thirty-six study sites likely have different levels of sediment loading. Despite these potential differences in sediment supply, Figure 3.16 demonstrates a trend of decreasing reach-average median surface grain size with increasing complexity of channel roughness, indicating that non-catastrophic sediment loading is subordinate to bedform and LWD roughness at the sites investigated. Although there is the potential for severe sediment impacts, and hence sediment-induced textural fining, in Pacific Northwest channels, natural catastrophic changes in sediment load tend to result from infrequent pulsed events (i.e., debris flows, fire storms, 50-100 year floods, etc.). Furthermore, because sediment impacts of this sort are typically not sustained, their influence on textural response will be transient compared to the pervasive influence of bedforms and LWD in forest channels. Consequently, LWD and stable barforms provide long-term influences that dominate surface textures of the study sites, while sediment supply effects are either relatively less significant or transient. The frequency with which channels are impacted by sediment loading, however, depends on geomorphic province and position within a channel network. Higher-gradient channels of the Pacific Northwest tend to be closer to debris flow sources, but lower-gradient channels are likely sites for debris flow deposition (e.g., Montgomery and Buffington, 1993).

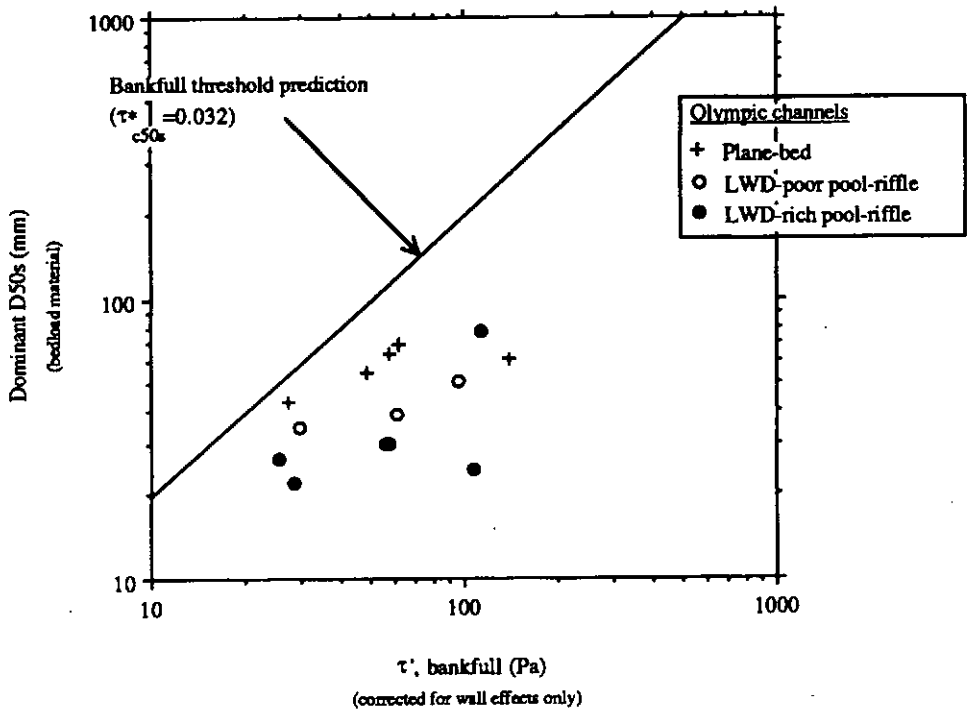

Figure 3.17 D_{50s} values of the dominant (i.e., most abundant) surface texture in each of the Olympic channels plotted relative to the bankfull threshold model prediction. Zones of response generally analogous to those of Figure 3.16 suggest that textural response to hydraulic roughness elements occurs on a reach scale, rather than solely on a local scale proximal to flow perturbances.

To further examine reach-scale textural response, the median grain size of the dominant (i.e., most abundant) surface texture of each Olympic channel was plotted versus shear stress (Fig. 3.17). A segregation of research sites by channel type similar to that of Figure 3.16 suggests that hydraulic roughness elements have a reach-wide impact on surface textures and are not just limited to local textural response.

Because Figure 3.16 illustrates a continuum of textural response, some overlap occurs between channel types. However, zones of response associated with specific channel types can be identified. Each zone describes a distribution of textural response (Fig. 3.18), with LWD-rich channels showing the broadest range and the highest magnitude of fining, expressed as the ratio of predicted-to-observed median surface grain size. Plane-bed channels exhibit the narrowest response range, but their distribution is based on considerably fewer data, and thus is less well defined.

The three types of gravel-bedded streams studied were chosen in order to distinguish textural response to different scales and styles of hydraulic roughnesses (i.e., bedforms versus LWD). Although LWD was present in both pool-riffle channel types, wood loading in the debris-poor channels is quite low, and for comparative purposes can be considered insignificant (Fig. 3.8). As such, LWD-poor pool-riffle channels predominantly represent grain and bedform roughness, while debris-rich channels represent the full suite of grain, bedform, and LWD resistance. Assuming negligible sediment supply effects, the relative magnitudes of textural response due to bedform and LWD roughness can be examined empirically by comparing median values of the response distributions (Fig. 3.18). These data show that bedform and LWD roughness are comparable, both causing a roughly two-fold decrease in reach-average median surface grain size. It is emphasized, however, that these magnitudes of textural response are median values of overlapping response distributions. Furthermore, surface textures of the plane-bed channels also deviate somewhat from the bankfull threshold prediction of surface

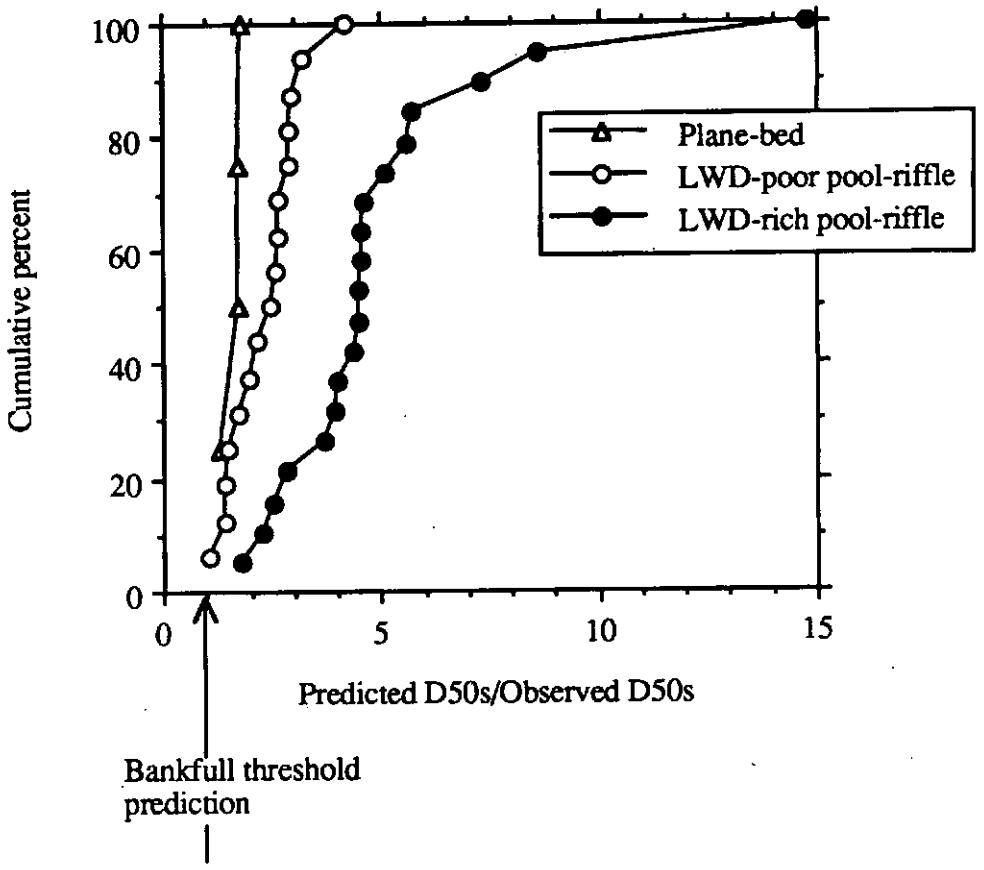

Figure 3.18 Distributions of reach-average textural response in plane-bed, LWD-poor, and LWD-rich channels. Textural response is expressed as deviation from unity for the ratio of predicted-to-observed D_{50s}. Due to some bedform roughness, the transitional plane-bed/pool-riffle channels are included with the LWD-poor pool-riffle data. The sediment-impacted Alder Creek and Lower Greens Creek are not included here.

grain size (Fig. 3.16 and 3.18), presumably due to background levels of sediment loading. As such, the magnitudes of textural fining due to bedform and LWD roughness determined from Figure 3.18 should be viewed as estimates, pending more rigorous discrimination of relative effects of sediment supply and hydraulic roughness. It is further cautioned that while relative magnitudes of textural response to bedforms and woody debris can be assessed from the empirical findings, the absolute degree of textural response inferred from the model is sensitive to the τ^*_{c50s} value used for the model predictions (cf. Fig. 2.2a-b).

Compatibility of Data Sets

Comparison of the Olympic and Alaskan data is based on the assumption that the methods of reach-average textural characterization are comparable. The two methods employed were: regularly spaced cross-channel pebble counts; and mapping of textural patches, accompanied by representative pebble counts of each texture. The two techniques are obviously identical for mono-textural channels, but for patchy streambeds accurate representation of channel grain sizes through regularly spaced pebble counts depends on the areal extent of sampling and the spatial distribution of textures within the channel [see also discussion by Wolcott and Church (1990)]. For example, the number and areal extent of pebble counts shown in Figure 3.19 are likely to approximate the true distribution of Figure 3.19a, but misrepresent that of Figure 3.19b simply due to differences in spatial distributions of textural patches in the two cartooned channels. Both estimates can be improved by either increasing the number of cross-channel transects or by increasing the area sampled in each pebble count. The Alaskan pebble counts are estimated to have sampled approximately 15-30% of the area of each study reach. This sampling area is probably sufficient for the LWD-rich channels, which have spatial distributions of textures similar to that shown in Figure 3.19a and Map 3, but is likely to be less accurate for the

debris-poor channels, as they typically have less well-distributed textural patches. Despite the uncertainty associated with the Alaskan LWD-poor channels, the bulk of the grain size data used in this analysis are likely compatible.

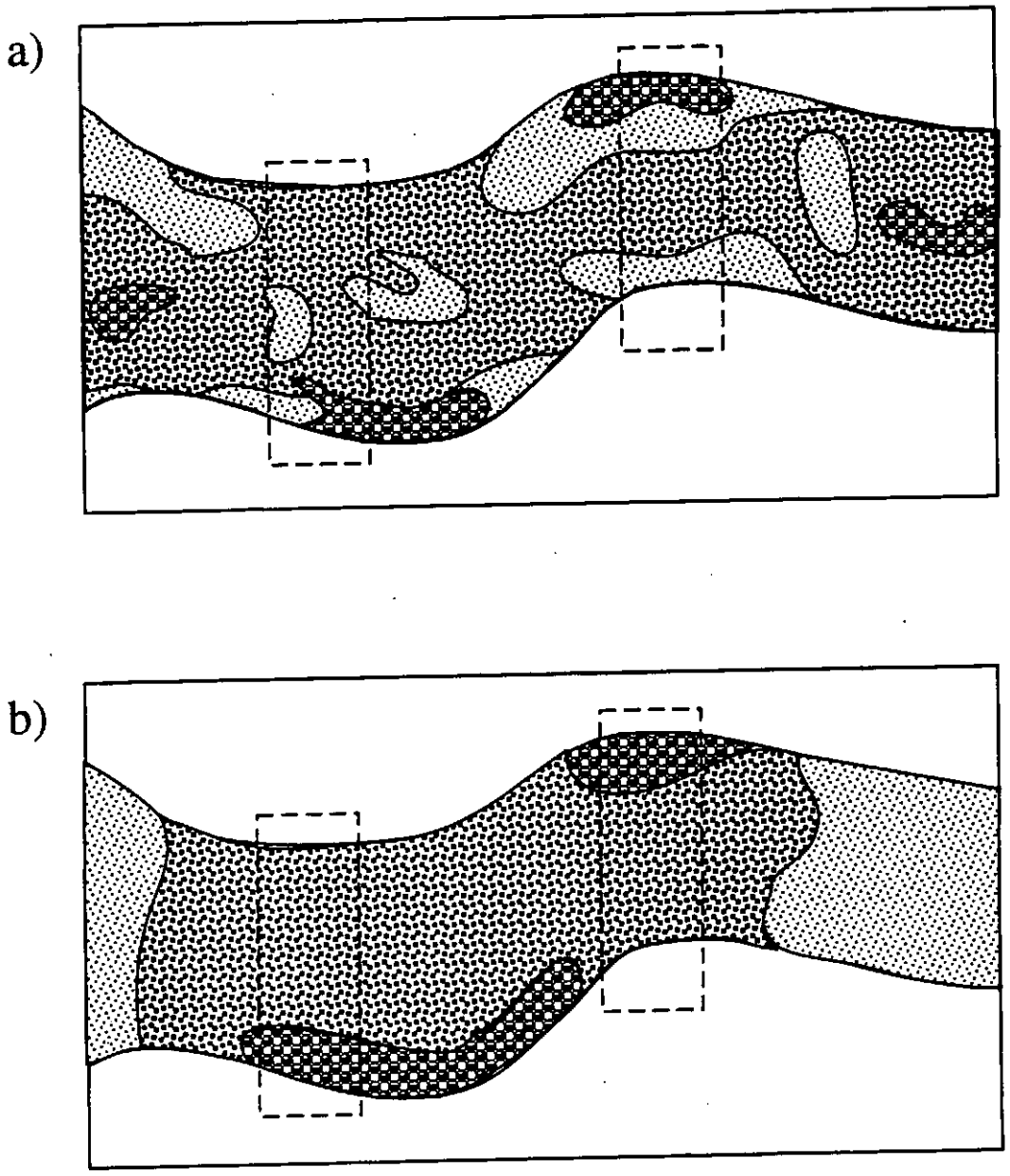

Figure 3.19 Illustration of the effectiveness of discrete pebble counts in a channel with a) highly complex and b) less complex spatial arrangements of surface textures.

Chapter 4: Land Management Implications

Assessment of Channel Condition and Prediction of Response Potential

Figures 4.1 and 4.2 summarize empirically determined ranges of textural response to bedform and LWD roughness inferred from the Olympic and Alaskan field data and also show the range of textural response to sediment supply determined from Kinerson's (1990) data. The empirical response distributions (Fig. 4.2) demonstrate that the combined influences of bedform and LWD roughness are of the same magnitude as that of potential textural fining due to sediment supply. Consequently, sediment supply and hydraulic roughness are both first-order controls on surface textures of forest gravel-bedded channels. If the interpretation made in Chapter 3 is correct, however, sediment supply impacts on surface textures, while potentially significant, may be infrequent and ephemeral compared to the pervasive effects of bedform and LWD roughness in forested environments like those studied.

The bankfull threshold model coupled with subsurface grain size analyses provides a valuable management tool for assessing channel condition. Predicted values of D_{50s} and measured values of D_{50ss} define theoretical limits of textural response to both sediment supply and other hydraulic roughness elements, as discussed in Chapters 1 and 2. Channel condition in terms of the degree of existing textural response to these factors can be assessed by comparing the observed textural fining relative to that of the potential fining represented by the theoretical limits

$$\frac{(\text{Predicted } D_{50s} - \text{Observed } D_{50s})}{(\text{Predicted } D_{50s} - \text{Observed } D_{50ss})} \qquad (7)$$

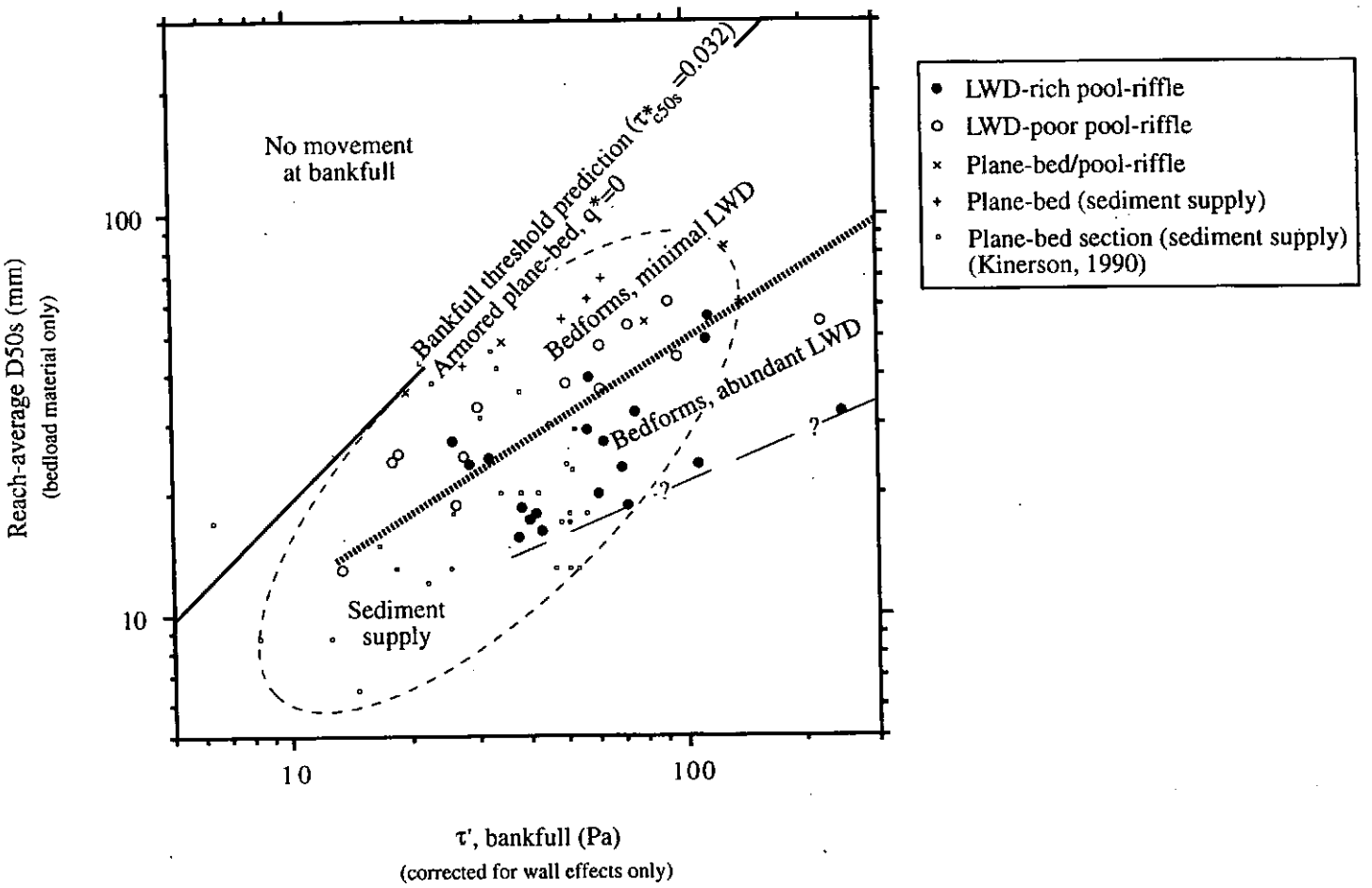

Figure 4.1 Summary of the bankfull threshold model and empirically determined ranges of textural response to sediment supply, bedforms, and LWD. Data are those shown in Figures 2.3 and 3.16.

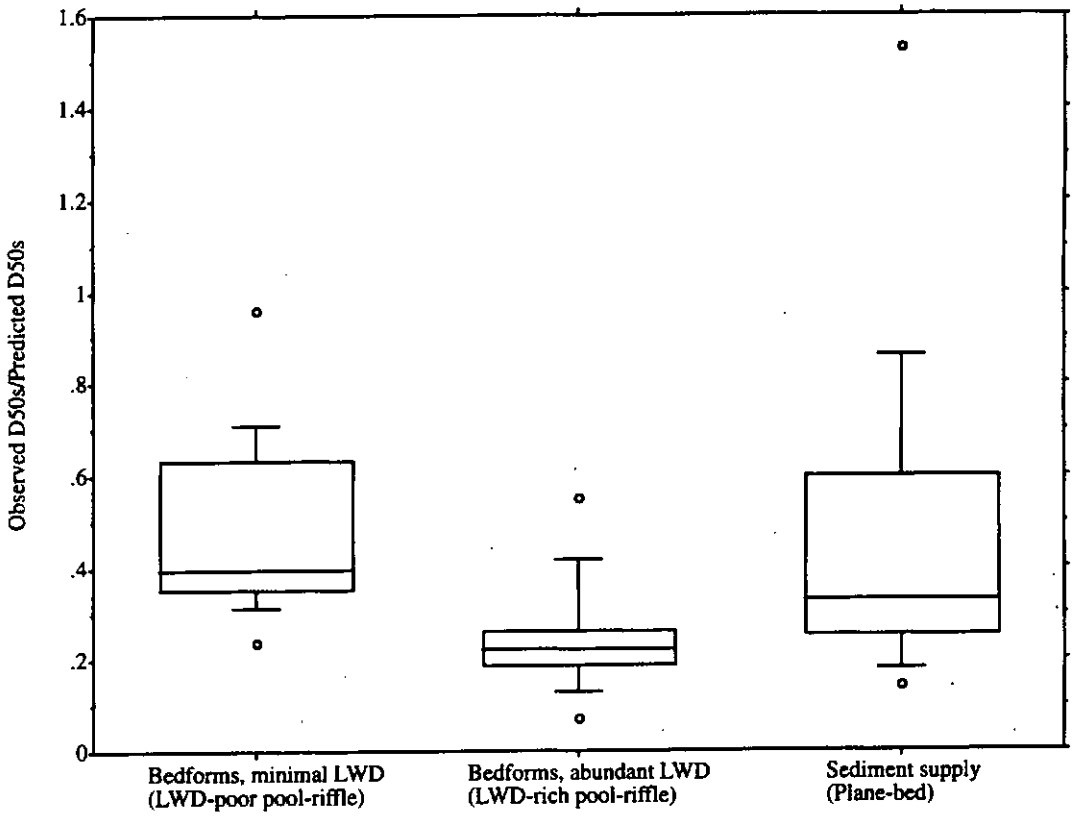

Figure 4.2 Empirical textural response ranges due to sediment supply, bedforms and minimal LWD, and bedforms and significant LWD. Line within each box plot represents the median value of the distribution, box ends are the inner and outer quartiles, whiskers are the inner and outer tenths, and circles are extrema. The sediment-impacted Lower Greens Creek is not included here.

The predicted D_{50s} is determined as $D_{50s}=\tau'/[(\rho_s-\rho)g\tau^*_{c50s}]$, where $\tau'=\tau_0-\tau_w$; other grain size values are measured in the field. Equation (7) is defined as the response ratio. While this ratio is quite similar to the q* formulation [i.e., (6)], it differs from q* in that it expresses textural response to both sediment supply and hydraulic roughness. A channel's ability to accommodate increased sediment loads or hydraulic roughness via textural fining will be exhausted as surface median grain sizes approach that of the subsurface; that is, as (7) approaches a value of 1. Further increases in sediment supply or hydraulic roughness can only be accommodated by sediment deposition and channel aggradation.

Of the channel types investigated, LWD-rich channels show the strongest magnitude of textural fining (Fig. 4.1). As such, it was expected that they would have larger response ratios and thus the least capacity for further textural response (Buffington and Montgomery, 1992; Buffington, 1993). Figure 4.3 shows that increased textural fining (expressed as the ratio of observed-to-predicted D_{50s}) roughly corresponds with an increasing response ratio. LWD-rich pool-riffle channels tend to exhibit greater textural fining and larger response ratios than plane-bed channels (Fig. 4.3), however the zonation of textural response by channel type is less clear than that of Figure 3.15 due to a paucity of available D_{50ss} data. The significant overlap of response ratios amongst channel types should preclude any *a priori* association of response ratio and channel type. The trend of decreasing response ratio with increasing complexity of channel roughness does, however, indicate that the potential for sediment supply to influence surface textures should decline in channels with greater bedform and LWD roughness, in that there is progressively less capacity for further textural response. Hence, the component of sediment-supply-induced textural fining in channels with significant structural roughness must be relatively small.

The bankfull threshold model can also be used to assess channel condition in terms of sediment supply alone, provided that roughness effects on shear stress have been

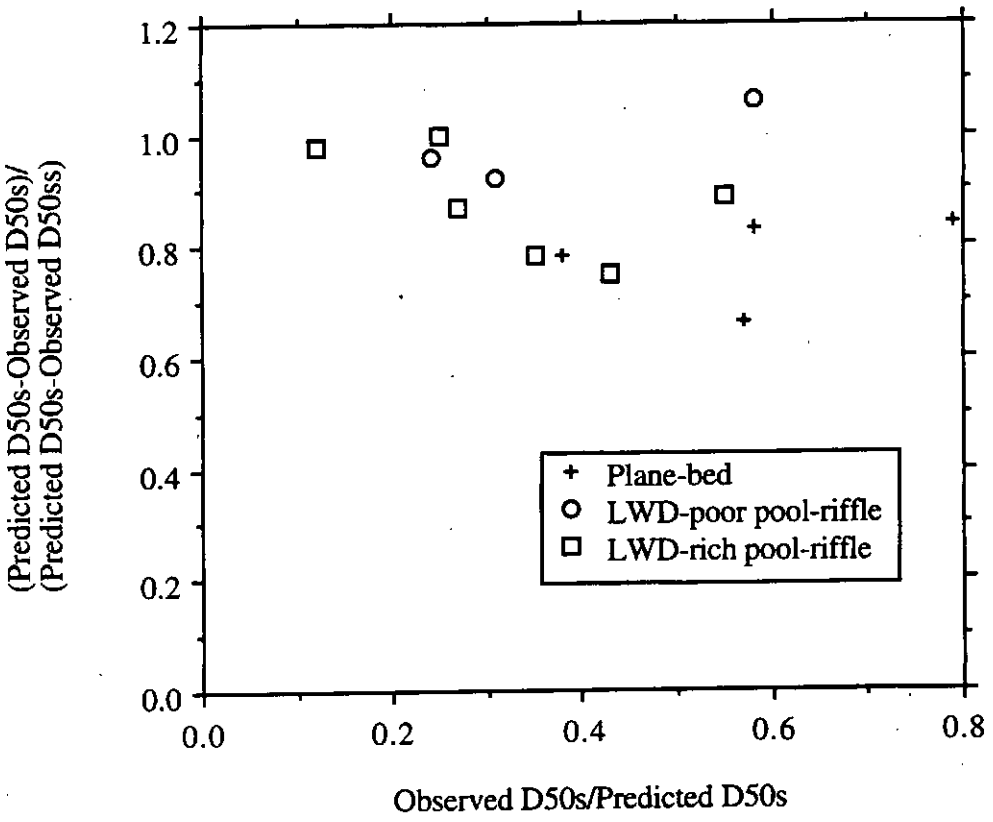

Figure 4.3 Textural fining relative to the bankfull threshold prediction of grain size (Observed D_{50s}/Predicted D_{50s}) versus response ratio [(Predicted D_{50s}-Observed D_{50s})/(Predicted D_{50s}-Observed D_{50ss})]. Note that the predicted D_{50s} value is calculated as $D_{50s}=\tau'/[(\rho_s-\rho)g\tau^*_{c50s}]$ using $\tau'=\tau_0-\tau_w$. The sediment-impacted Alder Creek is not included here.

accounted for. Assessment of sediment loading is made by evaluating (7), with τ' established as per (5), subtracting any shear stress dissipation caused by hydraulic roughness elements other than grain roughness. However, prediction of τ' in forest channels is difficult due to the spatial complexity and irregularity of both bedforms and LWD, and is a subject for future research. The difficulty in accounting for roughness effects during channel assessment is recognized in the watershed analysis manual developed by the State of Washington (WFPB, 1993). Its authors recommend that when estimating sediment loading with the q* technique (Dietrich et al., 1989), data should be collected in planar sections of channel away from roughness elements such as bedforms and LWD (WFPB, 1993). However, hydraulic roughness features have a reach-scale influence on surface textures and are not limited to local zones of response (i.e., Fig. 3.16). Furthermore, the full downstream extent of textural influence of an obstruction is uncertain. Velocity defects caused by much simpler flow obstructions can extend over downstream distances of several hundred obstruction-diameters (Grass, 1971). Without correction for roughness effects, q* measurements in most forest gravel-bedded channels are suspect. Because Kinerson (1990) worked in channels with bedform and LWD roughness and chose sample sites in a fashion analogous to that recommended by WFPB (1993), some of his q* values may also be affected by downstream persistence of energy dissipation and associated textural fining.

Once channel condition is established using (7), the empirical findings summarized by Figure 4.1 can be used to predict general trends of likely textural response to perturbations in sediment supply and hydraulic roughness. For example, channels with low response ratios will likely exhibit textural fining as a result of aquatic enhancement projects that add in-stream debris. Alternatively, textural coarsening is predicted for LWD-rich pool-riffle channels that are depleted of in-stream debris as a consequence of such

factors as debris flow scour, management stream cleaning (Meehan et al., 1969; Bryant, 1983), or recruitment decline following riparian harvest (Murphy and Koski, 1989). Channels directly receiving road drainage and associated sediment loads will exhibit textural fining if the response capacity is available; if not, deposition and channel aggradation is likely.

Textural response may, however, be more complicated than indicated by the above simple predictions. Changes in the caliber of supplied sediment will affect the assessment of channel condition. For example, if for some reason the caliber of the sediment load decreases, but the volume supplied does not change, then the bedload (and hence subsurface) grain size distribution will fine, increasing the response ratio and raising the channel capacity for surface textural fining. LWD can also cause complex textural responses. Because of the influence of woody debris on forest channel morphology (i.e., Fig. 3.13), changes in LWD loading may alter bedform configuration and roughness, which may intensify or counteract any LWD-induced textural response depending on the specific circumstances. To a large degree woody debris must also control bedload (and hence subsurface) grain sizes by influencing the magnitude of basal shear stress available. For example, addition of LWD and consequent shear stress dissipation will result in a reach-average decline in bedload (and subsurface) grain size caliber, extending the lower limit of potential textural response of the surface by decreasing D_{50ss}. Concomitant declines in surface grain size may, however, offset any potential increase in channel response ratio. Increased roughness due to the addition of LWD will also result in decreased velocity and water surface slope, causing increases in either water depth or width or both (Lisle, 1986a); changes in hydraulic variables such as this can alter τ_0. The point of these examples is to illustrate that textural response may not always follow a simple, predictable path.

In addition to predicting likely response trends, more specific predictions can also be made from the field data. Although there is considerable scatter, textural fining expressed as the ratio of observed-to-predicted D_{50s} generally declines with increasing LWD loading (Fig. 4.4). Furthermore, for a given LWD loading the degree of textural fining depends on channel shear stress (Fig. 4.4); higher shear stresses generally correspond with greater textural fining (i.e., lower ratio of observed-to-predicted D_{50s}). This is also evidenced in Figure 4.1 by the increase in range of textural fining observed in pool-riffle channels at greater shear stresses. Because larger channel shear stresses also mean greater velocities, identically placed obstructions will cause greater form drag, and hence greater textural fining, in higher-velocity channels. Textural response predictions made from Figure 4.4 should be viewed as estimates only, as the figure does not explicitly include bedform dimensions and other physical attributes of LWD which together control macro-scale form drag and textural fining. Form drag, and hence textural fining, should be correlated with: 1) bedform amplitude and wavelength; and 2) LWD size, orientation, position within the flow column, and abundance. Only the later is explicitly represented in Figure 4.4. Furthermore, sediment supply effects, while arguably small in these channels, are also not explicitly accounted for in Figure 4.4.

Specific magnitudes of textural response to changes in sediment supply are also predictable when examined within the threshold model framework. The magnitude of textural fining relative to model predictions (i.e., Predicted D_{50s}-Observed D_{50s}) is a power function of sediment loading (Fig. 4.5). In contrast, textural fining expressed as the ratio of observed-to-predicted D_{50s} is not a unique function of sediment supply (Fig. 4.6); rather, it is apparently dependent on the ratio of τ'/τ_{c50ss}, with the rate of textural fining less rapid for larger values of this shear stress ratio. Like the observed-to-predicted ratio of D_{50s}, q^* is a relative measure not singularly related to sediment supply (Fig. 4.7). While

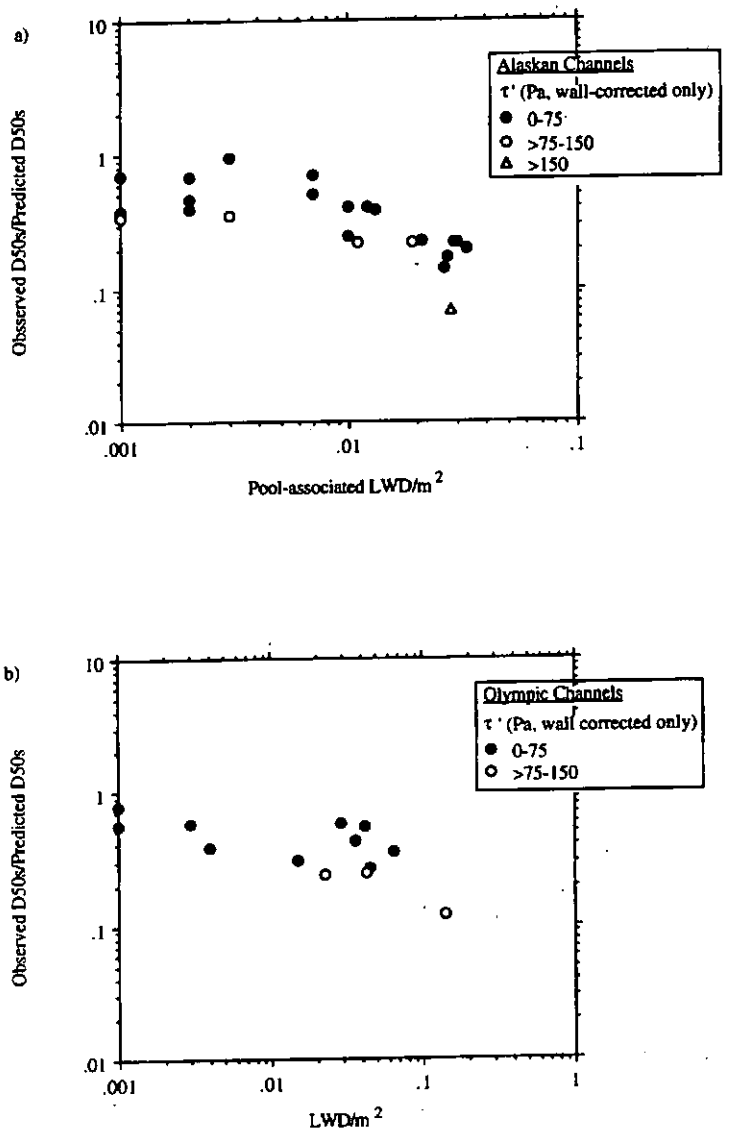

Figure 4.4 Textural fining as a function of LWD loading in the a) Alaskan and b) Olympic channels. Textural fining is expressed as deviation from unity for the ratio of observed-to-predicted D_{50s}, and LWD loading is represented by pool-associated pieces/m^2 and total pieces/m^2 for the Alaskan and Olympic sites, respectively. The sediment-impacted Alder Creek and Lower Greens Creek are not included here.

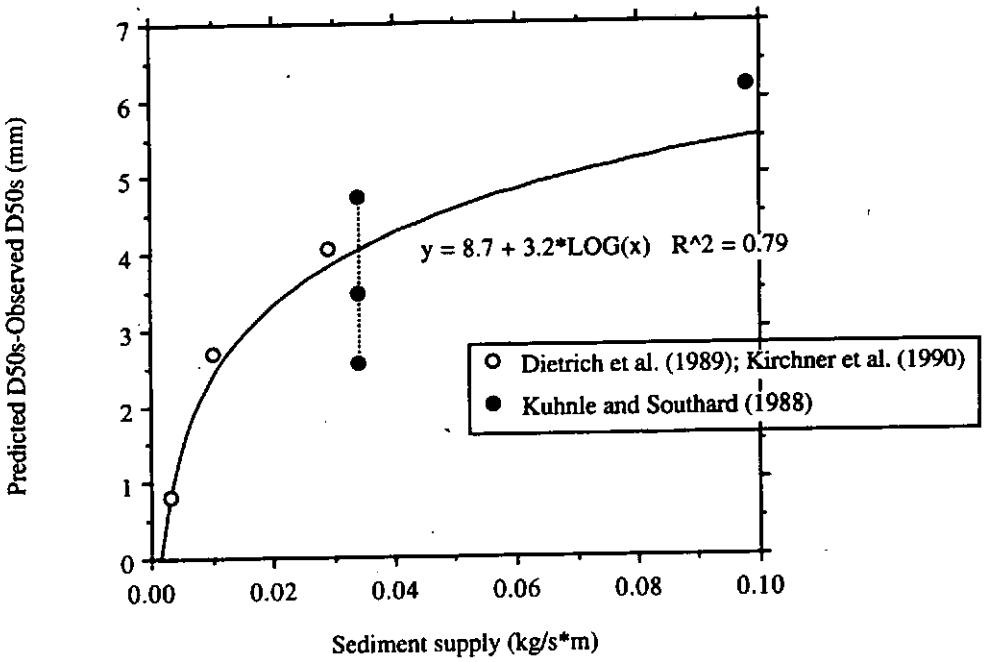

Figure 4.5 Sediment supply (kg/m•s) versus magnitude of textural fining relative to the bankfull threshold channel prediction (Predicted D_{50s}-Observed D_{50s}). D_{50s} is predicted based on τ^*_{c50s}=0.032.

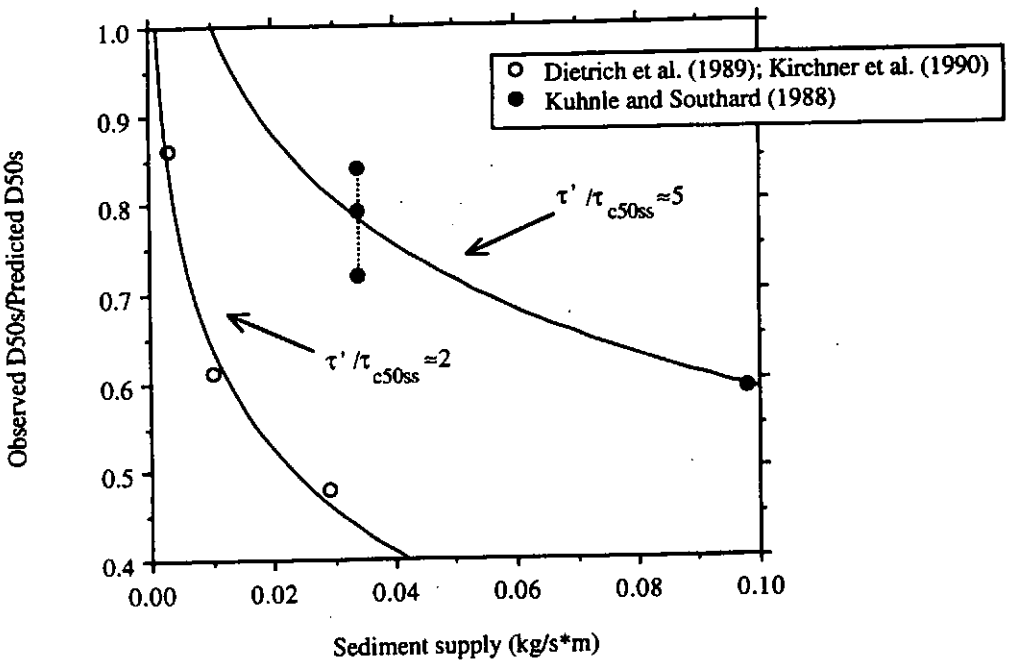

Figure 4.6 Sediment supply (kg/m•s) versus relative textural fining(Observed D_{50s}/Predicted D_{50s}). D_{50s} is predicted based on τ^*_{c50s}=0.032.

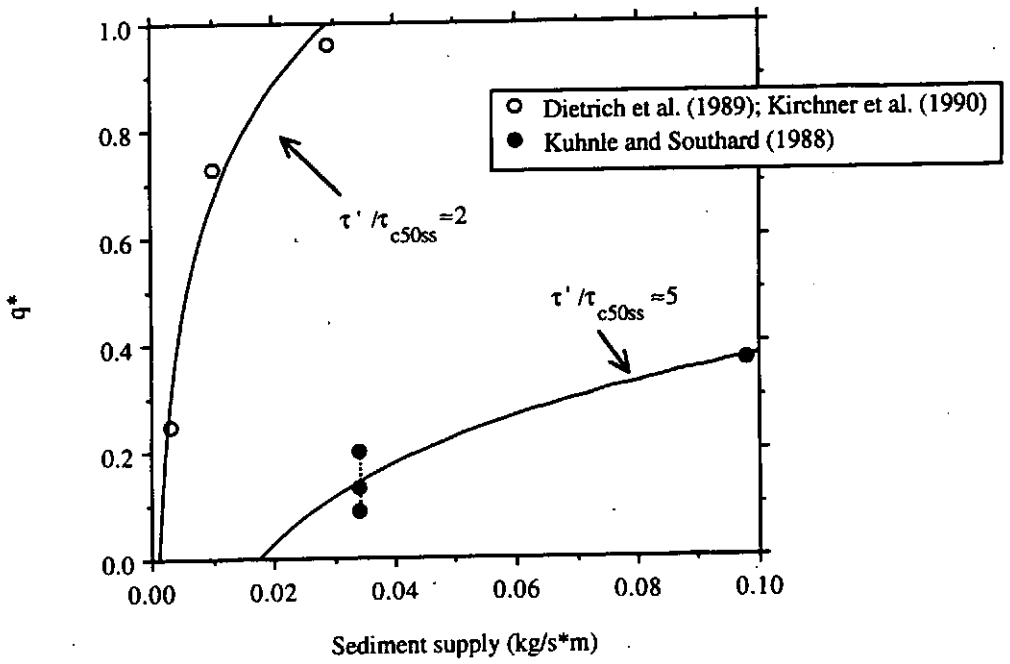

Figure 4.7 Sediment supply (kg/m·s) versus q*, based on τ^*_{c50s}=0.032.

q* can be used to infer qualitative degrees of sediment loading, magnitudes of textural fining measured within the bankfull threshold framework allow assessment of specific sediment loading (Fig. 4.5). The uniqueness of this relationship is, however, quite sensitive to the τ^*_{c50s} value used. Larger τ^*_{c50s} values produce families of curves for which the rate of textural fining with increasing sediment supply is inversely dependent on τ'/τ_{c50ss}. Smaller τ^*_{c50s} values result in a direct dependence of fining rate on τ'/τ_{c50ss}. Variation of τ^*_{c50s} does not affect the relative dependence on τ'/τ_{c50ss} shown in Figures 4.6 and 4.7.

TEXTURAL RESPONSE AND SALMONID HABITAT

Surface textures have direct implications for availability of salmonid spawning habitat. While channel characteristics such as temperature, depth, velocity, gravel "embeddedness" (e.g., Peterson et al., 1992), substrate content of fines, and intra-gravel flow and upwelling are believed to affect selection of spawning sites, perhaps the most important characteristic is the physical size of the gravel in which an adult salmon can excavate a redd. Typical median grain sizes of spawning gravels used by various salmonids as reported by Kondolf and Wolman (1993) are overlain on the empirical findings of the threshold channel model in Figure 4.8. Chinook salmon (*Oncorhynchus tshawytscha*) and chum salmon (*O. keta*) are tolerant of a broad range of spawning gravel sizes, while pink salmon (*O. gorbuscha*) and brook trout (*Salvelinus fontinalis*) are restricted to a very narrow range; spawning gravels preferred by the remaining salmonids have a total variance in median grain size of about 15 mm. Coupled with the empirical findings of the bankfull threshold model, these preferred spawning grain sizes allow examination of the geomorphic controls on species-specific spawning habitat availability. The level of examination afforded by this coupling is quite coarse, however, as the

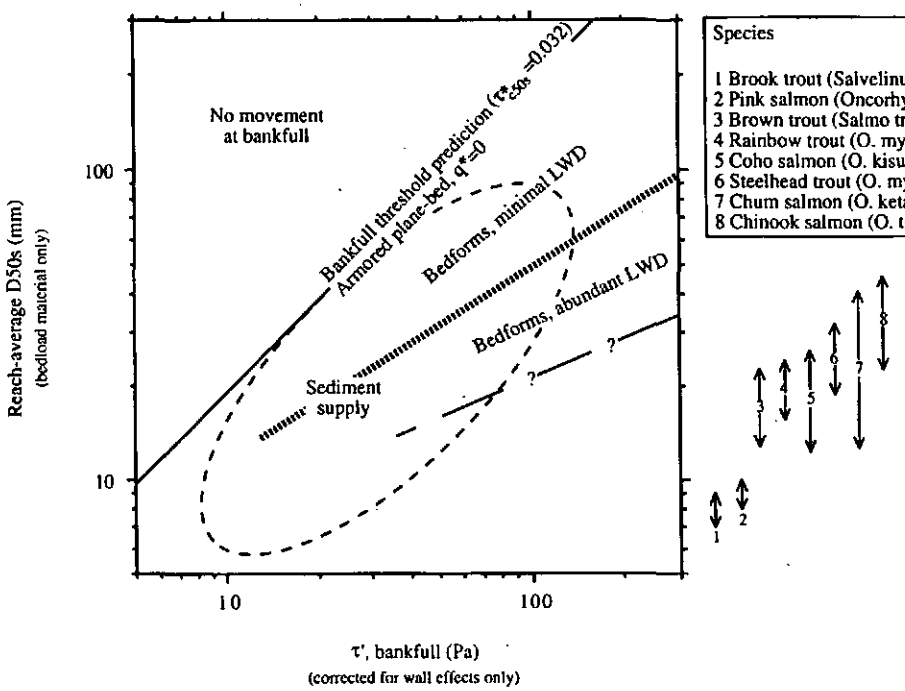

Species	Preferred median spawning grain size (mm)
1 Brook trout (Salvelinus fontinalis)	7.0-9.0
2 Pink salmon (Oncorhynchus gorbuscha)	8.0-10.0
3 Brown trout (Salmo trutta)	12.3-22.0
4 Rainbow trout (O. mykiss)	14.4-23.0
5 Coho salmon (O. kisutch)	11.8-27.7
6 Steelhead trout (O. mykiss)	17.7-32.0
7 Chum salmon (O. keta)	12.3-41.4
8 Chinook salmon (O. tshawytscha)	21.7-45.6

Figure 4.8 Comparison of the empirical results of the bankfull threshold model and median spawning grain sizes used by salmonids. Spawning gravel ranges represent the 25th and 75th percentiles of the median grain size distributions reported in Kondolf and Wolman's (1993) Figure 7. It is cautioned that these ranges should be viewed as estimates only, as Kondolf and Wolman's (1993) synthesis combines disparate and potentially erroneous data sets. Their data include both pre- and post-spawned gravels, grain size distributions of which are typically quite different (Kondolf et al., 1993; Montgomery et al., in review). Some sources used by Kondolf and Wolman (1993) ignored the larger grain sizes present in spawning gravels, skewing actual grain size distributions toward finer sizes. Most importantly, substrate samples in fisheries studies typically combine both surface and subsurface material and only measure a small volume of sediment; as such, grain size distributions may be erroneous (Church et al., 1987) and of uncertain application to the threshold model's prediction of D_{50s}. There is a need for more accurate and standardized characterization of preferred pre-spawning gravel sizes used for salmonid spawning.

empirical results of the current study represent reach-average D_{50s} values which unfortunately give no information on the actual variability and abundance of suitable spawning patches within a reach. Nevertheless, it is a useful starting point. Figure 4.8 shows that availability of preferred spawning grain sizes is significantly enhanced by textural response to sediment supply and hydraulic roughness. For example, preferred spawning gravel sizes for coho salmon (*O. kisutch*) in fully armored plane-bed channels (i.e., channels not exhibiting textural fining) only occur for bankfull shear stresses ranging from about 7-14 Pa (Fig. 4.8). However, as a result of textural fining, spawning sizes preferred by coho have the potential to occur in a variety of different channel types and over a greater range of bankfull shear stresses (7-146 Pa, Fig. 4.8). Consequently, textural response can significantly increase spawning habitat availability for a given salmonid species.

Figure 4.8 can also be used to examine the potential impacts of textural response on availability of species-specific spawning gravels. Textural response to changes in sediment supply or hydraulic roughness that extend beyond the range of median spawning sizes preferred by a particular species may cause them to abandon such reaches as spawning sites. For example, brown trout (*Salmo trutta*), which prefer relatively small spawning grain sizes, may abandon a LWD-rich pool-riffle channel as a spawning site if it coarsens significantly in response to a depleted wood supply. Wood loss may further compound impacts on a salmonid population by decreasing pool frequency and thus availability of potential rearing habitat (Montgomery et al., in press).

Forest channels with abundant LWD are widely recognized for the availability of potential spawning and rearing habitat that they offer (Everest et al., 1987; Sullivan et al., 1987; Bisson et al., 1987). The main significance of LWD is the channel "complexity" that it creates; that is, the obstruction-forced spatial variability of channel hydraulics, morphology, and grain size that satisfy some of the requirements of different salmonid

species and their life-stages. The increasing complexity and spatial variability of surface textures with greater wood loading is clearly noted in the current analysis. Ironically the LWD-rich pool-riffle channels may be the most valuable for salmonid usage and potentially the most sensitive to increased sediment supply or hydraulic roughness, in that they commonly have high response ratios (Fig. 4.3) and thus a small capacity for further textural response.

CONCLUSION

The bankfull threshold model provides a useful framework for examining textural response to sediment supply and other hydraulic roughness elements in gravel-bedded streams. Reach-average surface textures exhibit systematic fining in response to both of these factors. While sediment loading and hydraulic roughness are both first-order controls on reach-average median surface grain size, the infrequent nature of significant sediment input to forest channels likely causes sediment supply effects to be subordinate to the pervasive influence of LWD and bedforms in forest pool-riffle channels.

The interpretation of empirical results presented here and the assessment of relative magnitudes of textural influence caused by sediment supply and hydraulic roughness features of natural channels is preliminary and warrants further investigation. Future work will pursue this subject through rigorous partitioning of bedform and LWD shear stresses using theoretical boundary layer calculations. Theoretical calculations will be compared with field measurements of channel roughness. Once shear stress dissipation due to in-channel roughness features is accounted for, sediment supply effects on reach-average surface textures can be determined independently and compared with conclusions made in the current analysis.

Textural response to sediment supply and hydraulic roughness occurs on both a reach and local scale, and further investigation of the later is recommended. In particular, textural patch dynamics should be examined in order to better understand channel hydraulics and sediment transport at a subreach scale. When and how is sediment transported within and between patches and how do seasonal variations in shear stress and surface texture affect this? A better understanding of surface textures at a subreach scale would be valuable for assessing and predicting geomorphic controls on availability of spawning gravels for salmonids and other fishes.

NOTATION

C_D, C_L	drag, lift coefficient
D_{50}, D_{84}, D_i etc.	grain size for which 50%, 84%, i%, etc. of the grains are finer
D_{50s}, D_{50ss}, D_{50m}	median grain size of the surface material, subsurface material, laboratory mixture
D_{gs}	geometric mean grain size of the surface material
D^*	Dietrich's (1982) dimensionless grain size
D_i^*	Kirchner et al.'s (1990) dimensionless grain size, D_i/z_0
D_{maxs}, D_{maxss}	largest surface, subsurface grain size
D_n	nominal grain size
D_{sus}	maximum suspendable grain size at bankfull flow
e, e_i^*	Kirchner et al.'s (1990) dimensional and dimensionless grain exposure, e_i/D_i
f_i	fraction of grain size distribution comprised by D_i
g	gravitational constant
h	depth
h_c	critical depth for incipient motion
k_s	boundary roughness length scale (equivalent Nikuradse (1933) sand grain roughness)
m	mixed grain size
n_0, n_g	total, grain Manning (1891) roughness coefficient
p, p_i^*	Kirchner et al.'s (1990) dimensional and dimensionless grain projection, p_i/D_i
Q, Q_s	total volumetric fluid discharge, that over the bed only (Meyer-Peter and Müller, 1948)
q^*	Dietrich et al.'s (1989) dimensionless bedload transport rate
Re^*_c, Re^*_{ci}	critical grain/boundary Reynolds number for D_{50}, D_i

S	water surface/bed surface slope in m/m
T	texture
u	velocity
u	uniform grain size
u^*	shear velocity
V^*	Lisle and Hilton's (1992) sediment supply parameter
W	width
w_s	grain fall velocity
w^*	dimensionless grain fall velocity
z	height above the bed
z_0	total roughness length scale
z^*	Kirchner et al.'s (1990) dimensionless height above the bed, z/D_i
α	empirical coefficient
β	empirical exponent
γ	specific weight of fluid
θ	bed surface slope in degrees
κ	von Kármán's constant
ν	kinematic viscosity
ρ, ρ_s	fluid, sediment density
σ_{gs}, σ_{gss}, σ_{gm}	sorting coefficient [Folk's (1974) graphic standard deviation] of the surface material, subsurface material, laboratory mixture
τ_0	total *bankfull* boundary shear stress
τ'	effective *bankfull* boundary shear stress
τ_f	component of τ_0 expended on bedform drag
τ_g	component of τ_0 expended on skin friction and form drag of bed surface grains
τ_l	component of τ_0 expended on LWD (see text for mechanisms of energy dissipation)
τ_w	component of τ_0 dissipated by sidewall effects
τ_c	critical shear stress (value for incipient motion)

τ_{c_i}, τ_{c50s}	τ_c of D_i, D_{50s}
τ_{cq50s}	τ_c of D_{50s} based on empirical competence equations determined from coupled bedload sampling and shear stress measurement
τ_{cr50}, τ_{cr50m}	τ_c of D_{50}, D_{50m} for a specified reference bedload transport rate
τ_{cv50m}	τ_c of D_{50m} based on visual observation of incipient motion
τ^*	dimensionless shear stress
τ^*_c	dimensionless critical shear stress (value for incipient motion)
τ^*_{ci}, τ^*_{c50}, τ^*_{c50s}, τ^*_{c50ss}, τ^*_{c50m}	τ^*_c of D_i, D_{50}, D_{50s}, D_{50ss}, D_{50m}
τ^*_{cq}	τ^*_c based on empirical competence equations determined from coupled bedload sampling and shear stress measurement
τ^*_{cqi}, τ^*_{cq50}, τ^*_{cq50s}, τ^*_{cq50ss}	τ^*_c of D_i, D_{50}, D_{50s}, D_{50ss} based on empirical competence equations determined from coupled bedload sampling and shear stress measurement
τ^*_{cri}, τ^*_{cr50}, τ^*_{cr50s}, τ^*_{cr50m}	τ^*_c of D_i, D_{50}, D_{50s}, D_{50m} for a specified reference bedload transport rate
τ^*_{cvi}, τ^*_{cv50}, τ^*_{cv50m}	τ^*_c of D_i, D_{50}, D_{50m} based on visual observation of incipient motion
ϕ	$\log_2$ grain size
ϕ_{16}, ϕ_{84}, etc.	grain sizes for which 16%, 84%, etc. of the grains are finer
Φ	intergranular friction angle

REFERENCES

Ackers, P. and White, W. R., Sediment transport: New approach and analysis, *Journal of the Hydraulics Division, ASCE*, 99, 2041-2060, 1973.

Andrews, E. D., Effective and bankfull discharges of streams in the Yampa river basin, Colorado and Wyoming, *Journal of Hydrology*, 46, 311-330, 1980.

Andrews, E. D., Entrainment of gravel from naturally sorted riverbed material, *Geological Society of America Bulletin*, 94, 1225-1231, 1983.

Andrews, E. D., Bed-material entrainment and hydraulic geometry of gravel-bed rivers in Colorado, *Geological Society of America Bulletin*, 95, 371-378, 1984.

Andrews, E. D. and Erman, D. C., Persistence in the size distribution of surficial bed material during an extreme snowmelt flood, *Water Resources Research*, 22, 191-197, 1986.

Ashida, K. and Bayazit, M., Initiation of motion and roughness of flows in steep channels, Proceedings of the 15th Congress of the IAHR, Istanbul, Turkey, IAHR, 1, 475-484, 1973.

Ashida, K., Takahashi, T. and Sawada, T., Processes of sediment transport in mountain stream channels, Proceedings of the Symposium on Erosion and Sediment Transport in Pacific Rim Steeplands, Corvalis, Or., ed. T. R. H. Davies and A. J. Pearce, IAHS Publication 132, 166-178, 1981.

Ashworth, P. J. and Ferguson, R. I., Size-selective entrainment of bed load in gravel bed streams, *Water Resources Research*, 25, 627-634, 1989.

ASTM, Manual on test sieving methods, ASTM Special Technical Publication 447 B, 46 p., 1985.

Baker, V. R. and Ritter, D. F., Competence of rivers to transport coarse bedload material, *Geological Society of America Bulletin*, 86, 975-978, 1975.

Bathurst, J. C., Critical conditions for bed material movement in steep boulder-bed streams, Erosion and Sedimentation in the Pacific Rim, Corvalis, Or., ed. R. L. Beschta, R. Blinn, G. E. Grant, G. Ice and F. Swanson, IAHS Publication 156, 309-318, 1987a.

Bathurst, J. C., Measuring and modeling bedload transport in channels with coarse bed materials, In: River Channels: Environment and Process, ed. K. S. Richards, Basil Blackwell Ltd., Oxford, 272-294, 1987b.

Bathurst, J. C., Graf, W. H. and Cao, H. H., Initiation of sediment transport in steep channels with coarse bed material, In: Mechanics of Sediment Transport, ed. B. M. Sumer and A. Müller, Balkema, Rotterdam, The Netherlands, 207-213, 1983.

Bathurst, J. C., Graf, W. H. and Cao, H. H., Bed load discharge equations for steep mountain rivers, In: Sediment Transport in Gravel-bed Rivers, ed. C. R. Thorne, J. C. Bathurst and R. D. Hey, John Wiley & Sons, Chichester, U. K., 453-491, 1987.

Bathurst, J. C., Li, R. M. and Simons, D. B., Hydraulics of mountain rivers, Dept. of Civil Engineering, Colorado State University, Fort Collins, Co. Rep. CER78-79JCB-RML-DBS55, 229 p., 1979.

Bisson, P. A., Bilby, R. E., Bryant, M. D., Dolloff, C. A., Grette, G. B., House, R. A., Murphy, M. L., Koski, K. V. and Sedell, J. R., Large woody debris in forested streams in the Pacific Northwest: Past, present, and future, In: Streamside management: Forestry and Fishery Interactions, ed. E. O. Salo and T. W. Cundy, University of Washington Institute of Forest Resources, Seattle, 143-190, 1987.

Bisson, P. A., Nielsen, J. L., Palmason, R. A. and Grove, L. E., A system of naming habitat types in small streams, with examples of habitat utilization by salmonids during low streamflow, Proceedings of a Symposium on Acquisition and Utilization of Aquatic Habitat Inventory Information, Portland, Or., ed. N. B. Armantrout, Western Division of the American Fisheries Society, 62-73, 1982.

Booth, D. B., Bell, K. and Whipple, K. X, Sediment transport along the south fork and mainstem of the Snoqualmie River, King County Surface Water Management Division Basin Planning Program, Seattle, Wa., 1991.

Bray, D. I., Evaluation of effective boundary roughness for gravel-bed rivers, *Canadian Journal of Civil Engineering*, 7, 392-397, 1980.

Bridge, J. S. and Dominic, D. F., Bed load grain velocities and sediment transport rates, *Water Resources Research*, 20, 476-490, 1984.

Brush, L., Drainage basins, channels, and flow characteristics of selected streams in central Pennsylvania, USGS Professional Paper 282-F, 35 p., 1961.

Bryant, M. D., The role and management of woody debris in west coast salmonid nursery streams, *North American Journal of Fisheries Management*, 3, 322-330, 1983.

Buffington, J. M., Fluvial processes and interpretation of stream-bed surface textures, In: Geomorphological Watershed Analysis Project Biennial Report for the Period from 10/1/91 to 6/30/93, ed. D. R. Montgomery, T. Dunne and W. E. Dietrich, Prepared for the Washington State Department of Natural Resources under the Timber, Fish, and Wildlife Agreement, TFW-SH10-93-001, Appendix 9, 1993.

Buffington, J. M., Dietrich, W. E. and Kirchner, J. W., Friction angle measurements on a naturally formed gravel streambed: Implications for critical boundary shear stress, *Water Resources Research*, 28, 411-425, 1992.

Buffington, J. M. and Montgomery, D. R., Effects of hydraulic roughness and sediment supply on bed surface textures in gravel-bed streams, *EOS, AGU Transactions*, 73, 231, 1992.

Campbell, A. J. and Sidle, R. C., Bedload transport in a pool-riffle sequence of a coastal Alaska stream, *Water Resources Bulletin*, 21, 579-590, 1985.

Carling, P., The concept of dominant discharge applied to two gravel-bed streams in relation to channel stability thresholds, *Earth Surface Processes and Landforms*, 13, 355-367, 1988.

Carling, P. A., Threshold of coarse sediment transport in broad and narrow natural streams, *Earth Surface Processes and Landforms*, 8, 1-18, 1983.

Carling, P. A. and Hurley, M. A., A time-varying stochastic model of the frequency and magnitude of bed load transport events in two small trout streams, In: Sediment Transport in Gravel-bed Rivers, ed. C. R. Thorne, J. C. Bathurst and R. D. Hey, John Wiley & Sons, Chichester, U. K., 897-920, 1987.

Carling, P. A. and Reader, N. A., Structure, composition and bulk properties of upland stream gravels, *Earth Surface Processes and Landforms*, 7, 349-365, 1982.

Casey, H., Über geschiebebewegung, *Mitteilung der Preussischen Versuchsanstalt fur Wasserbau un Schiffbau*, Heft 19, 1935.

Çeçan, K. and Bayazit, M., Critical shear stress of armored beds, Proceedings of the 15th Congress of the IAHR, Istanbul, Turkey, IAHR, 1, 493-500, 1973.

Chang, Y. L., Laboratory investigation of flume traction and transportation, *ASCE Transactions*, 104, 1246-1313, 1939.

Chin, A., Step pools in stream channels, *Progress in Physical Geography*, 13, 391-407, 1989.

Chitale, S. V., River channel patterns, *Journal of the Hydraulics Division, ASCE*, 96, 201-221, 1970.

Church, M., Palaeohydrological reconstructions from a Holocene valley fill, In: Fluvial Sedimentology, ed. A. D. Miall, Canadian Society of Petroleum Geologists Memoir 5, 743-772, 1978.

Church, M., Channel morphology and typology, In: The Rivers Handbook, ed. P. Carlow and G. E. Petts, Blackwell Scientific Publications, Oxford, 126-143, 1992.

Church, M., Wolcott, J. and Maizels, J., Paleovelocity: A parsimonious proposal, *Earth Surface Processes and Landforms*, 15, 475-480, 1990.

Church, M. A., McLean, D. G. and Wolcott, J. F., River bed gravels: Sampling and analysis, In: Sediment Transport in Gravel-bed Rivers, ed. C. R. Thorne, J. C. Bathurst and R. D. Hey, John Wiley & Sons, Chichester, U.K., 43-88, 1987.

Clifford, N. J., Robert, A. and Richards, K. S., Estimation of flow resistance in gravel-bedded rivers: A physical explanation of the multiplier of roughness length, *Earth Surface Processes and Landforms*, 17, 111-126, 1992.

Cui, B. and Komar, P. D., Size measures and the ellipsoidal form of clastic sediment particles, *Journal of Sedimentary Petrology*, 54, 783-797, 1984.

Day, T. J., Preliminary results of flume studies into the armouring of a coarse sediment mixture, Geological Survey of Canada Report of Activities 76-1C, 277-287, 1976.

Day, T. J., A study of initial motion characteristics of particles in graded bed material, Geological Survey of Canada Current Research 80-1A, 281-286, 1980a.

Day, T. J., A study of the transport of graded sediments, Hydraulics Research Station, Wallingford, U.K., Report IT190, 1980b.

Dhamotharan, S., Wood, A., Parker, G. and Stefan, H., Bedload transport in a model gravel stream, St. Anthony Falls Hydraulic Laboratory, University of Minnesota, Minneapolis, Minn. Project Report 190, 1980.

Dietrich, W. E., Settling velocity of natural particles, *Water Resources Research*, 18, 1615-1626, 1982.

Dietrich, W. E., Kinerson, D. and Collins, L., Interpretation of relative sediment supply from bed surface texture in gravel bed rivers, *EOS, AGU Transactions*, 74, 151, 1993.

Dietrich, W. E., Kirchner, J. W., Ikeda, H. and Iseya, F., Sediment supply and the development of the coarse surface layer in gravel-bedded rivers, *Nature*, 340, 215-217, 1989.

Dietrich, W. E. and Smith, J. D., Influence of the point bar on flow through curved channels, *Water Resources Research*, 19, 1173-1192, 1983.

Dietrich, W. E. and Smith, J. D., Bed load transport in a river meander, *Water Resources Research*, 20, 1355-1380, 1984a.

Dietrich, W. E. and Smith, J. D., Processes controlling the equilibrium bed morphology in river meanders, Proceedings of the Conference Rivers '83, ed. C. M. Elliot, ASCE, 759-769, 1984b.

Dietrich, W. E., Smith, J. D. and Dunne, T., Flow and sediment transport in a sand bedded meander, *Journal of Geology*, 87, 305-315, 1979.

Dietrich, W. E., Smith, J. D. and Dunne, T., Boundary shear stress, sediment transport and bed morphology in a sand-bedded river meander during high and low flow, River Meandering, Proceedings of the Conference Rivers '83, ed. C. M. Elliot, ASCE, 632-639, 1984.

Diplas, P. and Fripp, J. B., Properties of various sediment sampling procedures, *Journal of Hydraulic Engineering, ASCE*, 118, 955-970, 1992.

Diplas, P. and Sutherland, A. J., Sampling techniques for gravel sized sediments, *Journal of Hydraulic Engineering, ASCE*, 114, 484-501, 1988.

Dunne, T., Montgomery, D. and Dietrich, W. E., Proposal for research in geomorphological watershed analysis, Prepared for the Washington State Department of Natural Resources under the Timber, Fish, and Wildlife Agreement, TFW-SH10-91-002, 27 p., 1991.

Egiazaroff, I. V., Calculation of nonuniform sediment concentrations, *Journal of the Hydraulics Division, ASCE*, 91, 225-247, 1965.

Einstein, H. A. and Barbarossa, N. L., River channel roughness, *ASCE Transactions*, 117, 1121-1146, 1952.

Emmett, W. W., Measurement of bedload in rivers, In: Erosion and Sediment Yield: Some Methods of Measurement and Modelling, ed. R. F. Hadley and D. E. Walling, Geo Books, Norwich, U.K., 91-109, 1984.

Engelund, F., Hydraulic resistance of alluvial streams, *Journal of the Hydraulics Division, ASCE*, 92, 315-326, 1966.

Everest, F. H., Beschta, R. L., Scrivener, J. C., Koski, K. V., Sedell, J. R. and Cederholm, C. J., Fine sediment and salmonid production: A paradox, In: Streamside Management: Forestry and Fishery Interactions, ed. E. O. Salo and T. W. Cundy, University of Washington Institute of Forest Resources, Seattle, 98-142, 1987.

Everts, C. H., Particle overpassing on flat granular boundaries, *Journal of the Waterways, Harbors, and Coastal Engineering, ASCE*, 99, 425-439, 1973.

Fahnestock, R. K., Morphology and hydrology of a glacial stream--White River, Mount Rainier, Washington, USGS Professional Paper 422A, 70 p., 1963.

FEMAT, Forest ecosystem management: An ecological, economic, and social assessment, report of the Forest Ecosystem Management Team, US Government Printing Office, Washington, D.C. 1993-793-071, 1993.

Fenton, J. D. and Abbott, J. E., Initial movement of grains on a stream bed: the effect of relative protrusion, *Proceedings of the Royal Society of London*, 352, 523-537, 1977.

Ferguson, R. I., Critical discharge for entrainment of poorly sorted gravel, *Earth Surface Processes and Landforms*, 19, 179-186, 1994.

Fernandez Luque, R. and van Beek, R., Erosion and transport of bed-load sediment, *Journal of Hydraulic Research*, 14, 127-144, 1976.

Flintham, T. P. and Carling, P. A., The prediction of mean bed and wall boundary shear in uniform and compositely rough channels, In: International Conference on River Regime, ed. W. R. White, John Wiley & Sons, 267-287, 1988.

Florsheim, J. L., Fluvial requirements for gravel bar formation in northwestern California, unpublished M.S. thesis, Humboldt State University, Humboldt, Ca., 105 p., 1985.

Folk, R. L., Petrology of Sedimentary Rocks, Hemphill Publishing Co., Austin, Tx., 182 p., 1974.

Furbish, D. J., Spatial autoregressive structure in meander evolution, *Geological Society of America Bulletin*, 103, 1576-1589, 1991.

Gehrels, G. E. and Berg, H. C., Geologic map of southeastern Alaska, USGS, Map I-1867, 1992.

Gehrels, G. E., McClelland, W. C., Samson, S. D., Patchett, P. J. and Jackson, J. L., Ancient continental margin assemblage in the northern Coast Mountains, southeast Alaska and northwest Canada, *Geology*, 18, 208-211, 1990.

Gessler, J., Beginning and ceasing of sediment motion, In: River Mechanics, ed. H. W. Shen, H. W. Shen, Fort Collins, Co., 7:1-7:22, 1971.

Gilbert, G. K., The transportation of débris by running water, USGS Professional Paper 86, 263 p., 1914.

Goldfarb, R. J., Leach, D. L., Pickthorn, W. J. and Paterson, C. J., Origin of lode-gold deposits of the Juneau gold belt, southeastern Alaska, *Geology*, 16, 440-443, 1988.

Gomez, B., Temporal variations in bedload transport rates: The effect of progressive bed armouring, *Earth Surface Processes and Landforms*, 8, 41-54, 1983.

Grant, G. E., Swanson, F. J. and Wolman, M. G., Pattern and origin of stepped-bed morphology in high-gradient streams, Western Cascades, Oregon, *Geological Society of America Bulletin*, 102, 340-352, 1990.

Grass, A. J., Initial instability of fine bed sand, *Journal of the Hydraulics Division, ASCE*, 96, 619-632, 1970.

Grass, A. J., Structural features of turbulent flow over smooth and rough boundaries, *Journal of Fluid Mechanics*, 50, 233-255, 1971.

Griffiths, G. A., Stochastic estimation of bed load yield in pool-and-riffle mountain streams, *Water Resources Research*, 16, 931-937, 1980.

Griffiths, G. A., Form resistance in gravel channels with mobile beds, *Journal of Hydraulic Engineering, ASCE*, 115, 340-355, 1989.

Guy, H. P., Simons, D. B. and Richardson, E. V., Summary of alluvial channel data from flume experiments, 1956-61, USGS Professional Paper 462-I, 96 p., 1966.

Haff, P. K., Basic physical models in sediment transport, Coastal Sediments '91, ed. N. C. Kraus, ASCE, New York, 1-14.

Hammond, F. D. C., Heathershaw, A. D. and Langhorne, D. N., A comparison between Shields' threshold criterion and the movement of loosely packed gravel in a tidal channel, *Sedimentology*, 31, 51-62, 1984.

Helley, E. J., Field measurement of the initiation of large bed particle motion in Blue Creek near Klamath, California, USGS Professional Paper 562-G, 19 p., 1969.

Henderson, F. M., Stability of alluvial channels, *ASCE Transactions*, 128, 657-720, 1961.

Henderson, F. M., Open Channel Flow, MacMillan Publishing Co., New York, 522 p., 1966.

Hey, R. D., Flow resistance in gravel-bed rivers, *Journal of the Hydraulics Division, ASCE*, 105, 365-379, 1979.

Hey, R. D., Bar form resistance in gravel-bed rivers, *Journal of Hydraulic Engineering, ASCE*, 114, 1498-1508, 1988.

Hey, R. D. and Thorne, C. R., Stable channels with mobile gravel beds, *Journal of the Hydraulics Division, ASCE*, 112, 671-687, 1986.

Higginson, N. N. J. and Johnston, H. T., Estimation of friction factor in natural streams, In: International Conference on River Regime, ed. W. R. White, John Wiley & Sons, 251-266, 1988.

Howard, A. D., Thresholds in river regimes, In: Thresholds in Geomorphology, ed. D. R. Coates and J. D. Vitek, Allen and Unwin Ltd., London, 227-258, 1980.

Inglis, C. C., discussion in: Henderson, F. M., Stability of alluvial channels, *ASCE Transactions*, 128, 710-713, 1961.

Jackson, W. L. and Beschta, R. L., A model of two-phase bedload transport in an Oregon coast range stream, *Earth Surface Processes and Landforms*, 7, 517-527, 1982.

Jiang, Z. and Haff, P. K., Multiparticle simulation methods applied to the micromechanics of bed load transport, *Water Resources Research*, 29, 399-412, 1993.

Johnson, M. A., Component and total friction factors of deep loose-boundary channels with bed sediment, gross depth and velocity distributions known but not energy slope, Proceedings of the 15th Congress of the IAHR, Istanbul, Turkey, IAHR, 1, 37-41, 1973.

Kalinske, A. A., Movement of sediment as bed load in rivers, *AGU Transactions*, 28, 615-620, 1947.

Kamphuis, J. W., Determination of sand roughness for fixed beds, *Journal of Hydraulic Research*, 12, 193-203, 1974.

Kappesser, G. B., Riffle stability index, a procedure to evaluate stream reach and watershed equilibrium, USDA Forest Service, Idaho Panhandle National Forests, Coeur d'Alene, 10 p., 1993.

Keller, E. A., Areal sorting of bed load material; the hypothesis of the velocity reversal, *Geological Society of America Bulletin*, 82, 753-756, 1971.

Keller, E. A. and Swanson, F. J., Effects of large organic material on channel form and fluvial processes, *Earth Surface Processes and Landforms*, 4, 361-380, 1979.

Kellerhals, R., Stable channels with gravel-paved beds, *Journal of the Waterways and Harbors Division, ASCE*, 63-83, 1967.

Kellerhals, R. and Bray, D. I., Sampling procedures for coarse fluvial sediments, *Journal of the Hydraulics Division, ASCE*, 8, 1165-1180, 1971.

Kinerson, D., Bed surface response to sediment supply, unpublished M.S. thesis, University of California Berkeley, Berkeley, Ca., 420 p., 1990.

Kirchner, J. W., Dietrich, W. E., Iseya, F. and Ikeda, H., The variability of critical shear stress, friction angle, and grain protrusion in water worked sediments, *Sedimentology*, 37, 647-672, 1990.

Knight, D. W., Boundary shear in smooth and rough channels, *Journal of the Hydraulics Division, ASCE*, 107, 839-851, 1981.

Knight, D. W., Demetriou, J. D. and Hamed, M. E., Boundary shear in smooth rectangular channels, *Journal of Hydraulic Engineering, ASCE*, 110, 405-422, 1984.

Komar, P. D., Selective grain entrainment by a current from a bed of mixed sizes: A reanalysis, *Journal of Sedimentary Petrology*, 57, 203-211, 1987a.

Komar, P. D., Selective gravel entrainment and the empirical evaluation of flow competence, *Sedimentology*, 34, 1165-1176, 1987b.

Komar, P. D. and Carling, P. A., Grain sorting in gravel-bed streams and the choice of particle sizes for flow-competence evaluations, *Sedimentology*, 38, 489-502, 1991.

Komar, P. D. and Li, Z., Applications of grain-pivoting and sliding analyses to selective entrainment of gravel and to flow-competence evaluations, *Sedimentology*, 35, 681-695, 1988.

Kondolf, G. M., Sale, M. J. and Wolman, M. G., Modification of fluvial gravel size by spawning salmonids, *Water Resources Research*, 29, 2265-2274, 1993.

Kondolf, G. M. and Wolman, M. G., The sizes of salmonid spawning gravels, *Water Resources Research*, 29, 2275-2285, 1993.

Kramer, H., Sand mixtures and sand movement in fluvial models, *ASCE Transactions*, 100, 798-878, 1935.

Kuhnle, R. A., Equal mobility on Goodwin creek, *EOS, AGU Transactions*, 74, 158, 1993.

Kuhnle, R. A. and Southard, J. B., Bed load transport fluctuations in a gravel bed laboratory channel, *Water Resources Research*, 24, 247-260, 1988.

Lacey, G., discussion in: Henderson, F. M., Stability of alluvial channels, *ASCE Transactions*, 128, 695-698, 1961.

Lane, E. W., Progress report on studies on the design of stable channels by the bureau of reclamation, *ASCE Proceedings*, 79, 1-30, 1953.

Lane, E. W., Design of stable channels, *ASCE Transactions*, 1234-1279, 1955.

Lane, E. W. and Carlson, E. J., Some factors affecting the stability of canals constructed in coarse granular materials, Proceedings of the Minnesota International Hydraulics Convention (joint meeting of the IAHR and the Hydraulics Division, ASCE), Minneapolis, Minn., IAHR, 37-48, 1953.

Langbein, W. B. and Leopold, L. B., River channel bars and dunes--Theory of kinematic waves, USGS Professional Paper 422-L, 20 p., 1968.

Leopold, L. B., Wolman, M. G. and Miller, J. P., Fluvial Processes in Geomorphology, W. H. Freeman and Company, San Francisco, 522 p., 1964.

Li, M. Z., Direct skin friction measurements and stress partitioning over movable sand ripples, *Journal of Geophysical Research, Oceans*, 99, 791-799, 1994.

Li, R., Simons, D. B. and Stevens, M. A., Morphology of cobble streams in small watersheds, *Journal of the Hydraulics Division, ASCE*, 102, 1101-1117, 1976.

Li, Z. and Komar, P. D., Laboratory measurements of pivoting angles for applications to selective entrainment of gravel in a current, *Sedimentology*, 33, 413-423, 1986.

Lindley, E. S., Regime channels, Proceedings of the Punjab Engineering Congress, 7, 63-74, 1919.

Lisle, T., A sorting mechanism for a riffle-pool sequence, *Geological Society of America Bulletin*, 90, II, 1142-1157, 1979.

Lisle, T. E., Effects of woody debris on anadromous salmonid habitat, Prince of Wales Island, southeast Alaska, *North American Journal of Fisheries Management*, 6, 538-550, 1986a.

Lisle, T. E., Stabilization of a gravel channel by large streamside obstructions and bedrock bends, Jacoby Creek, northwestern California, *Geological Society of America Bulletin*, 97, 999-1011, 1986b.

Lisle, T. E. and Hilton, S., The volume of fine sediment in pools: An index of sediment supply in gravel-bed streams, *Water Resources Bulletin*, 28, 371-383, 1992.

Lisle, T. E., Iseya, F. and Ikeda, H., Response of a channel with alternate bars to a decrease in supply of mixed-size bed load: A flume experiment, *Water resources Research*, 29, 3623-3629, 1993.

Lisle, T. E. and Madej, M. A., Spatial variation in armouring in a channel with high sediment supply, In: Dynamics of Gravel-bed Rivers, ed. P. Billi, R. D. Hey, C. R. Thorne and P. Tacconi, John Wiley & Sons, Chichester, U.K., 1992.

Little, W. C. and Mayer, P. G., Stability of channel beds by armoring, *Journal of the Hydraulics Division, ASCE*, 102, 1647-1661, 1976.

Lundgren, H. and Jonsson, I. G., Shear and velocity distribution in shallow channels, *Journal of the Hydraulics Division, ASCE*, 90, 1-21, 1964.

Manning, R., On the flow of water in open channels and pipes, *Transactions of the Institution of Civil Engineers of Ireland*, 20, 161-207, 1891.

Meehan, W. R., Farr, W. A., Bishop, D. M. and Patric, J. H., Some effects of clearcutting on salmon habitat of two southeast Alaskan streams, USDA Forest Service Research Paper PNW-82, 45 p., 1969.

Meyer-Peter, E. and Müller, R., Formulas for bed-load transport, Proceedings of the 2nd Meeting of the International Association for Hydraulic Structures Research (IAHR), Stockholm, Germany, IAHR, 39-64, 1948.

Middleton, G. V. and Southard, J. B., Mechanics of Sediment Movement, SEPM Short Course No. 3, SEPM, Tulsa, Ok., 401p., 1984.

Milhous, R. T., Sediment transport in a gravel-bottomed stream, unpublished Ph.D. dissertation, Oregon State University, Corvalis, Or., 232 p., 1973.

Millar, R. G. and Quick, M. C., Flow resistance of high-gradient gravel channels, in: Hydraulic Engineering, '94, Buffalo, New York, ed. G. V. Controneo and R. R. Rumer, ASCE, 1, 717-721, 1994.

Miller, M. C., McCave, I. N. and Komar, P. D., Threshold of sediment motion under unidirectional currents, *Sedimentology*, 24, 507-527, 1977.

Miller, R. T. and Byrne, R. J., The angle of repose for a single grain on a fixed rough bed, *Sedimentology*, 6, 303-314, 1966.

Misri, R. L., Garde, R. J. and Raju, K. G. R., Bed load transport of coarse nonuniform sediment, *Journal of Hydraulic Engineering, ASCE*, 110, 312-328, 1984.

Mizuyama, T., Bedload transport in steep channels, unpublished Ph.D. dissertation, Kyoto University, Kyoto, Japan, 118 p., 1977.

Montgomery, D. R., Buffington, J. M., Smith, R. D., Schmidt, K. M. and Pess, G., Pool spacing in forest channels, *Water Resources Research*, in press, 1995.

Montgomery, D. R. and Buffington, J. M., Channel classification, prediction of channel response, and assessment of channel condition, Prepared for the Washington State Department of Natural Resources under the Timber, Fish, and Wildlife Agreement, TFW-SH10-002, 84 p., 1993.

Montgomery, D. R., Buffington, J. M., Peterson, N. P., Schuett-Hames, D. and Quinn, T. P., Salmonid modifications of gravel streambeds: Implications for bed surface mobility and embryo survival, in review, 1995.

Murphy, M. L. and Koski, K. V., Input and depletion of woody debris in Alaska streams and implications for streamside management, *North American Journal of Fisheries Management*, 9, 427-436, 1989.

Nanson, G. C., Bedload and suspended-load transport in a small, steep, mountain stream, *American Journal of Science*, 274, 471-486, 1974.

Neill, C. R., Mean-velocity criterion for scour of coarse uniform bed-material, Proceedings of the 12th congress of the IAHR, Fort Collins, Co., IAHR, 3, C6.1-9, 1967.

Nelson, J. M. and Smith, J. D., Evolution and stability of erodible channel beds, In: River Meandering, ed. S. Ikeda and G. Parker, AGU, Washington, D.C., 321-378, 1989a.

Nelson, J. M. and Smith, J. D., Flow in meandering channels with natural topography, In: River Meandering, ed. S. Ikeda and G. Parker, American Geophysical Union, Washington, D.C., 69-126, 1989b.

Nikuradse, J., Stromungsgesetze in rauhen Rohren, *VDI Forschungsheft 361*, translated by the National Advisory Committee on Aeronautics, Technical Memo 1292, 1950, 22p., 1933.

Paintal, A. S., Concept of critical shear stress in loose boundary open channels, *Journal of Hydraulic Research*, 9, 91-113, 1971.

Parker, G., Self-formed straight rivers with equilibrium banks and mobile bed. Part 1. The sand-silt river, *Journal of Fluid Mechanics*, 89, 109-125, 1978a.

Parker, G., Self-formed straight rivers with equilibrium banks and mobile bed. Part 2. The gravel river, *Journal of Fluid Mechanics*, 89, 127-146, 1978b.

Parker, G., Surface-based bedload transport relation for gravel rivers, *Journal of Hydraulic Research*, 28, 417-436, 1990.

Parker, G. and Klingeman, P. C., On why gravel bed streams are paved, *Water Resources Research*, 18, 1409-1423, 1982.

Parker, G., Klingeman, P. C. and McLean, D. G., Bedload and size distribution in paved gravel-bed streams, *Journal of the Hydraulics Division, ASCE*, 108, 544-571, 1982.

Parker, G. and Peterson, A. W., Bar resistance of gravel-bed streams, *Journal of the Hydraulics Division, ASCE*, 106, 1559-1575, 1980.

Peterson, N. P., Hendry, A. and Quinn, T. P., Assessment of cumulative effects on salmonid habitat: Some suggested parameters and target conditions, Prepared for the Washington State Department of Natural Resources under the Timber, Fish, and Wildlife Agreement, TFW-F3-92-001, 75 p., 1992.

Petit, F., The evaluation of grain shear stress from experiments in a pebble-bedded flume, *Earth Surface Processes and Landforms*, 14, 499-508, 1989.

Petit, F., Evaluation of grain shear stresses required to initiate movement of particles in natural rivers, *Earth Surface Processes and Landforms*, 15, 135-148, 1990.

Prestegaard, K. L., Bar resistance in gravel bed steams at bankfull stage, *Water Resources Research*, 19, 473-476, 1983.

Proffit, G. T. and Sutherland, A. J., Transport of non-uniform sediments, *Journal of Hydraulic Research*, 21, 33-43, 1983.

Rakoczi, L., Selective erosion of noncohesive bed materials, *Geografiska Annaler*, 69 A, 29-35, 1987.

Reed, J. C., Southeastern Alaska, In: Landscapes of Alaska, ed. H. Williams, University of California Press, Berkeley and Los Angeles, 9-18, 1958.

Reid, I., Frostick, L. E. and Layman, J. T., The incidence and nature of bedload transport during flood flows in coarse-grained alluvial channels, *Earth Surface Processes and Landforms*, 10, 33-44, 1985.

Reid, L. M. and Dunne, T., Sediment production from forest road surfaces, *Water Resources Research*, 20, 1753-1761, 1984.

Rice, S., The spatial variation of bed material texture in coupled basins on the Queen Charlotte Islands, unpublished M.S. thesis, University of British Columbia, 127 p., 1990.

Rice, S., Towards a model of changes in bed material texture at the drainage basin scale, In: Process Models and Theoretical Geomorphology, ed. M. J. Kirkby, John Wiley & Sons, 160-172, 1994.

Richards, K., Rivers. Form and Process in Alluvial Channels, Methuen & Co. Ltd., New York, New York, 361 p., 1982.

Robert, A., Boundary roughness in coarse-grained channels, *Progress in Physical Geography*, 14, 42-70, 1990.

Rosato, A., Strandburg, K. J., Prinz, F., and Swendson, R. H., Why are the brazil nuts on the top: Size segragation of particulate matter by shaking, *Physical Review Letters*, 58, 1038-1040.

Sallenger, A. H., Inverse grading and hydraulic equivalence in grain-flow deposits, *Journal of Sedimentary Petrology*, 49, 553-562.

Sawada, T., Ashida, K. and Takahashi, T., Relationship between channel pattern and sediment transport in a steep gravel bed river, *Zeitschrift fur Geomophologie*, Supplementband 46, 55-66, 1983.

Schoklitsch, A., Handbuch des Wasserbaues, Springer, Vienna, 1962.

Shields, I. A., Anwendung der Aehnlichkeitsmechanik und der Turbulenzforschung auf die Geschiebebewegung, Mitteilunguen det Preussischen Versuchsanstalt fur Wasserbau und Schiffbau, translatted by W. P. Ott and J. C. van Uchelen, USDA Soil Conservation Service Cooperative Laboratory, California Institute of Technology, Pasadena, Ca. 36 p., 1936.

Shimizu, Y., Channel flow with lateral stress, unpublished(?) manuscript, available upon request from this author, 20 p., 1989.

Sidle, R. C., Bed load transport regime of a small forest stream, *Water Resources Research*, 24, 207-218, 1988.

Simons, D. B. and Albertson, M. L., Uniform water conveyance channels in alluvial material, *ASCE Transactions*, 128, 65-167, 1963.

Smith, J. D. and McLean, S. R., Spatially averaged flow over a wavy surface, *Journal of Geophysical Research*, 82, 1735-1746, 1977.

Smith, R. D. and Buffington, J. M., Effects of large woody debris on channel unit distribution in southeast Alaska, Proceedings of Watershed '91, USDA Forest Service R10-MB-217, 43-44, 1993.

Smith, R. D. and Buffington, J. M., Multivariate geomorphic analysis of forest streams: Implications for assessment of land use impact on channel condition, *Earth Surface Processes and Landforms*, in press, 1995.

Smith, R. D., Sidle, R. C. and Porter, P. E., Effects on bedload transport of experimental removal of woody debris from a forest gravel-bed stream, *Earth Surface Processes and Landforms*, 18, 455-468, 1993.

Sullivan, K., Hydraulics and fish habitat in relation to channel morphology, unpublished Ph.D. dissertation, Johns Hopkins University, Baltimore, Maryland, 407 p., 1986.

Sullivan, K., Lisle, T. E., Dolloff, C. A., Grant, G. E. and Reid, L. M., Stream channels: The link between forests and fishes, In: Streamside Management: Forestry and Fishery Interactions, ed. E. O. Salo and T. W. Cundy, University of Washington Institute of Forest Resources, Seattle, 39-97, 1987.

Tabor, R. W., Guide to the geology of Olympic National Park, University of Washington Press, Seattle, 144 p., 1975.

Tabor, R. W. and Cady, W. M., Geologic map of the Olympic Peninsula, Washington, USGS, Map I-994, 1978a.

Tabor, R. W. and Cady, W. M., The structure of the Olympic Mountains, Washington: Analysis of a subduction zone, USGS Professional Paper 1033, 38 p., 1978b.

Thompson, S. M. and Campbell, P. L., Hydraulics of a large channel paved with boulders, *Journal of Hydraulic Research*, 17, 341-354, 1979.

Thorne, C. R. and Lewin, J., Bank processes, bed material movement, and planform development in a meandering river, In: Adjustments of the Fluvial System, ed. D. D. Rhodes and G. P. Williams, Kendall/Hunt Publishing Co., Dubuque, Iowa, 117-137, 1979.

Tison, L. J., Recherches sur la tension limite d'entrainment des materiaux constitutifs du lit, Proceedings of the Minnesota International Hydraulics Convention (joint meeting of IAHR and Hydraulics Division, ASCE), Minneapolis, Minn., IAHR, 21-35, 1953.

USDA, A federal agency guide for pilot watershed analysis, vers. 1.2, USDA, 202 p., 1994.

USWES, Study of river-bed material and their use with special reference to the Lower Mississippi River, United States Waterways Experiment Station, Vicksburg, Miss. Paper 17, 1935.

Warburton, J., Observations of bed load transport and channel bed changes in a proglacial mountain stream, *Arctic and Alpine Research*, 24, 195-203, 1992.

Wentworth, C. K., A scale of grade and class terms for clastic sediments, *Journal of Geology*, 30, 377-392, 1922.

WFPB, Standard methodology for conducting watershed analysis, Washington Forest Practices Board, vers. 2.0, 1993.

White, C. M., The equilibrium of grains on the bed of a stream, *Royal Society of London*, Series A, 174, 322-338, 1940.

White, S. J., Plane bed thresholds of fine grained sediments, *Nature*, 228, 152-153, 1970.

Whiting, P. J. and Dietrich, W. E., Boundary shear stress and roughness over mobile alluvial beds, *Journal of Hydraulic Engineering, ASCE*, 116, 1495-1511, 1990.

Whiting, P. J., Dietrich, W. E., Leopold, L. B., Drake, T. G. and Shreve, R. L., Bedload sheets in heterogeneous sediment, *Geology*, 16, 105-108, 1988.

Wiberg, P. L. and Smith, J. D., Calculations of the critical shear stress for motion of uniform and heterogeneous sediments, *Water Resources Research*, 23, 1471-1480, 1987.

Wiberg, P. L. and Smith, J. D., Model for calculating bed load transport of sediment, *Journal of Hydraulic Engineering, ASCE*, 115, 101-123, 1989.

Wilcock, P. R., Bed-load transport of mixed-size sediment, unpublished Ph.D. dissertation, MIT, Cambridge, Mass., 205 p., 1987.

Wilcock, P. R., Methods for estimating the critical shear stress of individual fractions in mixed-size sediment, *Water Resources Research*, 24, 1127-1135, 1988.

Wilcock, P. R., Flow competence: A criticism of a classic concept, *Earth Surface Processes and Landforms*, 17, 289-298, 1992.

Wilcock, P. R. and McArdell, B. W., Surface-based fractional transport rates: Mobilization thresholds and partial transport of a sand-gravel sediment, *Water Resources Research*, 29, 1297-1312, 1993.

Wilcock, P. R. and Southard, J. B., Experimental study of incipient motion in mixed-size sediment, *Water Resources Research*, 24, 1137-1151, 1988.

Williams, G. P., Flume width and water depth effects in sediment-transport experiments, USGS Professional Paper 562-H, 37 p., 1970.

Williams, G. P., Bankfull discharge of rivers, *Water Resources Research*, 14, 1141-1154, 1978.

Wolcott, J. and Church, M., Strategies for sampling spatially heterogeneous phenomena: The example of river gravels, *Journal of Sedimentary Petrology*, 61, 534-543, 1990.

Wolman, M. G., A method of sampling coarse bed material, *AGU Transactions*, 35, 951-956, 1954.

Wolman, M. G. and Leopold, L. B., River flood plains: Some observations on their formation, USGS Professional Paper 282-C, 107 p., 1957.

Wolman, M. G. and Miller, J. P., Magnitude and frequency of forces in geomorphic processes, *Journal of Geology*, 68, 54-74, 1960.

Yalin, M. S., River Mechanics, Pergamon Press, Tarrytown, New York, p., 1992.

Yalin, M. S. and Karahan, E., Inception of sediment transport, *Journal of the Hydraulics Division, ASCE*, 105, 1433-1443, 1979.

Zimmerman, R. C., Goodlett, J. C. and Comer, G. H., The influence of vegetation on channel form of small streams, IAHS Publication 75, 255-275, 1967.

APPENDIX I: TABLE 1.1 NOTES

1 Using a dimensionless bedload transport formulation and a subset of Milhous' (1973) data, Parker and Klingeman (1982) extrapolated fractional bedload transport rates to a low reference value assumed representative of initial motion and calculated corresponding $\tau^*_{c_{ri}}$ values from the Shields equation. These values were in turn expressed as a function of D_i/D_{50s}. Only bedload transport data from armor-breaching events in the winter of 1971 were used (Parker and Klingeman, 1982; Komar, 1987a). $\tau^*_{c_{r50s}}$ is simply the value of this function with $D_i/D_{50s}=1$. The exponent of the Parker and Klingeman (1982) $\tau^*_{c_{ri}}$ function was estimated by JMB from their Fig. 3. Parker and Klingeman (1982) report $D_{50s}\approx 54$ mm [pg. 1411 and Table 1, Parker and Klingeman (1982)], however Milhous (1973) indicates that D_{50s} was 60-63 mm in 1971 [Tables 2 and 3, Milhous (1973)]. Using Milhous' (1973) median surface grain sizes and Parker and Klingeman's (1982) $\tau^*_{c_{ri}}$ function yields $\tau^*_{c_{50s}}=0.031$-0.032. σ_{gs} was calculated by JMB from data presented in Parker and Klingeman's (1982) Table 1.

2 Using Parker and Klingeman's (1982) technique (note *1*), $\tau^*_{c_{ri}}$ values were determined for Milhous' (1973) data and expressed as a function of the ratio D_i/D_{50ss} (Wilcock and Southard, 1988). $\tau^*_{c_{r50s}}$ was calculated by JMB from this function [Table 6, Wilcock and Southard (1988)], taking $D_i=D_{50s}=54$ mm (Parker and Klingeman, 1982) and $D_{50ss}=19.5$ mm [Table 1, Wilcock and Southard (1988)]; although it is not clear from Wilcock (1987), I assume that in following Parker and Klingeman's (1982) analysis Wilcock used the Oak Creek grain size data presented by them [Table 1, Parker and Klingeman, (1982)]. Wilcock's (1987) flume experiments were corrected for form drag and sidewall effects, but it is uncertain if Wilcock and Southard (1988) applied similar

corrections to the other data sources that they used [i.e., that of Milhous (1973)]. σ_{gs} is that reported for Parker and Klingeman (1982).

3 $\tau^*_{c_{ri}}$ values were determined using a simplified version of Parker and Klingeman's (1982) technique (note *1*) and regressed as a function of the ratio D_i/D_{50s} (Ashworth and Ferguson, 1989). $\tau^*_{c_{r50s}}$ values were determined by JMB from these functions [eqns (8a-c), Ashworth and Ferguson (1989)] with $D_i/D_{50s}=1$. D_{50s} values are averages of those reported in Ashworth and Ferguson's (1989) Table 1. In order to correct for form drag and other types of shear stress dissipation not accounted for by a simple depth-slope representation of critical shear stress, Ashworth and Ferguson (1989) used local point measures of shear stress to calculate τ_{c_i}. Nevertheless, their local estimates of boundary shear stress likely overestimate the effective bed shear stress, as they calculated boundary shear stress from the full velocity profile, rather than just over near-bed heights [see discussion of segmented velocity profiles in Middleton and Southard (1984) and Smith and McLean (1977)]. Their local velocity measures do, however, implicitly account for sidewall effects.

4 Parker's (1990) study simply re-visits the Parker and Klingeman (1982) study and expresses $\tau^*_{c_{ri}}$ in terms of the ratio D_i/D_{gs}, where D_{gs} is the geometric mean surface size defined as $\ln D_{gs}=\Sigma f_i \ln D_i$ (Parker, 1990); f_i is the fraction of the weight distribution comprised by D_i. $\tau^*_{c_{ri}}$ was calculated by JMB using D_{gs}=45.2 mm [pg. 428, Parker (1990)] and $D_i=D_{50s}$= 55 mm [Table 1, Parker (1990)]; note that these values are based on a grain size distribution for which the sand fraction was removed (Parker, 1990). σ_{gs} was calculated by JMB from data presented in Parker's (1990) Table 1.

5 $\tau^*_{c_{q50s}}$ was calculated by JMB from Andrews' (1983) eqn (2) using D_{50s} and D_{50ss} values reported by Andrews and Erman (1986). Although eqn (2) was developed from other data (Andrews, 1983) it shows reasonable agreement with the bedload transport data presented by Andrews and Erman (1986). Andrews' (1983) development of eqn (2) is, however, quite contorted. Using Shields' (1936) equation, dimensionless critical shear stresses were calculated for the geometric mean diameter of the largest grain size fraction sampled during bedload transport events in three North American rivers (Andrews, 1983). Critical shear stress was estimated from a depth-slope product employing a reach-average water surface slope and the flow depth over the zone of maximum bedload transport. The largest mobile particles for all of the sampled events in a given river were then grouped by size class and the average calculated critical shear stress was determined for each size class, $\overline{\tau}^*_{c_{qi}}$. These values from all three rivers were then regressed against the ratio D_i/D_{50ss}, yielding Andrews' (1983) equation (2). σ_{gs} was calculated by JMB from grain sizes estimated from Andrews and Erman's (1986) Fig. 4.

6 Using bedload transport data from Milhous (1973), Carling (1983), and Hammond et al. (1984), Komar (1987a) developed empirical competence equations for each study site, expressing competence as a power-law function between shear stress and the largest mobile grain size sampled during bedload events [Table 1, Komar (1987a)]. Each competence equation was re-written in terms of a power-law function for dimensionless critical shear stress of the form $\tau^*_{c_{qi}}=\alpha(D_i/D_{50})^{\beta}$ [similar to that used by Parker et al. (1982) and Andrews (1983)]. The Milhous $\tau^*_{c_{qi}}$ equation was determined through algebraic manipulation of the corresponding competence equation, taking D_{50} as the subsurface median grain size [pg. 207, Komar (1987a)]. Noting that the Milhous

competence equation crossed the Shields curve [*as defined by Miller et al. (1977)*] at $D_i \approx D_{50ss} \equiv D_{50}$, Komar (1987a) determined D_{50} values for the Carling and Hammond et al. $\tau^*_{c_{qi}}$ equations from the respective cross-over values of D_i [Fig. 3, Komar (1987a)]. Based on analogy with the Milhous data I assume that the Carling and Hammond et al. cross-over values correspond with D_{50ss}, making Komar's (1987a) reported $\tau^*_{c_{qi}}$ equations functions of D_i/D_{50ss}; however, cross-over points for Day's (1980b) competence functions apparently correspond with his reported D_{50m} values [Fig. 2, Komar (1987a)].

Using the empiricism that $D_i/D_{50} \approx 1$ at the cross-over, α values for the Carling and Hammond et al. $\tau^*_{c_{qi}}$ equations were fixed from cross-over points with the Miller et al. (1977) Shields curve [Fig. 4, Komar (1987a)], leaving β to be back-calculated. Komar (1987a) found that the resultant Carling $\tau^*_{c_{qi}}$ equation appeared to describe Milhous' data quite well, so he used it to represent Milhous' data, abandoning the algebraically defined Milhous $\tau^*_{c_{qi}}$ equation (cf. pg. 207, Fig. 5, and Table 1 of Komar (1987a)]. Rejecting this unsound rationale, I have maintained the original algebraically defined Milhous $\tau^*_{c_{qi}}$ equation in Table 1.1.

JMB calculated $\tau^*_{c_{q50s}}$ values from these "derived" $\tau^*_{c_{qi}}$ equations [Table 1, Komar (1987a)], using values of $D_i = D_{50s}$ and $D_{50} = D_{50ss}$ culled from other sources (see following notes).

7 $\tau^*_{c_{q50s}}$ was calculated by JMB from the originally defined Milhous equation, $\tau^*_{c_{qi}} = 0.044(D_i/D_{50})^{-0.43}$ [pg. 207, Komar (1987a)], using Komar's (1987a) reported values of $D_{50} = D_{50ss} = 20$ mm (Table 1) and $D_i = D_{50s} = 60$ mm (pg. 207). σ_{gs} was based on D_{90s} and D_{10s} from Milhous' (1973) Table 3.

8 The Carling $\tau^*_{c_{qi}}$ expression [Komar (1987a), Table 1] was based on a subset of Carling's (1983) bedload transport data; only data from Great Eggleshope Beck were used. JMB calculated $\tau^*_{c_{q50s}}$ from this expression using the cross-over value of $D_{50}=D_{50ss}\approx 20$ mm [Komar (1987a), Table 1] and $D_i=D_{50s}=62$ mm [Komar and Carling (1991), Table 1]. This D_{50s} value is derived from the framework gravel distribution, which is observationally very similar to the censored (i.e., armored) surface layer distribution (Carling and Reader, 1982).

9 $\tau^*_{c_{q50s}}$ was calculated by JMB from the Hammond et al. $\tau^*_{c_{qi}}$ equation [Komar (1987a), Table 1] using Komar's (1987a) reported value of $D_{50}=D_{50ss}=7.5$ mm (Table 1) and $D_i=D_{50s}=21$ mm [estimated by JMB from the Fig. 3 TV data of Hammond et al. (1984)].

10 JMB calculated $\tau_{c_{q50s}}$ from the Fahnestock (1963) competence equation reported by Komar (1987b, Table 1), and in turn used this value to determine $\tau^*_{c_{q50s}}$ from the Shields equation. For these calculations D_{50s} was determined from the composite White River grain size data [Fahnestock (1963), Table 2].

11 The data sets differ from those used by Komar (1987a) in that more data from Great Eggleshope Beck were included and, as with the Parker and Klingeman (1982) study, only the subset of Milhous' (1973) data corresponding with armor-breaching events was analyzed (Komar and Carling, 1991). $\tau^*_{c_{q50s}}$ values were calculated by JMB from relevant equations [Komar and Carling (1991), Fig. 9] and grain sizes [Komar and Carling (1991), Table 1]. Although the caption for Komar and Carling's (1991) Fig. 9 indicates that the Great Eggleshope Beck $\tau^*_{c_{qi}}$ equation is expressed as a function of

median subsurface grain size, the normalizing grain size used by the authors (62 mm) is that of the framework gravel [pg. 498, Komar and Carling (1991)], which is equivalent to the censored (i.e., armored) *surface* size (Carling and Reader, 1982); Komar and Carling's (1991) Table 1 also indicates that the 62 mm median framework size is a surface value analogous to that of the surface material in Oak Creek. Despite the caption for Komar and Carling's (1991) Fig. 9, only the Oak Creek $\tau^*_{c_{qi}}$ equation is expressed as a function of D_{50ss}; the Great Eggleshope Beck $\tau^*_{c_{qi}}$ equation is a function of D_{50s}.

12 $\tau^*_{c_{q50s}}$ was based on Milhous' (1973) Fig. 21 which is a plot of the maximum mobile grain size sampled in a pit bedload trap versus τ/γ; $\tau^*_{c_{q50s}}$ was estimated by JMB from contoured Shields stresses shown on this plot. Virtually the full range of grain sizes sampled during Milhous' (1973) experiments share a common minimum $\tau^*_{c_q}$ value of 0.025, re-enforcing the concept of "equal mobility" (Parker et al., 1982). Grain sizes plotted in Milhous' (1973) Fig. 21 are nominal diameters calculated from weights of the largest particle captured by the trap. Cui and Komar (1984) argue that the nominal diameter of a grain is on average equivalent to the grain's intermediate diameter; this similarity of measures is assumed here. τ_c was calculated from the maximum depth-slope product during a bedload transport event. σ_{gs} was based on D_{90s} and D_{10s} from Milhous' (1973) Table 3.

13 Carling (1983) expressed incipient motion in terms of a power function between total boundary shear stress (calculated as a depth-slope product) and the average size of the five largest bedload particles sampled during an event. Similarly, Shields stress was expressed as a power function of Re* ($=u^*D_i/\nu$) (Carling, 1983). JMB calculated $\tau^*_{c_{q50s}}$ from these expressions and other reported data. For example, the following

procedure was used for Great Eggleshope Beck: taking D_{50s} as the median grain size of the framework distribution [Table 1, Komar and Carling (1991)], $\tau_{c_{q50s}}$ was determined from Carling's (1983) equation (7); with this value, u^*_c and in turn Re^*_c was estimated, allowing calculation of $\tau^*_{c_{q50s}}$ from Carling's (1983) equation (9). In calculating Re^*_c it was assumed that $\nu=10^{-6}$ m^2/s. $\tau^*_{c_{q50s}}$ for Carl Beck was estimated in a similar fashion using appropriate equations for Carl Beck and the mean framework gravel size reported by Carling and Reader (1982).

14 $\tau^*_{c_{q50s}}$ values are fit from a semi-theoretical critical discharge formulation employing Bathurst's (1987a) bedload transport data which is expressed in terms of the average maximum grain size mobilized during a given peak discharge (Ferguson, 1994). Ferguson's (1994) formulation combines an Andrews-type (1982) equation (assuming conditions of near equal mobility) with the Schoklitsch (1962) equation. Form drag and sidewall corrections are not explicitly considered, but may be indirectly accounted for to some degree by the Thompson and Campbell (1979) roughness empiricism used by Ferguson (1994); this empiricism, however, is likely only representative of the roughness conditions examined by Thompson and Campbell (1979).

15 Using empirically determined values in a theoretical critical shear stress formulation similar to that of White's (1940), Kalinske (1947) argues that $\tau_c=4D$ for uniform, sand-sized grains with $Re^*_c>3.5$; this equality is expressed in English units. $\tau^*_{c_{50s}}$ was calculated by JMB by re-writing Kalinske's (1947) competence expression in terms of the Shields equation.

16 Çeçen and Bayazit (1973) examined transport rates and grain size distributions of bedload material in an armored channel typical of natural, mountain streams. Equality of

armor and bedload grain size distributions was used to define incipient motion of the bed surface. The corresponding critical shear stress was found to equal that required for incipient motion of D_{50s} according to Egiazaroff's (1965) critical shear stress formulation (Çeçen and Bayazit, 1973).

17 $\tau^*_{c_{50s}}$ was based on a theoretical critical shear stress formulation (Kirchner et al., 1990) employing friction angle and grain protrusion measurements made from flume-worked heterogeneous bed surfaces. Grain mobility here is for that of particles placed on a bed surface. $\tau^*_{c_{50s}}$ values are calculated in the absence of form drag and sidewall effects. The specific $\tau^*_{c_{50s}}$ value reported here was read from Kirchner and others' (1990) Fig. 18 for $D/K_{50}=1$ and n=10.

18 $\tau^*_{c_{50s}}$ was determined from Kirchner et al.'s (1990) theoretical critical shear stress formulation employing friction angle measurements made from bed surfaces of a natural pool-riffle stream (Buffington et al., 1992). Grain mobility here is for that of particles placed on a bed surface. $\tau^*_{c_{50s}}$ values are calculated in the absence of form drag and sidewall effects. The specific $\tau^*_{c_{50s}}$ value reported here was read from Buffington and others' (1992) Fig. 13 for $D/K_{50}=1$ and n=0.1.

19 Using a simple "slab" shear model Jiang and Haff (1993) simulated particle motion of a heterogeneous bed surface, accounting for individual relative grain velocities, intergranular friction, and grain-to-grain collisions. Reported $\tau^*_{c_{50s}}$ values bracket the calculated threshold of "continuous" motion, defined as one or more particles moving at all times (Jiang and Haff, 1993) during a simulation. Bedform drag and sidewall effects were not present in the simulations.

20 Using his own experiments and data reported by Casey (1935), Kramer (1925), USWES (1935), and Gilbert (1914), Shields (1936) calculated $\tau^*_{c_{r50m}}$ values for each laboratory sediment mixture using a reference critical shear stress corresponding to an extrapolated near-zero bedload transport rate of the mixture. Shear stresses were corrected for sidewall effects in Shields' (1936) experiments, but it is uncertain if such corrections were made for the other data sources used by Shields (1936). Some $\tau^*_{c_{r50m}}$ and Re^*_c values were read from Tison's (1953) Table II, but most were estimated by JMB from the Shields curve presented in Rouse's comments to Chang (1939). D_{16m} and D_{84m} values used to calculated σ_{gm} were estimated from Shields' (1936) Fig. 16. While Shields (1936) reports D_{50m} values used in his experiments, it is unclear which values correspond with a given point on the Shields curve. As such, assignment of D_{50m} values in Table 1 is based on a sensible match of grain size with reported $\tau^*_{c_{r50m}}$ and Re^*_c pairs for a particular sediment type.

21 D_{50m} values used in Casey's (1935) experiments were 0.85 mm, 1.23 mm, and 2.44 mm (Shields, 1936), however, assignment of these values to reported $\tau^*_{c_{r50m}}$ and Re^*_c pairs is uncertain. Shields (1936) chose D_{50m} values for his granitic grain experiments to mimic those of Casey (1935). If similarity of grain size distributions is also assumed, then Casey's (1935) experiments employed near-uniform sizes [$\sigma_{gm} \approx 0.23$ for Shields' (1936) granitic grains]. Other details of Casey's (1935) experiments were not reported by Shields (1936) and are unknown to JMB.

22 Kramer (1935) began measurements of bedload transport and other parameters at the start of each experiment, unlike other investigators who waited for some sort of equilibrium condition before making measurements [e.g., Gilbert (1914), Williams

(1970), Wilcock and Southard (1988)]. Reported D_{50m} values were estimated by JMB from Kramer's (1935) Fig. 1, and are again a best fit to reported $\tau^*_{c_{r50m}}$ and Re^*_c pairs.

23 Sediment was sand-sized, but other experimental details were not reported by Shields (1936) and are unknown to JMB. These mixtures are likely non-uniform, based on Day's (1980b) estimates of the USWES (1935) σ_{gm} values.

24 Grain sizes reported are the mean nominal diameters of the laboratory sediment mixture. The first $\tau^*_{c_{r50m}}$ and Re^*_c pair correspond with Gilbert's (1914) grade H sediment mixture; no bedform types were reported for these runs (Gilbert, 1914). Bedload and other measurements were begun when the bed slope equilibrated with the sediment feed rate (Gilbert, 1914). σ_{gm} values were based on the reported range of grain sizes in a given mixture.

25 Paintal (1971) questions the existence of a definitive threshold for mobility, arguing that grains exposed to any current will move if one observes them long enough. Nevertheless, two potential $\tau^*_{c_{r50m}}$ values can be estimated from Paintal's (1971) analysis. Extrapolating high bedload transport rates to a zero value yields $\tau^*_{c_{r50m}} \approx 0.05$ for D_{50m} values of 2.5 mm and 7.95 mm [Paintal (1971), Fig. 8]. Alternatively, a straight line fit through a plot of low dimensionless bedload transport rates versus Shields stresses of Paintal's (1971) composite data yields $\tau^*_{c_{r50m}} \approx 0.02$ at a transport rate of 10^{-9} [Paintal (1971), Fig. 6].

26 Mizuyama (1977) examined the influence of slope and relative roughness on grain mobility, and proposed a modified formulation for the Shields stress, accounting for slope and intergranular friction angle. However, a slight mistake in Mizuyama's (1977)

force balance resulted in a proposed modified Shields stress of $\tau^*_{c_{r50m}}=\tau_{c_{r50m}}/[(\rho_s-\rho)gD_{50m}\{\tan\Phi\cos\theta-\sin\theta\,\rho_s/(\rho_s-\rho)\}]$, rather than the correct expression $\tau^*_{c_{r50m}}=\tau_{c_{r50m}}/[(\rho_s-\rho)gD_{50m}(\tan\Phi\cos\theta-\sin\theta)]$; a buoyancy term was neglected on the left-hand side of Mizuyama's (1977) eqn (3.27) [see Wiberg and Smith (1987) for a similar correct derivation]. Furthermore, the reported intergranular friction angles, Φ, are actually angles of repose for the mass sediment mixture [cf. Miller and Byrne (1966)]. Using the correct Shields stress expression (with the erroneous Φ values), JMB calculated $\tau^*_{c_{r50m}}$ values with data from Mizuyama's (1977) Tables 3.1 and 3.2. Mizuyama (1977) determined $\tau_{c_{r50m}}$ values by extrapolating bedload transport rates to a near-zero reference level. Reported grain sizes are nominal values of the median (?) grain size of the laboratory sediment mixture; nominal diameters are assumed equivalent to b-axes here (see note *12*). σ_{gm} was estimated by JMB from reported sieve ranges. Although the data are not presented here, Mizuyama (1977) also conducted experiments with mixed-grain sediments. It was found that mixed-grain sediments have higher modified Shields stresses than near-uniform grains and that $\tau^*_{c_{r50m}}$ increases systematically with decreasing sorting, contrary to more recent findings (Misri et al. 1984; Buffington et al., 1992).

27 Misri and others' (1984) Fig. 6, which is a plot of Einstein's (1950) dimensionless bedload transport parameter versus Shields stress stratified by D_i of their N-2 sediment mixture, indicates that dimensionless shear stress is a function of D_i and, more importantly, has no definable critical value over the transport rates that they examined; these findings agree with those of Einstein (1950) and Paintal (1971). The "critical" Shields stress reported in Table 1 was estimated by JMB from Misri and others' (1984) Fig. 6 based on the lowest transport rate (10^{-4}) of D_i values that bracket D_{50m}.

28 The following criteria were used by Bridge and Dominic (1984) in selecting data sources: use of laboratory sediment mixtures of near-uniform size and density, allowing a mean grain size to be taken as characteristic and avoiding potential armoring effects; and experiments resulting in lower or upper stage plane-beds, minimizing form drag effects. Wall effects were corrected "where necessary" (Bridge and Dominic, 1984). $\tau^*_{c_{r50m}}$ values were determined empirically by plotting dimensionless bedload transport rates versus Shields stress, with the critical reference value assumed to be the Shields stress asymptotically approached at low transport rates (Bridge and Dominic, 1984).

29 Collection of bedload and other data began only after attainment of equilibrium conditions, defined by uniformity of bedforms and steady sediment transport rates (Guy et al., 1966). Time to equilibrium varied from hours to several days. The 0.19 mm and 0.32 mm runs had water temperatures close to 20° C, but the 0.28 mm runs had water temperatures closer to 15° C; as such, $\nu=1.139 \cdot 10^{-6}$ m^2/s was used in calculating Re^*_c for the 0.28 mm runs.

30 Bedload and other measurements made after attainment of a constant bed slope and equilibrium of sediment input and output (Williams, 1970).

31 $\tau^*_{c_{r50m}}$ determined from the composite experiments of Fernandez Luque and van Beek (1976). Five different laboratory sediment mixtures were used with mean (by weight) grain sizes of 0.9-3.3 mm and densities of 1340-4580 kg/m^3. See also note *42*.

32 $\tau^*_{c_{r50m}}$ values correspond with extrapolated zero or near-zero bedload transport rates and were calculated by JMB using Bathurst and others' (1987) eqn (15.1) and values in Table 15.3. Equation (15.1) is a modified Shields stress, accounting for slope and

intergranular friction angle. However, reported friction angles are actually angles of repose of the mass sediment mixture, not intergranular friction angles [cf. Miller and Byrne (1966)]. Re^*_c values estimated from Bathurst and others' (1987) Fig. 15.3.

33 Reported grain sizes and relative roughnesses are from Bathurst et al. (1983). Details of Bathurst and others' (1979) flume experiments are unknown to JMB. $\tau^*_{c_{r50m}}$ values were determined by Bathurst et al. (1979) as per note *32* and were estimated by JMB from Bathurst and others' (1987) Fig. 15.3. It is uncertain, however, if Bathurst and others' (1979) values were corrected for sidewall effects.

34 Using the Ackers and White (1973) bedload transport equation, Day (1980b) extrapolated fractional bedload transport rates to a low reference value assumed representative of incipient motion and determined corresponding initial motion parameters for D_i of bedload experiments conducted by USWES (1935) and Day (1980a). $\tau^*_{c_{r50m}}$ values were determined by JMB from Day's (1980b) Fig. 41.4 for dimensionless particle sizes corresponding with D_{50m} values of the flume experiments [Table 41.1, Day (1980b)]; the Ackers and White (1973) initial motion parameter in Fig. 41.4 is simply the square root of the Shields equation. Few details of the experimental methods and conditions were presented by Day (1980b). Using Day's (1980b) reported values of $(D_{84m}/D_{16m})^{0.5}$ (Table 41.1), σ_{gm} was calculated by JMB as $\sigma_{gm}=[\log_2(D_{84m}/D_{16m})-\log_2(1)]/2$.

35 Using Parker and Klingeman's (1982) technique (note *1*), $\tau^*_{c_{ri}}$ values were determined and expressed as a function of the ratio D_i/D_{50m} (Wilcock and Southard, 1988). $\tau^*_{c_{r50m}}$ values were calculated by JMB from these functions [Table 6, Wilcock and

Southard (1988)], taking $D_i/D_{50m}=1$. Wilcock's (1987) data were corrected for form drag and sidewall effects, but it is uncertain if Wilcock and Southard (1988) applied similar corrections to the other data sources that they used. Misri et al. (1984) applied sidewall and (?) form drag corrections, but analytical procedures of Day (1980a) and Dhamotharan et al. (1980) are unknown to JMB. For the data of Misri et al. (1984), Dhamotharan et al. (1980), and Wilcock and Southard (1988), σ_{gm} was calculated from D_{15m} and D_{85m} values reported by Wilcock and Southard (1988, Table 1). σ_{gm} values for Day's (1980a) experiments are the same as those described in note *34*.

36 Bedload and other measurements were made after attainment of equilibrium conditions, defined by steady sediment transport and stable bedforms (Wilcock and Southard, 1988). To better establish initial motion conditions several runs for each sediment mixture involved lower stage plane-bed morphologies. Bedload transport rates for these runs were close to the assumed reference value (Wilcock and Southard, 1988). Water temperatures were typically about 25° C and as such I used $\nu \approx 0.893 \cdot 10^{-6}$ m^2/s in calculating Re^*_c values.

37 Kramer (1935) recognized three types of visual grain movement: weak, characterized by infrequent movement of a small number of the finest grain sizes of the sediment mixture; medium, characterized by movement of a significant number of the mean grain sizes (and smaller), but with insignificant bedload transport and maintenance of a plane-bed morphology; and general, characterized by significant movement of all grain sizes, an appreciable quantity of bedload transport, and dune-ripple development. Because mobility of the median grain size is the issue here, the data reported in Table 1.1 are

values corresponding with "medium" bed surface mobility of each sediment mixture. D_{50m} values estimated by JMB from Kramer's (1935) Fig. 1.

38 $\tau^*_{c_{v50m}}$ was calculated from the Meyer-Peter and Müller (MPM) bedload equation employing the observed τ_c and assuming a zero transport rate at incipient motion (Meyer-Peter and Müller, 1948). The MPM equation expresses bedload transport of the composite bed material in terms of the "effective diameter" of the laboratory sediment mixture, defined as $\Sigma D_i f_i$, where D_i is the average grain size within a given size class of the weight distribution and f_i is that class' fraction of the distribution. The effective diameter was typically equivalent to $D_{50\text{-}60m}$ (Meyer-Peter and Müller, 1948).

39 Threshold of mobility defined by visual observation of either the initiation or cessation of motion (White, 1940). The first two $\tau^*_{c_{v50m}}$ and Re* pairs were calculated by JMB from White's (1940) Table 1 (experiments 1a-b and 2a) assuming ρ_s=2650 kg/m^3 and $\rho \approx 900$ kg/m^3; the density of the fluid was estimated by comparing the reported depth-slope products [Table 1, "from d," White (1940)] with those calculated by JMB for a fluid medium of water. The third $\tau^*_{c_{v50m}}$ and Re* pair was calculated by JMB from data on pg. 328 assuming $\nu=10^{-6}$ m^2/s. All other values from White's (1940) Table 2.

40 Boundary shear stress was measured from photographed velocity profiles defined by hydrogen bubbles traces (Grass, 1970). Two measures of shear stress are reported by Grass: 1) an average value determined from 25 of the instantaneous velocity profiles *selected at random throughout the measuring period*; 2) an instantaneous value interpolated from the instantaneous velocity profiles just before and after incipient motion (as identified from photographs of the bed surface). $\tau^*_{c_{v50m}}$ values determined from the later measures are reported in Table 1 in parentheses. $\tau^*_{c_{v50m}}$ values calculated

from the former measures are more comparable to a depth-slope value in that they are a time-averaged measure; however, it is unclear if the randomly selected velocity profiles of a given run are sampled from similar conditions of flume-average flow depth and slope. Direct shear stress measures of this sort implicitly account for sidewall effects.

41 $\tau^*_{c_{v50m}}$ values calculated by JMB using the Shields equation and data in Everts' (1973) Table 1. Re^*_c was calculated with $\nu=0.893 \cdot 10^{-6}$ m^2/s, as Everts (1973) reports a water temperature of about 25° C.

42 Fernandez Luque and van Beek (1976) examined the effects of bed surface slope on $\tau^*_{c_{v50m}}$ values and as expected found a systematic increase in $\tau^*_{c_{v50m}}$ with slope; the Shields equation as originally written neglects the downslope gravitational component of the driving force. $\tau^*_{c_{v50m}}$ values reported in Table 1.1 are for 0° bed slopes and were estimated by JMB from Fernandez Luque and van Beek's (1976) Fig. 2. $\tau_{c_{v50m}}$ values were calculated from a standard Moody diagram, using measured velocities and an hydraulic radius corresponding with the center 0.05 m of the flume bed (Fernandez Luque and van Beek, 1976); this technique implicitly accounts for sidewall effects.

43 σ_{gm} was estimated by JMB from D_{10m} and D_{90m}, knowing that $1.6 \leq D_{90m}/D_{10m} \leq 2.1$ for the sediment mixtures employed in Yalin and Karahan's (1979) experiments. The estimation is $\sigma_{gm} \approx [\log_2(D_{90m}/D_{10m}) - \log_2(1)]/2$.

44 The same technique was used as in note *1*, however, $\tau^*_{c_{ri}}$ values were expressed as a function of D_i/D_{50ss}. σ_{gss} was calculated by JMB from data presented in Parker and Klingeman's (1982) Table 1.

45 $\tau^*_{c_{q50ss}}$ values were determined by JMB from reported $\tau^*_{c_{qi}}$ functions [Komar (1987a), Table 1], with $D_i/D_{50ss}=1$. Note that $\tau^*_{c_{q50}}$ values were fit by Komar to the Shields curve developed by Miller et al. (1977), and as such are fixed by default at values of 0.045 for high Re^*_c values (see note *6*). σ_{gss} was calculated by JMB from D_{10ss} and D_{90ss} values presented in Milhous' (1973) Table 3.